PUBLISHED BY THE ACADEMY OF SCIENCES OF ALBANIA

JNTS

JOURNAL OF NATURAL
AND TECHNICAL SCIENCES

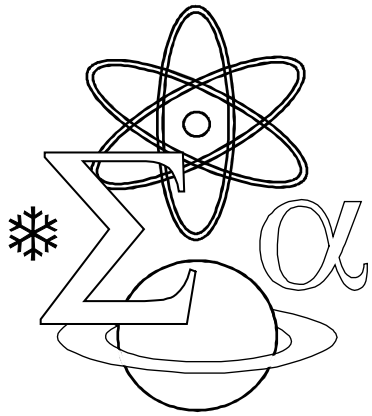

2015, Vol. XX (1)

THE EILENBERG-MAC LANE COHOMOLOGY OF AN INVERSE MONOID AND THE MAXIMUM GROUP IMAGE

Anjeza KRAKULLI
Department of Mathematics, Faculty of Technology and Information,
University Aleksandër Moisiu, Durrës, Albania
Elton PASKU
Department of Mathematics, Faculty of Natural Sciences,
University of Tirana, Albania

ABSTRACT

The present paper investigates the extent homological properties of an inverse monoid determined from those of its maximum group image. We provide several evidences that the maximum group image contains vital homological information which can be used to study certain properties of the monoid itself. For instance, we prove that an inverse monoid S is of type FP_∞, if and only if it contains a minimal idempotent and its maximum group image is of the same type. Regarding cohomological dimensions, we show that the cohomological dimension of a free Clifford monoid and that of its maximum group image agree and are equal to one. Also, we define the index of a full submonoid of an inverse monoid in terms of their maximum group images and show that if the index is finite then, the monoid is of type FP_∞ if and only if its submonoid is of the same type.

Keywords: Inverse monoid, semilattice, maximum group image, cohomology groups, Ext , Tor, homological finiteness condition FP_∞, direct limits, direct products, unitarily finitely generated, cohomological dimension
Mathematics Subject Classification: 18G10, 18G15, 13D02, 16E30, 18A30, 20M12, 20M18

1. INTRODUCTION AND PRELIMINARIES

A useful way to look for homological information for an inverse monoid is to study homological properties of its maximal subgroups and see at what extent they determine certain properties of the monoid. There are several evidences given in (Gray and Pride, 2011) that this approach is indeed useful. In this paper the authors have shown that a Clifford monoid S is of type FP_n if and only if S contains a minimal idempotent e and the maximal subgroup of S

containing e is of type FP_n. For the wider class of inverse semigroups, they prove under the assumption that the semigroup contains a minimal idempotent, that it is of type FP_n if and only if its maximal subgroup containing that idempotent is of the same type. Differently from (Gray and Pride, 2011), in our paper we relate homological properties of an inverse monoid S to those of its maximum group image G. We prove that S is of type FP_∞ if and only if S contains a minimal idempotent and G is of type FP_∞. We also prove that the cohomological dimension of a free Clifford monoid and that of its maximum group image agree. In this case we prove that the cohomological dimension is one, which makes a free Clifford monoid another candidate to prove an analogue of the Stalling Swan theorem for inverse semigroups. At the end of the paper we define the index of a full submonoid of an inverse monoid in terms of their maximum group images and show that if the index is finite then, the monoid is of type FP_∞ if and only if its submonoid is of the same type. This property has its counterpart in the theory of cohomology of groups. These results provide enough evidence that the maximum group image of an inverse monoid contains vital homological information which can be used to study homological properties of the monoid itself, and therefore deserves to be studied further on.

By definition, S is an inverse semigroup if for each element x there is a unique x^{-1} such that $x = xx^{-1}x$ and $x^{-1} = x^{-1}xx^{-1}$. A key property of inverse semigroups is that their idempotents commute. If S is an inverse monoid and E its semilattice of idempotents, then we let G be the maximum group image of S; that is $G \cong S/\pm$ where $\pm$ is the congruence on S defined as follows. For every $a, b \in S$, $a \pm b$ if and only if there is an $e \in E$ such that $ae = be$, or equivalently, if there is $f \in E$ such that $fa = fb$. The unit of G will be denoted by 1.

We can regard the monoids S and G as small categories with a single object, denoted by $*_S$ and $*_G$ respectively, and with morphisms, the elements of the respective monoids. Define $J : S \to G$ by $J(*_S) = *_G$ and for every $s \in S$ we let $J(s) = «(s)$ where $« : S \to S/\pm$ is the canonical epimorphism. One can easily prove that J is a functor using the fact that it arises for an epimorphism of monoids. The functor J induces a functor $J^* : \mathbf{Ab}^G \to \mathbf{Ab}^S$ by the rule $J^*(M) = MJ$, for every G-module $M \in \mathbf{Ab}^G$.

The following construction is a special case of the comma category (Mac Lane, 1997). Denote by $\Im \downarrow *_G$ the category of J-objects over $*_G$ as follows. An object of $\Im \downarrow *_G$ is a pair $(*_S, a)$ where $a : *_G \to *_G$ is a morphism in G. A morphism $s : (*_S, a) \to (*_S, b)$ is a morphism $s : *_S \to *_S$ such that the

diagram commutes. In other words, there is a morphism $s:(*_S,a)\to(*_S,b)$ if $bJ(s)=a$.

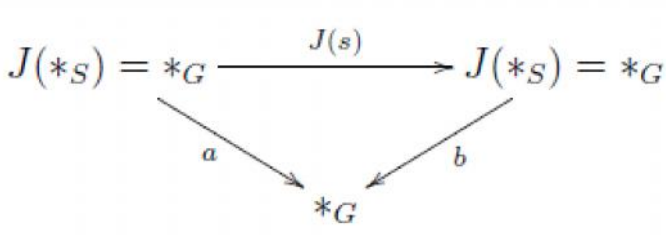

We record the following lemma for future use.

Lemma 1.1. *For every monoid S, there is an isomorphism between additive categories $\mathbf{Ab}^S$ and $\mathbf{Ab}^{\mathbb{Z}S}$, where $\mathbb{Z}S$ is the additivization of S.*

Proof. Define $\mathcal{I}_S:\mathbf{Ab}^S\to\mathbf{Ab}^{\mathbb{Z}S}$ by $\mathcal{I}_S(F)=\mathbb{Z}F$ on objects and by $\mathcal{I}_S(\phi)=\mathbb{Z}\phi$ on morphisms $\phi:F_1\cdot\to F_2$. ■

2. Cohomology of inverse monoids

As long as we are trying to relate the homological properties of an inverse monoid to those of its maximum group image, it is natural to consider the Eilenberg-MacLane cohomology of monoids which by definition is given by

$$H^n(S,M)=Ext^n_{\mathbb{Z}S}(Z,M).$$

Here, S is a monoid, M is a left S-module and $\mathbb{Z}$ is the trivial S-module.

The following lemma is crucial in the proof of theorem 2.1.

Lemma 2.1 *$\Im\downarrow *_G$ is filtered and if S contains a minimal idempotent, then $\Im\downarrow *_G$ is strongly filtered in the sense of* (Schubert, 1972).

Proof. Let $(*_S,a)$ and $(*_S,b)$ be two objects of $\Im\downarrow *_G$. We can chose $\sim$ and $\in S$ such that $\alpha(\sim)=a$ and $\alpha(\ )=b$, then, from the definition $\sim:(*_S,a)\to(*_S,1)$ and $:(*_S,b)\to(*_S,1)$ are arrows in $\Im\downarrow *_G$. Secondly, if $s_1,s_2:(*_S,a)\to(*_S,b)$ are parallel arrows, then we have $b\alpha(s_1)=a=b\alpha(s_2)$, which means that $s_1\pm s_2$ and as a result there is an $e\in E$ such that $es_1=es_2$. But evidently, $e:(*_S,b)\to(*_S,b)$ is an arrow in $\Im\downarrow *_G$, hence the above equality is an equality of arrows in $\Im\downarrow *_G$. This

shows that $\Im\downarrow *_G$ is a filtered category. Lastly, we assume that S contains a minimal idempotent $\pounds$ and let $s_i : (*_S, a) \to (*_S, a_i)$ with $i \in I$ be a pencil in $\Im\downarrow *_G$. For every $i \in I$, chose $t_i \in S$ such that $\ll(t_i) = a_i$. For every i and $j \in I$ we have that $a_i \ll(s_i) = a = a_j \ll(s_j)$, hence $\ll(t_i s_i) = \ll(t_j s_j)$. Then there exists and idempotent $e_{ij} \in E$ such that $e_{ij} t_i s_i = e_{ij} t_j s_j$. Multiplying through on the left by $\pounds$ and recalling that $\pounds$ is a minimal idempotent, we obtain $\pounds t_i s_i = \pounds t_j s_j$. As before, $\pounds : (*_S, 1) \to (*_S, 1)$ is an arrow in $\Im\downarrow *_G$, therefore the family of arrows $\pounds t_i$ with $i \in I$ is a commutative completion of the given pencil showing that $\Im\downarrow *_G$ is strongly filtered. ■

The following is an analogue of theorem 4.1 of (Pasku, 2011) for inverse monoids in general and also an analogue of proposition 3.6 of (Loganathan, 1981) which relates the Lausch cohomology of an inverse monoid to the Eilenberg-Mac Lane cohomology of its maximum group image.

Theorem 2.1 For every $n \geq 0$ and every left $\mathbb{Z}G$ module M there is a natural isomorphism

$$Ext^n_{\mathbb{Z}G}(\mathbb{Z}, M) \cong Ext^n_{\mathbb{Z}S}(Z, \mathbf{J}^* M) \qquad (1)$$

where $\mathbf{J}^* = \mathcal{I}_S J^* \mathcal{I}_G^{-1}$, with $\mathcal{I}_G$ and $\mathcal{I}_S$ being the isomorphisms of lemma 1.1 and $\mathbb{Z}$ is the trivial module.

Proof. We show first that J^* has a left adjoint $\tilde{J}$ by using standard categorical arguments and then we show that both, J^* and are exact functors. Since all colimits exist in $\mathbf{Ab}$, then the dual of theorem 1, p. 237 of (Mac Lane, 1997) shows that every functor $T \in \mathbf{Ab}^S$ has a left Kan extension $Lan_J T$ along J defined by

$$Lan_J T(*_G) = \underline{Lim}(\Im\downarrow *_G \xrightarrow{P} S \xrightarrow{T} \mathbf{Ab}) \qquad (2)$$

where P is the projection $(*_S, a) \mapsto *_S$. Now the dual of the argument given in p. 237 of (Mac Lane, 1997) shows that the function $T \mapsto Lan_J T$ determines a left adjoint $\tilde{J}$ of J^*. As a left adjoint, preserves cokernels, so to prove it is exact it remains to show that preserves monics too. Let $T_1 \to T_2$ be

a monic in $\mathbf{Ab}^S$, then Proposition 3.1, p. 258 of (Mac Lane, 1963) shows that the induced morphism $T_1P \to T_2P$ is also monic in $\mathbf{Ab}^{\Im\downarrow *_G}$. Regarding $\mathbf{Ab}$ as the category of right $\mathbb{Z}$ modules and recalling from lemma 2.1 that $\Im\downarrow *_G$ is filtered, we can apply theorem 2.6.15 of (Weibel, 1994) to show that the other induced morphism $\underline{Lim}(T_1P) \to \underline{Lim}(T_2P)$ is monic which from (2) is the same as to say that $Lan_J T_1(*_G) \to Lan_J T_2(*_G)$ is monic too. Proposition 3.1, p. 258 of (Mac Lane, 1963) again shows that $Lan_J T_1 \to Lan_J T_2$ is monic proving the exactness of $\tilde{J}$.

We show that also J^* is exact. For this recall first that J^* preserves kernels as a right adjoint. It remains to show that it preserves epics too. Indeed, if $M_1 \twoheadrightarrow M_2$ is an epic in $\mathbf{Ab}^G$, then the induced homomorphism $M_1 J(*_S) = M_1 \to M_2 = M_2 J(*_S)$ is a surjective homomorphism of left S modules.

The composite $\tilde{\mathbf{J}} = \mathcal{I}_G \tilde{J} \mathcal{I}_S^{-1} : \mathbf{Ab}^{\mathbb{Z}S} \to \mathbf{Ab}^{\mathbb{Z}G}$ is exact since $\mathcal{I}_G$ and $\mathcal{I}_S^{-1}$ are exact. In the same way we can get another exact functor $\mathbf{J}^* = \mathcal{I}_S J^* \mathcal{I}_G^{-1} : \mathbf{Ab}^{\mathbb{Z}G} \to \mathbf{Ab}^{\mathbb{Z}S}$. In fact this functor is the change of ring functor in the sense of (Hilton and Stammbach, 1997). Since each isomorphism is adjoint to its inverse, we see from theorem 1, p. 103 of (Mac Lane, 1997) that $\tilde{\mathbf{J}}$ is a left adjoint to $\mathbf{J}^*$. Now we can apply theorem 12.1, p. 162 of (Hilton and Stammbach, 1997) to obtain for every $n \geq 0$ a natural isomorphism

$$\Phi^n : Ext^n_{\mathbb{Z}G}(\tilde{\mathbf{J}}N, M) \to Ext^n_{\mathbb{Z}S}(N, \mathbf{J}^* M) \qquad (3)$$

for every $M \in \mathbf{Ab}^{\mathbb{Z}G}$ and $N \in \mathbf{Ab}^{\mathbb{Z}S}$. If we take N to be the trivial left $\mathbb{Z}S$ module $\mathbb{Z}$, then $\tilde{\mathbf{J}}N$ coincides with the trivial $\mathbb{Z}G$ module $\mathbb{Z}$. Indeed, as proved in (Hilton, and Stammbach, 1997), the change of ring functor $\mathbf{J}*$ has a left adjoint (which has to be naturally isomorphic to $\tilde{\mathbf{J}}$) given by the rule $N \mapsto \mathbb{Z}G \otimes_{\mathbb{Z}S} N$. For $N = \mathbb{Z}$ we see that any generator $g \otimes_{\mathbb{Z}S} z$ of $\mathbb{Z}G \otimes_{\mathbb{Z}S} \mathbb{Z}$ can be reduced as follows: $g \otimes_{\mathbb{Z}S} z = 1 \otimes_{\mathbb{Z}S} s \cdot z = 1 \otimes_{\mathbb{Z}S} z$ where $s \in \kappa^{-1}(g)$. Therefore, $\tilde{\mathbf{J}}\mathbb{Z} \cong \mathbb{Z}$. Applying (3) for $N = \mathbb{Z}$, we get the natural isomorphism $Ext^n_{\mathbb{Z}G}(\mathbb{Z}, M) \cong Ext^n_{\mathbb{Z}S}(\mathbb{Z}, \mathbf{J}*\mathbf{M})$. ■

The isomorphism of theorem 2.1 shows that $\mathrm{cd}G \leq cdS$. We prove in the following proposition that in the case of inverse monoids containing a minimal idempotent cohomological dimensions are the same and then obtain as a corollary that free clifford monoids have cohomological dimension one.

Proposition 2.1 *Let S be an inverse monoid containing a minimal idempotent $£$. Then the cohomological dimension of S and that of its maximum group image G agree.*

Proof. We give first the strategy of the proof and then proceed with the technical details. The crux of the proof is to show that $\mathbf{J}^*\mathbb{Z}G$ is a projective left $\mathbb{Z}S$ module via $«$ and then utilize proposition 12.3 of (Hilton and Stammbach, 1997) which gives in this case a natural isomorphism $Ext^n_{\mathbb{Z}G}(\mathbb{Z}, Hom_{\mathbb{Z}S}(\mathbf{J}*\mathbb{Z}G, B)) \cong Ext^n_{\mathbb{Z}S}(\mathbb{Z}, B)$ for every $n \geq 0$ and $B \in \mathbf{Ab}^{\mathbb{Z}S}$. This implies immediately that $\mathrm{cd}S \leq \mathrm{cd}G$. This, together with the remark after theorem 2.1, imply that $\mathrm{cd}S = \mathrm{cd}G$. Let us show that $\mathbf{J}^*\mathbb{Z}G$ is projective. From theorem 2.1 we see that $\mathbf{J}^*\mathbb{Z}G$ is a flat $\mathbb{Z}S$ module, so to prove it is projective it is enough to show that it is finitely presented. Indeed, there is an exact sequence

$$\mathbb{Z}S \xrightarrow{\cdot} \mathbb{Z}S \xrightarrow{\tilde{«}} \mathbf{J}*\mathbb{Z}G \longrightarrow 0 \qquad (4)$$

where $\tilde{«}$ is the linear extension of $«$ and $\cdot$ is defined by $\cdot(s) = s - s£$. It is easy to see that $\cdot$ is a left $\mathbb{Z}S$ module homomorphism which maps $\mathbb{Z}S$ onto $\mathrm{Ker}(\tilde{«})$. The latter follows easily from the fact that $\mathrm{Ker}(\tilde{«})$ is generated as an abelian group from elements of the form $s - s£$. ■

We recall from (Howie, 1995) that a free Clifford monoid on a set X is the set

$$CM_X = \{(u, A) \in FG_X \times \mathcal{P}(X) \mid c(u) \subseteq A\},$$

where FG_X is the free group on X, $\mathcal{P}(X)$ is the set of all subsets of X, and by $c(u)$ we denote the content of the word u, that is, the set of all letters from X represented in the word u. The multiplication on CM_X is defined by

$$(v, B)(u, A) = (vu, B \cup A).$$

Corollary 2.1 *If CM_X is the free Clifford monoid on a set X, then the cohomological dimension of CM_X and that of its maximum group image $G = CM_X/\pm$ agree and are equal to one.*

Proof. As one can see from above, a free clifford monoid contains the minimal idempotent $(1, X)$, therefore from proposition 2.1 we have that $\mathrm{cd}CM_X = \mathrm{cd}G$, so it remains to show that $\mathrm{cd}G = 1$. This can be achieved if we prove that G is free on some set. In fact it is free on the set of equivalence classes $\{(\overline{x,\{x\}}) \mid x \in X\}$ modulo $\pm$. This can be proved easily using the universal property of CM_X as depicted in the following diagram

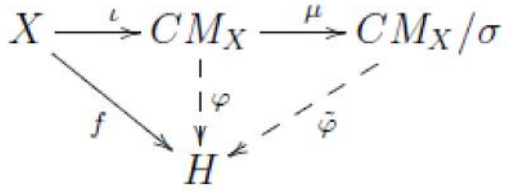

where H is any group and $f : X \to H$ is any map, $\S(x) = (x,\{x\})$, « is the natural epimorphism, ¨ is the monoid morphism which extends uniquely f and ¨˜ is given by ¨˜$((\overline{u,c(u)})) =$ ¨$((u,c(u)))$. ■

Corollary shows that free Clifford monoids are among other candidates to prove an analogue of the Stalling Swan theorem for inverse semigroups in terms of the Eilenberg-Mac Lane cohomology. Though it should be mentioned that, similarly to the Lausch cohomology, the dimension zero case for the Eilenberg MacLane cohomology is quite different from that of groups. More specifically, for E-unitary inverse monoids we have this

Corollary 2.2 *Let S be an E-unitary inverse monoid. Then S has cohomological dimension zero if and only if S is a semilattice with zero.*

Proof. From theorem 2.1 the maximum group image G has to be zero, therefore for every $s \in S$, $(s, 1_S) \in \pm$. Since S is E-unitary, it follows that s is an idempotent. The fact that S has a zero follows from (Laudal, 1972) and also from (Guba and Pride 1998). The converse is obvious. ■

We can get another application of theorem 2.1 in the case of abelian inverse monoids. We recall from (Nico, 1972) the following problem discussed there for abelian monoids in general. If S is an abelian monoid and T its maximal cancellative homomorphic image, then for any $\mathbb{Z}S$ module D we form the $\mathbb{Z}T$ module $D' = \mathrm{Hom}_{\mathbb{Z}S}(\mathbb{Z}T, D)$. It is well known the existence of a natural homomorphism $H^n(T, D') \to H^n(S, D)$. If D is a trivial $\mathbb{Z}S$ module, then D' is just D regarded as a trivial $\mathbb{Z}T$ module. The above homomorphism turns out to be an isomorphism for D trivial and $n = 1, 2$ but it was unknown what happens for $n \geq 3$. If S is an abelian inverse monoid, then it is obvious that T is just G, the maximum group image of S. In this case we can utilize the isomorphism (1) to obtain an isomorphism $Ext^n_{\mathbb{Z}G}(\mathbb{Z}, D') \cong Ext^n_{\mathbb{Z}S}(\mathbb{Z}, \mathbf{J}^* D')$. The following is now immediate.

Corollary 2.3 *If S is an abelian inverse monoid and G its maximum group image, then for any trivial $\mathbb{Z}S$ module D there is a natural isomorphism $H^n(S, D) \cong H^n(G, D)$ for every $n \in N$.*

The proof of theorem 2.2 will use a characterization of the FP_∞ property for modules M in terms of the functors $\mathrm{Ext}(M, \bullet)$ and $\mathrm{Tor}(M, \bullet)$.

Theorem 2.2 *Let S be an inverse monoid and G its maximum group image. If S is of type FP_∞, then S contains a minimal idempotent and G is of type FP_∞. Conversely, if S contains a minimal idempotent and G is of type FP_∞, then S is of type FP_∞.*

Proof. In particular S is of type FP_1, therefore there is free partial resolution of finite type of the trivial $\mathbb{Z}S$ module $\mathbb{Z}$:

$$\oplus_{i \in I_1} \mathbb{Z}S \to \oplus_{i \in I_0} \mathbb{Z}S \to \mathbb{Z} \to 0. \qquad (5)$$

We can regard $\mathbb{Z}E$ as a right $\mathbb{Z}S$ module via the conjugation of S on E: $e \cdot s = s^{-1}es$ for all $s \in S$ and $e \in E$. If we tensor (5) on the left by $\mathbb{Z}E$ regarded as a left $\mathbb{Z}E$ module and a right $\mathbb{Z}S$ module, we obtain the following exact sequence in $\mathbb{Z}E - Mod$

$$\oplus_{i\in I_1}\mathbb{Z}E\otimes_{\mathbb{Z}S}\mathbb{Z}S\to\oplus_{i\in I_0}\mathbb{Z}E\otimes_{\mathbb{Z}S}\mathbb{Z}S\to\mathbb{Z}E\otimes_{\mathbb{Z}S}\mathbb{Z}\to 0 \qquad (6)$$

Next we show that $\mathbb{Z}E\otimes_{\mathbb{Z}S}\mathbb{Z}$ is the trivial $\mathbb{Z}E$ module $\mathbb{Z}$. Indeed, any generator $e\otimes_{\mathbb{Z}S}z$ can be reduced as follows: $e\otimes_{\mathbb{Z}S}z=1_S\otimes_{\mathbb{Z}S}e\cdot z=1_S\otimes_{\mathbb{Z}S}z$, hence $\mathbb{Z}E\otimes_{\mathbb{Z}S}\mathbb{Z}\cong\mathbb{Z}$ as abelian groups. On the other hand, the action of any idempotent f on the generator $1_S\otimes_{\mathbb{Z}S}z$ leaves fixed this generator.Similarly one can show that $\mathbb{Z}E\otimes_{\mathbb{Z}S}\mathbb{Z}E\cong\mathbb{Z}E$. Indeed, any generator $e\otimes_{\mathbb{Z}S}s$ of $\mathbb{Z}E\otimes_{\mathbb{Z}S}\mathbb{Z}S$ can be reduced as follows: $e\otimes_{\mathbb{Z}S}s=s^{-1}es\otimes_{\mathbb{Z}S}1_S$ which shows that the elements of $\mathbb{Z}E\otimes_{\mathbb{Z}S}\mathbb{Z}S$ are $\mathbb{Z}$-linear combinations of elements of the form $e\otimes_{\mathbb{Z}S}1_S$. From this it is easy to see why $\mathbb{Z}E\otimes_{\mathbb{Z}S}\mathbb{Z}S\cong\mathbb{Z}E$ as left $\mathbb{Z}E$ modules. Now using the exactness of (6) and above isomorphisms, we can obtain the following exact sequence

$$\oplus_{i\in I_1}\mathbb{Z}E\to\oplus_{i\in I_0}\mathbb{Z}E\to\mathbb{Z}\to 0,$$

proving that E is of type FP_1. The main result of (Y. Kobayashi 2007) shows that E is unitarily finitely generated and then in the same way as in the proof of theorem 9 of (Gray, Pride 2011) we can show that E contains a minimal idempotent.

To prove that G is of type FP_∞, as shown in (Brown, 1982) (see also (Brown, 1975)), we need to prove that $Ext^n_{\mathbb{Z}G}(\mathbb{Z},\bullet)$ commutes with direct limits. Let $\underrightarrow{lim}M_i$ be a direct limit of a diagram of modules M_i with $i\in I$. Then we have the following natural isomorphisms

$$\begin{aligned}
Ext^n_{\mathbb{Z}G}(\mathbb{Z},\underrightarrow{Lim}M_i) &\cong Ext^n_{\mathbb{Z}S}(\mathbb{Z},\mathbf{J}^*\underrightarrow{Lim}M_i) && \text{from (1)}\\
&\cong Ext^n_{\mathbb{Z}S}(\mathbb{Z},\underrightarrow{Lim}\mathbf{J}^*M_i) && \text{the functor } \mathbf{J}^* \text{ has a right adjoint}\\
&\cong \underrightarrow{Lim}Ext^n_{\mathbb{Z}S}(\mathbb{Z},\mathbf{J}^*M_i) && S \text{ is of type } FP_\infty\\
&\cong \underrightarrow{Lim}Ext^n_{\mathbb{Z}G}(\mathbb{Z},M_i) && \text{from the naturality of (1)}
\end{aligned}$$

which proves that G is of type FP_∞ as required.

Before we prove the converse under the given hypothesis, we will make an observation. We denote by $\mathbb{Z}$ the trivial right $\mathbb{Z}S$ module $\mathbb{Z}$ and by $\mathbb{Z}'$ the trivial right $\mathbb{Z}G$ module $\mathbb{Z}$. For every abelian group C, the left $\mathbb{Z}S$ modules $\mathbf{J}^*Hom_{\mathbb{Z}}(\mathbb{Z}',C)$ and $Hom_{\mathbb{Z}}(\mathbb{Z},C)$ coincide. Of course, as abelian groups

they are equal. To see that they are equal as modules, we recall that the action of S on the elements f of $\mathbf{J}^* Hom_{\mathbb{Z}}(\mathbb{Z}', C)$ is defined by posing $s \cdot f(x) = \kappa(s) \cdot f(x) = f(x \cdot \kappa(s))$ for every $s \in S$ and $x \in \mathbb{Z}'$. But from the definition of $\mathbb{Z}'$, $f(x \cdot \kappa(s)) = f(x)$, and as a result $s \cdot f = f$ which means that $\mathbf{J}^* Hom_{\mathbb{Z}}(\mathbb{Z}', C)$ is trivial as a left $\mathbb{Z}S$ module. Similarly, we can prove that the abelian group $Hom_{\mathbb{Z}}(\mathbb{Z}, C)$ is trivial as a left $\mathbb{Z}S$ module, therefore we have the equality. For any left $\mathbb{Z}S$ module A and every abelian group C we have the following natural isomorphisms.

$$
\begin{array}{lcll}
Hom_{\mathbb{Z}}(\mathbb{Z}' \otimes_{\mathbb{Z}G} \tilde{\mathbf{J}}A, C) & \cong & Hom_{\mathbb{Z}\mathbb{G}}(\tilde{\mathbf{J}}A, Hom_{\mathbb{Z}}(\mathbb{Z}', C)) & \text{from the adjoint associativity} \\
 & \cong & Hom_{\mathbb{Z}S}(A, \mathbf{J}^* Hom_{\mathbb{Z}}(\mathbb{Z}', C)) & \text{from theorem 2.1} \\
 & = & Hom_{\mathbb{Z}S}(A, Hom_{\mathbb{Z}}(\mathbb{Z}, C)) & \text{from our observation} \\
 & \cong & Hom_{\mathbb{Z}}(\mathbb{Z} \otimes_{\mathbb{Z}S} A, C) & \text{from the adjoint associativity.}
\end{array}
$$

It follows that we have the natural isomorphism in $\mathbf{Ab}$

$$Nat(Hom_{\mathbb{Z}}(\mathbb{Z}' \otimes_{\mathbb{Z}G} \tilde{\mathbf{J}}A, \bullet), \mathbb{Z} \otimes_{\mathbb{Z}} \bullet) \cong Nat(Hom_{\mathbb{Z}}(\mathbb{Z} \otimes_{\mathbb{Z}S} A, \bullet), \mathbb{Z} \otimes_{\mathbb{Z}} \bullet)$$

Yoneda lemma now implies the existence of a natural isomorphism

$$\mathbb{Z}' \otimes_{\mathbb{Z}G} \tilde{\mathbf{J}}A \cong \mathbb{Z} \otimes_{\mathbb{Z}S} A$$

Since $\tilde{\mathbf{J}}$ preserves projective resolutions (theorem 12.1, p. 162 of (Hilton and Stammbach, 1997), the naturality of the above isomorphism implies that for every $n \geq 0$ there are natural isomorphisms

$$Tor_n^{\mathbb{Z}G}(\mathbb{Z}', \tilde{\mathbf{J}}A) \cong Tor_n^{\mathbb{Z}S}(\mathbb{Z}, A). \qquad (7)$$

Similarly one can prove that for any $K \in \mathbf{Ab}^G$ there is a natural isomorphism

$$Tor_n^{\mathbb{Z}G}(\mathbb{Z}', \mathcal{I}_G K) \cong Tor_n^G(\mathcal{I}_G^{-1}\mathbb{Z}', K) \qquad (8)$$

To prove that the trivial $\mathbb{Z}S$ module $\mathbb{Z}$ is of type FP_∞ we must show that $Tor_n^{\mathbb{Z}S}(\mathbb{Z}, \bullet)$ commutes with direct products. Let A_i for $i \in I$ be a family of left $\mathbb{Z}S$ modules. The following natural isomorphisms hold true.

$$
\begin{aligned}
Tor_n^{\mathbb{Z}}(\mathbb{Z}, \prod_{i\in I} A_i) &\cong Tor_n^{\mathbb{Z}G}(\mathbb{Z}', \tilde{\mathbf{J}} \prod_{i\in I} A_i) && \text{from (7)}\\
&\cong Tor_n^{\mathbb{Z}G}(\mathbb{Z}', \mathcal{I}_G \tilde{J} \mathcal{I}_S^{-1}(\prod_{i\in I} A_i)) && \text{from the definition of } \tilde{\mathbf{J}}\\
&\cong Tor_n^{\mathbb{Z}G}(\mathbb{Z}', \mathcal{I}_G \tilde{J}(\prod_{i\in I} \mathcal{I}_S^{-1} A_i))\\
&\cong Tor_n^{\mathbb{Z}G}(\mathbb{Z}', \mathcal{I}_G \underrightarrow{Lim}((\prod_{i\in I} \mathcal{I}_S^{-1} A_i)P) && \text{from theorem 2.1}\\
&\cong Tor_n^{\mathbb{Z}G}(\mathbb{Z}', \mathcal{I}_G \underrightarrow{Lim}((\prod_{i\in I} \mathcal{I}_S^{-1} A_i)P) && (\prod_{i\in I} \mathcal{I}_S^{-1} A_i)P \cong \prod_{i\in I}(\mathcal{I}_S^{-1} A_i P)\\
&\cong Tor_n^{G}(\mathcal{I}_G^{-1}\mathbb{Z}', \underrightarrow{Lim}((\prod_{i\in I} \mathcal{I}_S^{-1} A_i)P) && \text{from (8)}\\
&\cong Tor_n^{G}(\mathcal{I}_G^{-1}\mathbb{Z}', \prod_{i\in I} \underrightarrow{Lim} \mathcal{I}_S^{-1} A_i P)\\
&\cong Tor_n^{\mathbb{Z}G}(\mathbb{Z}', \mathcal{I}_G \prod_{i\in I} \underrightarrow{Lim} \mathcal{I}_S^{-1} A_i P)\\
&\cong Tor_n^{\mathbb{Z}G}(\mathbb{Z}', \prod_{i\in I} \mathcal{I}_G \underrightarrow{Lim} \mathcal{I}_S^{-1} A_i P) && \mathcal{I}_G \text{ is a right adjoint}\\
&\cong \prod_{i\in I} Tor_n^{\mathbb{Z}G}(\mathbb{Z}', \mathcal{I}_G \underrightarrow{Lim} \mathcal{I}_S^{-1} A_i P) && G \text{ is of type } FP_\infty\\
&\cong \prod_{i\in I} Tor_n^{G}(\mathcal{I}_G^{-1}\mathbb{Z}', \underrightarrow{Lim} \mathcal{I}_S^{-1} A_i P)\\
&\cong \prod_{i\in I} Tor_n^{G}(\mathcal{I}_G^{-1}\mathbb{Z}', \tilde{J} \mathcal{I}_S^{-1} A_i)\\
&\cong \prod_{i\in I} Tor_n^{\mathbb{Z}G}(\mathbb{Z}', \mathcal{I}_G \tilde{J} \mathcal{I}_S^{-1} A_i)\\
&\cong \prod_{i\in I} Tor_n^{\mathbb{Z}G}(\mathbb{Z}', \tilde{\mathbf{J}} A_i) && \text{from the definition of } \tilde{\mathbf{J}}\\
&\cong \prod_{i\in I} Tor_n^{\mathbb{Z}S}(\mathbb{Z}', A_i) && \text{from (7)}
\end{aligned}
$$

Now comparing the left with the right hand side in the above sequence of isomorphisms, we get the result. ■

We use the above result to show that property FP_∞ behaves nicely with respect to inverse subsemigroups of finite index in the following sense.

Definition 2.1 Let H be a full inverse subsemigroup of an inverse monoid S. We say that H is of finite index in S if the maximum group image of H has finite index in the maximum group image of S.

This definition makes sense since the maximum group image of H can be regarded as a subgroup of the maximum group image of S as one can easily check.

Proposition 2.2 *Let S be an inverse monoid and H be an inverse*

subsemigroup of S *of finite index. Then,* S *is of type* FP_∞ *if and only if* H *is of the same type.*

Proof. If S if of type FP_∞ then it contains a minimal idempotent e and its maximum group image S is of the same type. Since H is a full inverse subsemigroup of S, it will contain e. On the other hand, as we mentioned before, $H \leq S$ where H is the maximum group image of H, and from the condition $[H:S] < \infty$. Proposition 5.1 of (Brown, 1982) now implies that H is of type FP_∞ and therefore H is of that type. Conversely, if H is of type FP_∞, then H and therefore S contains a minimal idempotent.

On the other hand, H is of type FP_∞, hence S is of the same type as $[H:S] < \infty$. The result of theorem 2.2 finishes the proof. %

REFERENCES

Brown K. 1975. Homological criteria for finiteness. *Comment Math. Helvetici* **50**, 129-135.

Brown K. 1982. *Cohomology of groups.* Graduate Texts in Mathematics, 87. *Springer-Verlag, New York-Berlin,* Springer-Verlag.

Gray R, Pride SJ. 2011. Homological finiteness properties of monoids, their ideals and maximal subgroups. *Journal of Pure and Applied Algebra*, **215 (12)**: 3005-3024.

Guba VS, Pride SJ. 1998. On the left and right cohomological dimension of monoids. *Bulletin of the London Mathematical Society.***30 (3):** 391-396.

Hilton PJ, Stammbach U. 1997. *A Course in Homological Algebra.* Second Edition, Springer-Verlag.

Howie JM. 1995. *Fundamentals of Semigroup Theory*, Clarendon Press Oxford.

Kobayashi Y.2007. The homological finiteness property and finite generation of monoids. *International Journal of Algebra and Computation,* **17(3)**:593-605.

Laudal OA. 1972. Note on the projective limit of small categories, *Proceedings of the American Mathematical Society*, **33,** 307-309.

Lawson MV. 1998, *Inverse Semigroups. The Theory of Partial Symmetries,* World Scientific

Loganathan M. 1981. Cohomology of Inverse Semigroups, *Journal of Algebra*.**70,** 375-393.

Mac Lane S. 1963, *Homology*, Academic Press, New York.

Mac Lane S. 1997.*Categories for the Working Mathematician*, Springer Verlag.

Nico WR. 1972, *A counterexample in the cohomology of monoids*, Semigroup Forum, 493-94.

Pasku E. 2011, *Clifford semigroups as functors and their cohomology*, Semigroup Forum, **83 (1)**, 75-88.

Schubert H. 1972. *Categories,* Springer Verlag.

Weibel Ch. 1994. A., An introduction to homological algebra, Cambridge studies in advanced mathematics 38, Cambridge University Press.

THE EFFECT OF COOLING FLOW (CF) ON THE TEMPERATURE PROFILE OF THE HOT ELECTRONIC GAS AND THE CALCULATION OF THE COMPTON PARAMETER *Y*0

Enkelejd ÇAÇA
Department of Physics, Faculty of Mathematics Engineering and Physics Engineering, Polytechnic University of Tirana, Albania

ABSTRACT

Building more accurate profiles for temperature and density of hot electronic gas which is concentrated at the centre of clusters of galaxies is a constant problem for the survey of the Sunyeav Zel'dovich effect (SZ). The latter consists of the inverse Compton effect of the hot electronic gas interacting with cosmic microwave background (CMB) photons passing through intra cluster medium (ICM). So far, the isothermal model is used for temperature profiling in the calculation of the inverse Compton effect. Recent improved observations from satellites showed that the hot electronic gas presents a feature that is called the cooling flow (CF). Temperature in this model is different towards the edges of the clusters of galaxies, leading to a change on the Compton parameter in comparison with Isothermal model. In the present paper the data provided by Chandra, the X-ray satellite, are investigated based on two models for the electron density and temperature profile. A sample of 8 clusters of galaxies was analyzed. The results reported that the differences on the Compton parameter are 10-100% in comparison with Isothermal model when building the temperature profiles using CF model. Consequently, the change of the electronic gas temperature which affect both, CMB spectrum and temperature, from SZ effect is very important for an accurate evaluation of the Compton parameter.
***Keywords*:** cluster of galaxies, X-ray, comptonization, cooling flow, S-Z effect

1. INTRODUCTION AND PRELIMINARIES

The Synyaev-Zel'dovich (SZ) effect was first introduced in 1970s (Sunyaev and Zeldovich, 1969; 1972) as a consequence of Compton interaction between cosmic microwave background (CMB) photons and highly energetic electrons present in the hot plasma of intergalactic space within cluster of galaxies (intra-cluster medium, ICM). Since then, efforts have been made to detect and image the Synyaev-Zel'dovich (SZ) effect from cluster of galaxies. The effect

resulting in a CMB anisotropy characterized by a spectral signature and spatial correlation with cluster position in the sky is almost independent from the cluster redshift. This effect soon became a means to address cluster physics and cosmology due to its simplest physical interpretation and marginal detection possibilities even with outdated observation techniques and detector technology. After few observation performed in the early stages of SZ search programs (Birkinshaw 1991; 1999), the last 15 years have finally marked the first systematic SZ measurements, operating at wavelengths from a few cm to the mm/submm region. The larger contribution to the effect is expected to fully exploit its spectral signature and thus justifies the application of multi-band techniques for good systematic control and foreground removal. While imaging of the SZ effect has already been performed at radio frequencies (Carlstrom *et al*., 1996; Grego *et al*., 1996) using interferometric detectors, higher frequency measurements have been mostly performed via single-pixel detectors. The latter was characterized by multi-band selection and higher spectral discrimination of the signal from unwanted contributions. The current progress made in the area of bolometer technology ensures the right emphasis on near-future microwave instruments pretending to extract the largest astrophysical and cosmological information from SZ observation; must be able to combine multi-frequency techniques with moderate-to-high imaging capabilities. In order to significantly reduce the bulk of systematic and statistical uncertainty coming from the modelling of ICM density and temperature distributions and, for ground-based experiment, take full advantage of long integration and on-site operator control to optimally customize the observation strategy. Moreover, giving the growing sky coverage capabilities of the new experiments, it will soon be possible to perform routine observations and produce untargeted surveys of potentially more than 100 clusters, to determine statistically robust cosmological parameter estimates and deeply probe the universe at high red-shift. These surveys will provide a direct view of growth large scale structures and help building catalogues of cluster that will possibly extend past z ’ 2 with significantly low observational biasing.

1. TEMPERATURE PROFILES.

In the case of the CF clusters in order to model the gas temperature we use a non-isothermal model for the temperature (Piffaretti *et al*., 2005; Piffaretti and Kaastra, 2006; Gitti *et al*., 2007). The temperature declines from the maximum cluster temperature at a break radius r_{br} moving outwards and shows a typical temperature decline towards the X-ray emission peak. As the central cooling region is of great interest and the cooling radius for a cooling time of 15 *Gyr*, *Rcool* is smaller than r_{br} for all the CF clusters, the temperature profiles

can be simply modelled by a function that is monotonically raising with radius. Hence, for each cluster we select temperature bins inside the radius *RT, max* = r_{br} and fit them using the following expressions:

$$T_T = T_0 + T_1 \frac{\left(\frac{r}{r_T}\right)^{«}}{1+\left(\frac{r}{r_T}\right)^{«}} \qquad (1)$$

$$\widetilde{T}_r = \widetilde{T}_0 - \widetilde{T}_1 \exp\left(-\frac{r^2}{2\tilde{r}_T^2}\right) \qquad (2)$$

In order to reduce the number of parameters here, we set T(r = 0) equal to the temperature of the central bin for both fits and use μ=2 in Eq.1 (Allen et al., 2001). Both temperature parameterizations (Eq. 1 and Eq. 2) are used in the computation temperature profile and modelling of the gas pressure that depends from the temperature and the density of the electronic gas present at the centre of the cluster. The main results were achieved using the parameterization in Eq. 1. The second parameterization given in Eq. 2 only is used to explore the effect of a different modelling on the main results. The changes occurred by using the Eq. 2 are almost insignificant and do not change the results obtained using Eq. 1. The main problem on the definition of the temperature of the gas is the correctly definition from the X-ray observation. These observations suffer from a great uncertainty. Uncertainties depart from the way as one weighs the temperatures of the bins. Much important research has been carried out in the area with subsequent publication of many noted papers (see Mazzotta *et al*., (2004)). The present paper does not aim at reviewing these papers though those fall within the aim of the present paper. The second uncertainty relates to the differences in the observations of the various detectors on same target.

Another parameter to be defined is the electronic density of the gas and its profile. Gas density is modeled by using a single *β*-model given by:

$$n_r = n_0 \left(1+\left(\frac{r}{r_C}\right)^2\right)^{-\frac{э}{2}} \qquad (3)$$

The density profile is fitted within *Rn,max*, which is the radius at the centre of the last radial bin, where a robust estimate of gas density and temperature is possible (see Piffaretti *et al.*, (2005)). An alternative parameterization of the

gas density profile is the more complex double β-model (Mohr *et al*., 1999), which is a popular generalization of the single β-model (Cavaliere and Fusco-Femiano, 1976; 1978), used to model the central surface brightness excess observed in CF clusters.

The clusters sample is in the Table 1 reported:

Table 1. Cluster sample.

Cluster	Right ascension *J2000.0*	Declination *J2000.0*	z	
ABELL 773	09h17m59s	51.7064	0.217000 (1)	CF
MS 1358.4+6245	13h59m54.3s	62.5101	0.328000 (2)	CF
ZW 3146	10h23m39.63s	4.18621	0.290600 (3)	CF
ABELL 1795	13h49m00s	26.5852	0.062476	CF
ABELL 2204	16h32m45s	5.5785	0.152158 (1)	CF
ABELL 2390	21h53m34s	17.6697	0.228000 (1)	CF

(1) Right ascension, Declination and z reference (Struble and Rood, 1999)

(2) Right ascension, Declination and z reference (Luppino and Gioia, 1995; Gioia and Luppino, 1994)

(3) Right ascension, Declination and z reference (Allen *et al.*, 1992)

$$n_r = n_1\left(1+\left(\frac{r}{r_{C1}}\right)^2\right)^{-\frac{э_1}{2}} + n_2\left(1+\left(\frac{r}{r_{C2}}\right)^2\right)^{-\frac{э_2}{2}} \qquad (4)$$

Unfortunately in this case, the gas density is modelled using the sum of two single-models, so the number of free parameters is doubled: $n0,i$, βi, and r_c,i, with $i = 1, 2$. Consequently, while fitting the single β-model to the density profiles gives statistically significant values for the best-fit parameters, the large number of parameters adopted in the double β-model, together with the small number of bins in which the gas density is measured, do not allow a significant determination of the best-fit parameters. Table 2 reports the results obtained using the single β-model. Nonetheless, in order to constrain to which extent the double β-modelling changes the results, the density profiles was fit using a double β-model with a reduced number of fitting parameters (only for 3 clusters: Abell 1795, Abell 2204 and Abell 2390), which the density data were found. Once obtained, the profiles were used to model the gas pressure as done by using the single β-model results (Fig. 2). Specially for the cluster A2004 and A2390 we use a double β-model having better results in comparison with single β-model (see Fig. 2), the $\chi 2$ for the double β-model is small than single β-model

(see Tab. 4). Abell 1795 showed no difference between the first two clusters, the single β-model and the double β-model. In addition, using the second model is unecessary. For all other clusters the single β-model has been assumed (r_c along with the density data for the β-model Tab. 3 (Bonamente *et al*., 2006).

All parameters of this fit are showed in the table booth with the central density *n*0 and *rc* of the gas (Tab. 3). Once the parameters of temperature and the central electronic density are known, the pressure of the electronic gas and the parameter of comptonization *y*0 of the CMB photons could be defined from the hot electrons present at the centre of the cluster.

Table 2. *Rc* is the cooling radius obtained from the best fit parameters fitting temperature profile with Eqs. 1 and 2. Here, μ = 2 in Eq. 1 is used. *T*0 is set equal to the temperature of the central bin For both fitting functions.

Cluster	$R_{T,max}$ (kpc)	R_c (kpc)	T_0 (keV)	T_1 (keV)	β	
ABELL 773	1500	291.4	6	6.79	0.564	CF
MS 1358.4	454	57	4.02	5.8	0.675	CF
ZW 3146	450	49	3.6	5.02	0.668	CF
ABELL 1795	800	45	5.73	3.5	0.52	CF
ABELL 2204	200	72.86	3.1	6.6	0.710	CF
ABELL 2390	870	50.2	4.9	4.45	0.47 (3)	CF

(1) Density and temperature reference (CHANDRA) (LaRoque *et al*., 2006).
(2) Density and temperature reference (CHANDRA) (Tamura *et al*., 2004)
(3) This paper.
β-reference (Bonamente *et al*., 2006)

Table 3. *Rc* for the density profile that are used to fit the data. Also β, β1 and β2 for the double-β model including r_{c1} and r_{c2} (CHANDRA).

Cluster	r_c (kpc)	β	n_0 $x10^{-3}$	β_1	β2	r_{c1} (kpc)	r_{c2} (kpc)
ABELL 773	136	0.564	$9.8x10^{-3}$(1)				
MS 1358.4	137	0.675	$9.6x10^{-2}$(1)				
ZW 3146	110	0.668	$1.7x10^{-1}$(1)				
ABELL 1795	38(3)	0.52	0.05(1)				
ABELL 2204	160	0.710	$2.1x10^{-1}$(1)	0.55(3)	1.43(3)	17.1(3)	7.1(3)
ABELL 2390	35(kpc)	0.47 (3)	0.8(2)	0.35(2)	2.38(3)	23(3)	7.5(3)

(1) r_c, Density and β reference (LaRoque et al., 2006).
(2) Density reference (CHANDRA) (Tamura et al., 2004)
(3) This paper

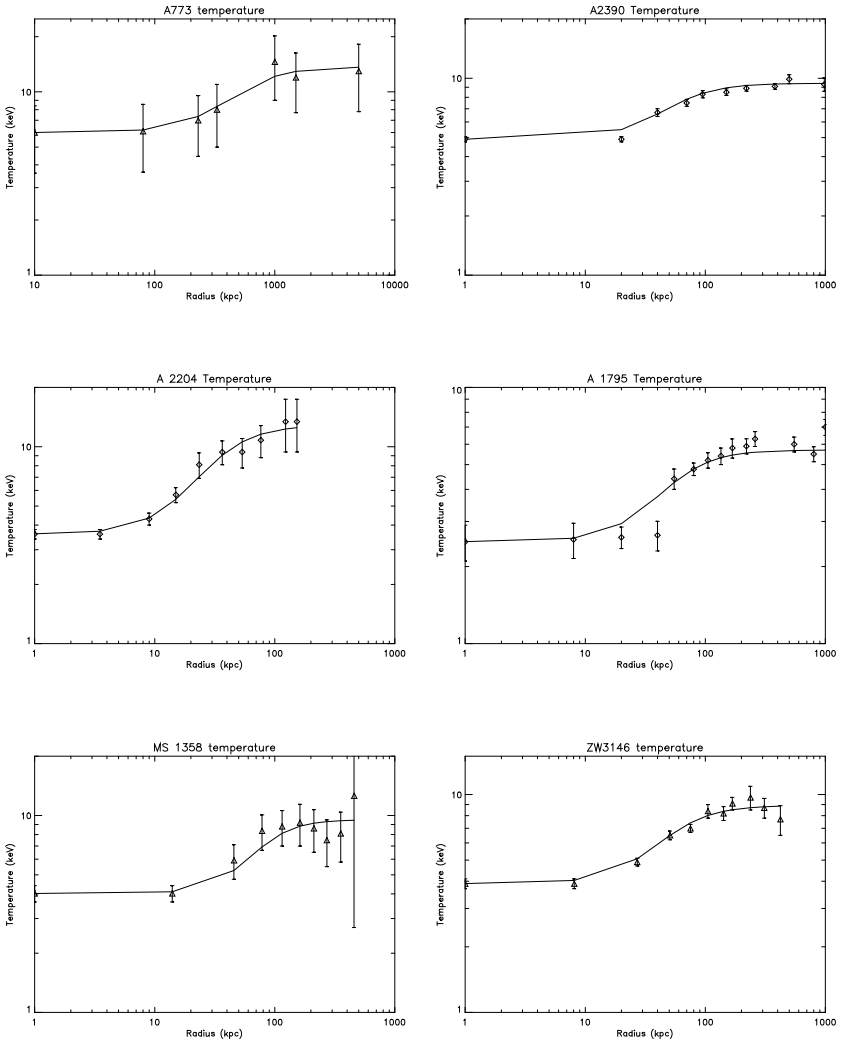

Fig. 1. The best fit-profiles of temperature for the clusters: MS 1358, ZW3146 and RXJ1120 (cooling flow).

Table 4. χ^2 for the two models.

Cluster	χ^2 β-model	χ^2 double β-model
ABELL 2204	0.29	0.023
ABELL 2390	0.24	0.01

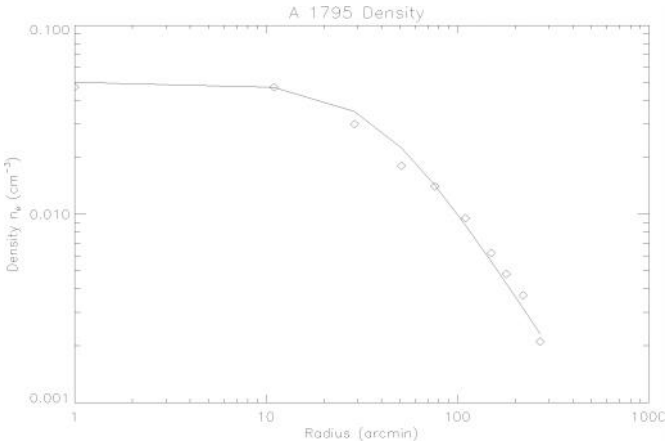

Fig. 2. β-model is applied to fit the density profile for the cluster: A1795.

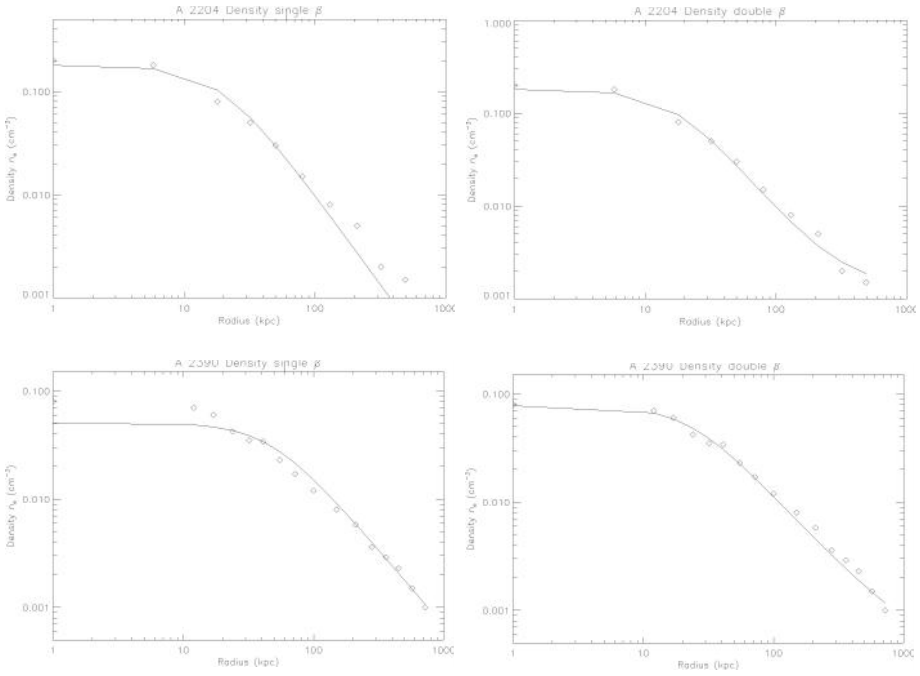

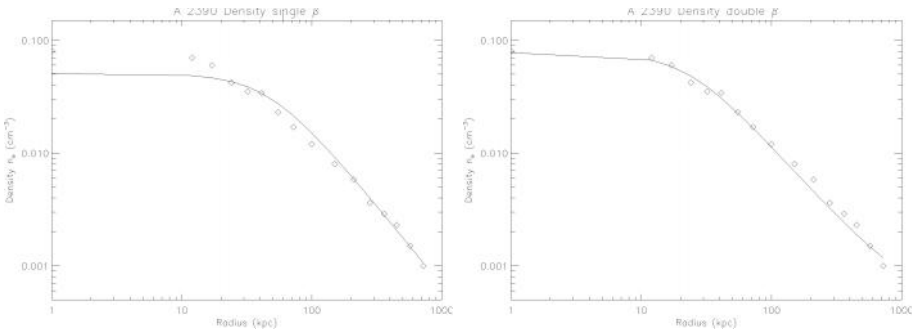

Fig. 3. Abell 2204 and Abell 2390 density profile (comparison between β and double β model).

2. COMPTONIZATION PARAMETER *Y*

The aforementioned profiles could be used to calculate the Comptonization parameter. The original treatment from the (Sunyaev and Zeldovich, 1972) is based on a solution to the (Kompaneets, 1957) equation, which is a non-relativistic (Fokker-Planck) diffusion, approximation to the exact integrals in equation 5, written for the average occupation number of the radiation energy levels:

$$\frac{\partial \bar{n}}{\partial n} = \frac{kT}{m_e C} \frac{\pm_T n_e}{x^2} \frac{\partial}{\partial x} \left[x^4 \left(\frac{T_e}{T} \frac{\partial \bar{n}}{\partial x} + \bar{n} + \bar{n}^2 \right) \right] \qquad (5)$$

n_e and T_e are the electron gas temperature and number density profiles (under the assumption that the electron population is thermally relaxed), T is the radiation temperatures (in the case of blackbody spectrum) and x is the non-dimesional frequency, $h\nu/kT$. Since for the case of ICM electrons and CMB photons $Te \gg T = T_{CMB}$, the first term in parentheses dominates over the others, allowing to reduce equation 5 to:

$$\frac{\partial \bar{n}}{\partial n} = \frac{kT_{CMB}}{m_e C} \frac{\pm_T n_e}{x^2} \frac{\partial}{\partial x} \left[x^4 \left(\frac{T_e}{T_{CMB}} \frac{\partial \bar{n}}{\partial x} \right) \right] \qquad (6)$$

A solution to this equation could be found under the hypothesis that the radiation field undergoes weak diffusion from the gas (*i.e.* multiple scattering events of a single photon are strongly unlikely), so that the right part of the equation 6 can be rewritten with the expression of a planckian occupation number for n

$$\overline{n_p}(x) = \frac{1}{e^x - 1} \tag{7}$$

Finally, integrating over the line of sight (l.o.s) through the cluster yields the non-relativistic (*i.e* low electron temperature) expression for the spectrum of the thermal SZ effect:

$$\Delta I_t = i_0 y g(x) \tag{8}$$

where $i_0 = 2(kT_{CMB})^3/(hc)^2$, and y is the comptonization parameter defined as:

$$y = \int_{l.o.s} n_e(l) \frac{kT_e}{m_e C^2} \pm_T dl = \frac{kT_e}{m_e C^2} \tau \tag{9}$$

i.e. an integral of electron density and temperature profiles across the cluster; σT is the Thomson cross section, and τ is the cluster optical depth with respect to the Thomson scattering process. The dependence from the non dimensional frequency is entirely described by:

$$g(x) = \frac{x^4 e^x}{(e^x - 1)} \left[x \frac{e^x + 1}{e^x - 1} - 1 \right] \tag{10}$$

Eq. 10 shows that the distortion is negative at low frequencies below the critical *crossover* value x_0 3.83 (corresponding to $\sim 217 GHz$) and positive in the high frequency region. Typical values of the y parameter are $\sim 10^{-4}$ in rich and/or moderately hot clusters; from the corresponding expression for the CMB temperature fluctuation induced from the effect,

$$\frac{\Delta T_{CMB}}{T_{CMB}} = \left[x \frac{e^x + 1}{e^x - 1} - 4 \right] y \tag{11}$$

and being the spectral function of order unity, one gets for the induced CMB anisotropy a value of $\Delta TCMB/TCMB \approx 10^{-4}$, indicating that the thermal SZ effect (especially when compared to the primary CMB anisotropy power spectrum at high *ls*) is the dominating anisotropy observable in the direction of an even moderately rich and warm galaxy cluster. In the above calculation of the comptonization parameter, the angular separation from the cluster centre

has been inserted by means of well known transformation $r \approx \theta D_A$ which makes use of the angular diameter distance D_A.

Table 5. In this table we show the comptonization parameter for the cluster in question. For the cluster with cooling flow (CF) has been obtained applying the temperature profile see Eqs. 1 and 2. For a complete view of the effect I apply Eqs. 1 and 2 for all clusters.

Cluster	y_0 (CF)	y_0 (Isothermal)	y_0 (T_e*profile*)	
ABELL 773	$4.5x10^{-4}$	$7.06x10^{-4}$	–	CF
MS 1358.4	$7.88x10^{-4}$	$12.8x10^{-4}$	–	CF
ZW 3146	$6.2x10^{-4}$	$9.1x10^{-4}$	–	CF
ABELL 1795	8.02^{-6}	$1.5x10^{-5}$	–	CF
ABELL 2204	$5.3x10^{-4}$	$8.11x10^{-4}$	–	CF
ABELL 2390	$3.99x10^{-4}$	$6.18x10^{-4}$	–	CF

Table 6. The same table, but this time comptonization parameters obtained from SZ observations, has been included.

Cluster	y_0 (CF)	y_0 (Isothermal)	y_0 (T_e*profile*)	Y_0 (SZ observation)
ABELL 773	$4.5x10^{-4}$	$7.06x10^{-4}$	–	$4.23x10^{-4}$
MS 1358.4	$7.88x10^{-4}$	$12.8x10^{-4}$	–	
ZW 3146	$6.2x10^{-4}$	$9.1x10^{-4}$	–	$3.62x10^{-4}$
ABELL 1795	$8.02x10^{-6}$	$1.5x10^{-5}$	–	–
ABELL 2390	$5.3x10^{-4}$	$8.11x10^{-4}$	–	$2.53x10^{-4}$
ABELL 2390	$3.99x10^{-4}$	$6.18x10^{-4}$	–	$3.56x10^{-4}$

SuZIE II data Benson et al., (2004)

All the clusters have been set at the same Angular Distance (20 arcmin), comparable with the total field of bolometer array (17arcmin), to a resolution of 4.5'/pixel. We use in this simulation the temperature profile from the Eq. 1 and Eq. 2, for the entire cluster that shows a CF centre. The Tab. 6 is equal with Tab. 5, but now the comptonization parameter *Y*0 obtained from the SZ observation has been included to.

4. RESULTS

In order to calculate the S-Z effect on the CMB, the change on the intensity and the temperature of the CMB passing through the ICM, we use a different

model, the cooling flow model (Piffaretti *et al*., 2005; Gitti *et al*., 2007), for the electronic gas temperature instead of isothermal model. We use the beta model for the gas density (Cavaliere and Fusco-Femiano, 1976; 1978) to calculate S-Z effect, except for two clusters where it's used the double-beta model (Mohr *et al*., 1999). Temperature profile is modelled by the equations 1 and 2. Equation 3 and 4 were used for the density profile.

Fig 2 depicts the best fit to the data available (X-Ray data Bonamente *et al*., 2006; LaRoque *et al*., 2006; Peterson *et al*., 2001) for the temperature profile of the clusters sample. The Fig. 2 depicts the best fit for the density using the double-β model (2 clusters), for all the other clusters the single-β model has been used (one example of 2 clusters is shown in Fig 2).

In order to obtain the best fitting temperature profile, the parameter $\mu = 2$ was fixed and the temperature $T0$ was set equal to the temperature of the central bin. For two clusters; Abell1835 and Abell2390, the slope parameter β was provided; all other parameters are shown in the Tab. 2. The density parameters are reported in the Tab. 3, for the best fit parameters we provide rc in the case of two clusters; Abell1835 and Abell2390. For the double-β model both parameters; $\beta 1$, $\beta 2$ and $rc1$, $rc2$ for the clusters Abell2204 and Abell2390 were calculated. The difference between these models is in the Fig. 2 depicted. Table 4 reports the difference in the terms of $\chi 2$, smaller in the case of the double-β, ten times than the single-β model. As data for the other clusters lack, the single-β model was used involving the central density $n0$, Tab. 3.

4.1. Comptonization parameter Y results.

The Comptonization parameter was obtained applying the equation:

$$y = \int_{l.o.s} n_e(l) \frac{kT_e}{m_e c^2} \pm_T dl = \frac{kT_e}{m_e c^2}^2 \qquad (12)$$

where the temperature *Te* and the density *ne* are already defined. Results are in the Tab 5 and Tab 6 reported. Table 5 reports the comptonisation parameter $y0$ for 6 CF clusters. The second column shows the comptonisation parameter $y0$ that isothermal model yield for these clusters.

The two models of the cluster MS 1358.4 have different the values; isothermal model $y0$ is 60% higher than CF temperature profile model. For the other 5 clusters the isothermal model overestimate the comptonisation parameter $20 \div 100\%$.Table 6 reports the same results including the $Y0$ obtained from the S-Z observations (see Benson *et al*., 2004; Zemcov et al., 2007), unfortunately only for 4 clusters.

For the cluster Abell773, the CF profile fits very good with S-Z data. On the other hand, the isothermal model overestimates $y0$ more than 50%. In the case of ZW3146 both models do not agree with S-Z observations, but they overestimate $y0$. CF profile model is closer to the observed value, while the isothermal model value, is 2.5 time greater than observed value. Regarding the Abell2204, the comptonisation value is higher than S-Z value, 2 and 3.5 times, respectively. For the last cluster Abell2390, CF model value fits the S-Z data, while the isothermal model overestimates $y0$ by about two times.

5. CONCLUSIONS

The paper investigates the possibility of a new error when calculating the Compton inverse effect (known as S- Z effect) on the CMB radiation induced by the use of the Isothermal model, profiling the temperature of the hot electronic plasma, residing inside the gravitational wail of the clusters of galaxies. A different approach for the temperature profile, the Cooling Flow profile was used involving the Eq.1 and Eq.2. The temperature profile of 8 clusters was built involving X-ray data observation. In order to have a good view, the Comptonisation parameter from both models were calculated and compared the results with S-Z data provided from the observations. In addition, the change in ΔI and ΔT was simulated.

The CF temperature profiles is different from those obtained using the isothermal model. In most cases the isothermal model overestimated the Comptonisation parameter. Consequently, new error occurred into calculating cosmological parameters derived from combined observations; S-Z and X-ray. The difference between temperature profile models covers a wide range from 30% to 100% Abell1795. As these profiles with S-Z data $y0$ fit, the difference with the isothermal temperature profile model becomes even greater—for Abell2204 about 3.5 times.

For the clusters that showed this feature (CF), the new model reflects better the real condition of the hot electronic plasma that resides in the centre of the clusters of galaxies. Given that, however we can see from the comparison of $y0$ and the simulations on the intensity and temperature change, we have a discrepancy between simulated data from X-ray observations with those obtained from the direct S-Z observations.

REFERENCES

Allen SW, Edge AC, Fabian AC, Bohringer H, Crawford CS, Ebeling H, Johnstone RM, Naylor T, Schwarz RA. 1992. Optical spectroscopy of the ROSAT X-ray brightest clusters. *Monthly Notices of the Royal Astronomical Society*. **259**:67–81.

Allen S. W, Schmidt R. W, and Fabian A. C. 2001. The X-ray virial relations for relaxed lensing clusters observed with Chandra. *Monthly Notices of the Royal Astronomical Society*. **328**:L37–L41, doi: 10.1046/j.1365-8711.2001.05079.x.

Benson BA, Church SE, Ade PAR, Bok JJ, Ganga KM, Henson CN, Thompson KL.2004. Measurements of Sunyaev-Zel'dovich effect scaling relations for clusters of galaxies. *The Astrophysical Journal*. **617**:829–846, doi: 10.1086/425677.

Birkinshaw M. 1991. Measurement of the Sunyaev-Zel'dovich effect. In A. Blanchard, L. Celnikier, M. Lachieze- Rey, and J. Tran Thanh Van, editors, *Physical Cosmology*, 177.

Birkinshaw M. 1999. The Sunyaev-Zel'dovich effect. *Physics Reports*. **310**:97–195. doi: 10.1016/S0370- 1573(98)00080-5.

Bonamente M, Joy MK, LaRoque SJ, Carlstrom JE, Reese ED, Dawson KS. 2006. Determination of the cosmic distance scale from Sunyaev-Zel'dovich effect and Chandra X-Ray measurements of high- redshift galaxy clusters. *The Astrophysical Journal*, **647 (1)**:25–54, doi: 10.1086/505291.

Carlstrom JE, Joy M, Grego L. 1996. Interferometric imaging of the Sunyaev-Zeldovich effect at 30 GHz. *The Astrophysical Journal Letters*, **456**:L75. doi: 10.1086/309866.

Cavaliere A, Fusco-Femiano R. 1976. X-rays from hot plasma in clusters of galaxies. *Astronomy & Astrophysics.* 49:137–144.

Cavaliere A, Fusco-Femiano R. 1978. The distribution of hot gas in clusters of galaxies. *Astronomy & Astrophysics*. **70**:677- 684.

Gitti M, Piffaretti R, Schindler S. 2007. Mass distribution in the most X-ray-luminous galaxy cluster RX J1347.5-1145 studied with XMM-Newton. *Astronomy & Astrophysics*, **475**:441–441, doi: 10.1051/0004- 6361:20077580e.

Gioia IM, Luppino GA. 1994. The EMSS catalog of X-ray-selected clusters of galaxies. 1: an atlas of CCD images of 41 distant clusters. *The Astrophysical Journal Letters*, **94**:583–614, doi: 10.1086/192083.

Kompaneets AS. 1957. The establishment between quanta and electrons. *Soviet Physics. Journal of Experimental and Theoretical Physics*. **4**:730-737.

Grego L, Carlstrom J, Joy M, and Holzapfel W. 1996. The Sunyaev–

Zel'dovich effect imaged in galaxy clusters. In *American Astronomical Society Meeting Abstracts, Bulletin of the American Astronomical Society*, **28**, 115.05

LaRoque SJ, Bonamente M, Carlstrom JE, Joy MK, Nagai D, Reese ED, Dawson KS. 2006. X-Ray and Sunyaev-Zel'dovich effect measurements of the gas mass fraction in galaxy clusters. *Astronomy & Astrophysics*, **652**:917–936, doi: 10.1086/508139.

Luppino GA, Gioia IM. 1995. Constraints on cold dark matter theories from observations of massive x-ray- luminous clusters of galaxies at high redshift. *The Astrophysical Journal Supplemen*t, **445**:L77–L80, doi: 10.1086/187894.

Mazzotta P, Rasia E, Borgani S, Moscardini L, Dolag K, Tormen G. 2004. Spectroscopic-like temperature of clusters of galaxies and cosmological implications. *ArXiv Astrophysics e-prints*.

Mohr JJ, Mathiesen B, Evrard AE. 1999. Properties of the intracluster medium in an Ensemble of Nearby Galaxy Clusters. *The Astrophysical Journal*, **517**:627–649, doi: 10.1086/307227.

Piffaretti R, Kaastra JS. 2006. Effervescent heating: constraints from nearby cooling flow clusters observed with XMM-Newton. *Astronomy & Astrophysics*, **453**:423–431, doi: 10.1051/0004-6361:20054365.

Piffaretti R, Jetzer P, Kaastra JS, Tamura T. 2005. Temperature and entropy profiles of nearby cooling flow clusters observed with XMM-Newton. *Astronomy & Astrophysics*, **433**:101–111, doi: 10.1051/0004-6361:20041888.

Struble MF, Rood HJ. 1999. A Compilation of Redshifts and velocity dispersions for ACO clusters. *The Astrophysical Journal Supplement*. **125**: 35–71, doi: 10.1086/313274.

Sunyaev RA, Zeldovich YB. 1969. Distortions of the background radiation spectrum. *NATURE*, 223:721–722. doi: 10.1038/223721a0.

Sunyaev RA, Zeldovich YB. 1972. The observations of relic radiation as a test of the nature of X-ray radiation from the clusters of galaxies. *Comments on Astrophysics and Space Physics*, **4**:173.

Tamura S, Kaastra JS, den JWA Herder, Bleeker JAM, Peterson JR. 2004. Abundances in intracluster medium with XMM (Tamura, 2004). *VizieR Online Data Catalog*, **342**:135.

Zemcov M, Borys C, Halpern M, Mauskopf P, Scott D. 2007. A study of the Sunyaev-Zel'dovich increment using archival SCUBA data. *Monthly Notices of the Royal Astronomical Society*, **376**:1073–1098, doi: 10.1111/ j.1365-2966.2007.11443.x.

OPTIMIZATION OF MEDICAL EXPOSURES IN INTERVENTIONAL RADIOLOGY

Drilona KISHTA
University Hospital Center, Mother Theresa, Tirana, Albania
Antoneta DEDA
Department of Physics, Faculty of Natural Sciences,
University of Tirana, Albania
Uarda GJOKA
University Hospital Center, Mother Theresa, Tirana, Albania

ABSTRACT

Optimization of medical exposures is of immediate importance for the interventional radiology as it seeks to avoid detrimental effects of radiation. Here, staff training and optimization of these exposures would be of immediate importance, as high doses procedures are in some cases required. Three principles of radiation protection must be followed: i) justification, ii) optimization and, iii) dose limits. Periodic check of the components in a diagnostic x-ray imaging system is very important. In addition, recommendations of Basic Safety Standards (BSS), regarding the classifications of areas dose limits must be followed. Moreover, thermoluminescent dosimeters (TLD) that monitor personal doses are in constant use by the medical staff working at University Hospital Centre (UHC). Periodical check of physical and geometrical characteristics of X and the use of shielding screens are unavoidable for the diagnostic radiology as they divide areas which are unrelated to the examination. Applying periodically the quality control (QC) methods is necessary for an accurate ionizing radiation or use of radioactivity materials and monitoring patient dose (by evaluating Entrance Skin Dose (ESD)). In the present investigation 100 patients (adults and children) suffering from heart and brain diseases are involved and the exposure data were recorded fluoroscopically. The type of procedure, fluoroscopic time, higher values of voltage and current, the dose rate and dose-area product values obtained by Dose Air Production (DAP) of each patient were recorded. Staff radiation dose level should be monitored and reviewed in order to not exceed the permitted levels.

Keywords: quality control (QC), quality assurance (QA), interventional radiology, TLD dosimeters, miliSivert, dose, dose rate

1. INTRODUCTION

The present paper aims at: i) investigating the dose rate of patients in interventional radiology (IR) and compare the reference levels of dose to patients and staff in IR, ii) describing and understanding better the basic elements of the methods and techniques used to perform Quality Control (QC) and Quality Assurance (QA) and measurement of radiation doses in IR (Wagner, 1994), iii) optimizing medical exposures in IR which is closely related to the improvement of the information received from these exposures using the smallest possible doses of radiation to patients (Vañó,1997) and, iv) increasing radiation protection measures for personnel performing IR procedures to minimize their occupational exposures (Faulkner,1986).

The present investigation was carried out at the labs of hemodynamic and angiography, Interventional Radiography, University Hospital Center (UHC), Tirana, Albania involving "Coroskop Top" and an angiograph manufactured from Siemens. The angiograph is equipped with the Dose Air Production (DAP) device which determines the doses administered during various procedures (Vañó *et. al*., 2013).

2. METHOD AND MEASUREMENTS

Figure 1 depicts the Siemens Angiography used for cardiologic purposes. Figure 2 depicts the Siemens Angiography used for neurologic purposes. The two devices were produced in 2007. A continuous fluoroscopic monitoring was carried out for the catheterization of the peripheral parts. Voltage and current of the fluorescent tube (automatic lighting control system) are automatically adjusted based on the examined anatomical area and the physical feature of the patient.

Fig .1: Coroskop Top.

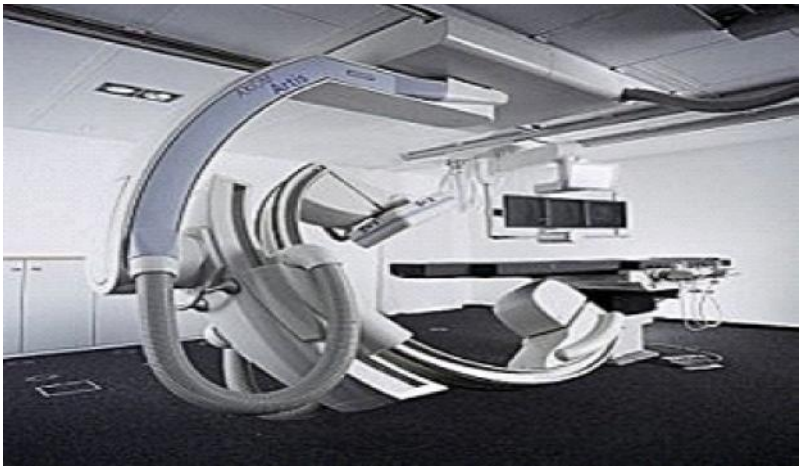

Fig. 2: Angiograph used in neurology.

During a routine procedure of quality control (QC), the output of radiation (O / P) by X device was measured at a distance of 75 cm to the whole range of possible fluoroscopic voltage of the tube (Marshall *et. al.*, 1995).

All measurements were carried out using a digital multimeter (PMX-III R / CT RTI Electronics, Molndal, Sweden) equipped with a detector (R25) and calibrated at a standard laboratory.

Dose Air Production (DAP) consists of a room ionization meters and a Cp type "DIAMENTOR E2", where the data of the radiation rate and the dose-surface product given by the ionization chamber are displayed.

In the present investigation 100 patients (adults and children) suffering from heart and brain diseases are involved. Exposure data were recorded fluoroscopically (A Survival Guide 2010). Procedures, fluoroscopic time, higher values of voltage and current, the dose rate and dose-area product values obtained by DAP for each patient were recorded (Ferral and Lorenz 2010).

3. RESULTS AND DISCUSSION

The annual limit for effective dose in persons exposed is 20 mSv and the limits for equivalent dose to the skin (including hands and feet) and the eyes are 500 mSv and 150 mSv, respectively. Consequently, more than 320 procedures are annually carried out to obtain dosimeter readings equal to 20 mSv (for personal dosimeters located in the thoracic level and outside protective lead apron). If aprons and protective collar are using the actual effective dose, there will be only a small fraction of the estimated dose, i.e., more than 3000 of such procedures performed before the medical practitioner receives the annual

limited effective dose. Hands, feet and eyes require more than 1900, 4440 and 17800 procedures annually. Table 1 reports that IR is not risky for the operator and his assistants. In the present investigation, the scattered dose in a distance of 2 m for an average procedure with fluoroscopic time and exposure factors is only 0.01 mSv; equal to the daily dose limit in uncontrolled areas.

Table 1. Measured personal dose values in comparison with allowed dose values of the staff.

Profession	**Average dose values for 2 months (mSv)**	**Allowed dose values for 2 months (mSv)**	**Annual average dose values (mSv)**	**Annual allowed dose values (mSv)**
Cardiologist 1	0.53	3.4	3.5	20
Cardiologyst 2	0.42	3.4	2.7	20
Neurologist 1	0.47	3.4	3.2	20
Nurse (Cardiology)	0.35	3.4	2	20
Nurse (Neurology)	0.27	3.4	1.5	20

Table2. The data for the doses of surgeon, during various types of surgical in cardiology and neurology procedures for 100 patients at hospital center

Surgical Procedure	**Nr. Of patients**	**Exposure Time (min)**		**Voltage kVp**	**Intesity mA**	**DAP** μGym^2		**Dose rate** μGy m^2/s	
		Limit min, max	**Average ±SD**	**Average ±SD**	**Average ±SD**	**Limit Min Max**	**Average±SD**	**Limit Min Max**	**Average ±SD**
Pacemaker	10	0.4 1.7	0.9±0.5	70 ±5	4.4±2.3	1942.3 2349.7	2056.90±123	54 82	73±0.8
PTCA+STENT	17	6.4 25	14.58±7	180 ±7	12.3±3.9	6028.4 23048.9	15079.2±428	75 354	210±45
SAK II APP	32	1.2 3.9	2.7±0.6	90 ±3	14.3±4.7	2350.49 6473.24	5854.95±162	64 159	128.±32
SAK II APQ	27	1.1 3.5	2.5±0.4	90 ±5	13.9±5.3	1937.65 5698.13	4758.82±157	47 138	110±28
Celebral Hemorrhage	14	7.9 18	16.47±2	190 ±8	10.7±4.5	8025.46 21045.9	19433.2±423	180 392	357.±52
All Procedures	100	0.4 25	7.43±0.5	124±9	9.12 ±3.7	1937.65 23048.9	9847.99±258	47 392	175.6±28

Therefore, any hospital non-professional staff member or anyone that stands at a distance of 2 m or more during fluoroscopy can participate one procedure a week, without exceeding the annual effective dose of 1 mSv. Exposure data for each procedure are in table 2 reported.

4. CONCLUSIONS

The rapid development of imaging technology has contributed to the growth of interventional radiology (IR) in the last 25 years. The patients who underwent IR aged from 40 to 80 years. The children who underwent these procedures had heart mutations. Patients are exposed to a much higher dose of radiation in IR compared to the patients undergoing diagnostic X-ray examinations due to long fluoroscopy time, large power during these procedures and the required number of radiographic images.

In some cases, dose levels exceed the threshold due to deterministic effects.

Stochastic effects should be taken into consideration for IR procedures for specific groups such as children. A low quality of the image in order to reduce patient dose would be very important for the optimization of IR procedures. Great efforts have been made to ensure that the equipments on the market optimize the quality of the image /dose and not to maximize dose and image. Applying periodically the quality control (QC) methods is necessary for an accurate ionizing radiation or use of radioactivity materials and monitoring patient dose (by evaluating Entrance Skin Dose (ESD)). Staff radiation dose level should be monitored and reviewed in order to not exceed the permitted levels.

REFERENCES

A Survival Guide. **2010.** *Interventional Radiology*: 3rd Edition**,** 154-159.

Faulkner K, Love GH, Sweeney JK Bardsley RA. 1986. Radiation doses and somatic risk to patients during cardiac radiological procedures. *The British Journal of Radiology*. **59,** 359-363.

Ferral H, Lorenz JM. 2010. Interventional Radiology. *RadCases*, 123-129.

Marshall NW, Noble J, Faulkner K. **1995.** Patient and staff dosimetry in neuroradiological procedures. *The British Journal of Radiology*. **68**, 495- 501.

Vañó E, Fernández JM, Sánchez RM, Ten JI. **2013.** Diagnostic reference levels in interventional radiology. *Radiologia* **2**, 55, Dec; Suppl 2:17-24.

Vañó E, Guibelalde E, Fernandes JM, Gonzales L. **1997.** Patient dosimetry in Interventional Radiology using Slow Films. *The British Journal of Radiology*. **70**, 195- 200.

Wagner LK, Eifel PJ, Geise RA. **1994.** Potential biological effects following high x-ray dose interventional procedures. *Journal of Vascular Interventional Radiology***, 5(1)**, 71- 84.

THE ASSESMENT OF SODIUM AND POTASSIUM CONCENTRATRION IN THE BLOOD SERUM OF ALBANIAN WOMEN

Marjena BIXHI
Clinic of Gynecology, New Life, Durrës, Albania
Pranvera LAZO and **Joana GJIPALAJ**
Department of Chemistry, Faculty of Natural Sciences,
University of Tirana, Albania

ABSTRACT

The present paper aims to investigate the concentrations of sodium and potassium in the serum samples of pregnant and non-pregnant women and prove the effectiveness of the therapy with substitute of sodium and potassium during the pregnancy. In the present investigation 76 women divided into two groups; pregnant (n=36) and non-pregnant women (n=40) are involved. Sampling took place from February to March 2013 following the World Health Organization (WHO) protocol. The serum samples were prepared using the high speed centrifugation (3600 rpm, in gel tubes) of blood samples after the dilution at 1:10 ratio with 0.25% Triton X-100 prepared in de-ionized water. The flame Atomic Emission Spectroscopy (FAES) was involved to investigate the serum samples. Results reported normal values of sodium and potassium on most of blood samples of pregnant women compared with those of non-pregnant women, and a normal recommended range of concentration of K and Na in blood samples. The pregnant women underwent the treatment with substitute of sodium and potassium and effectiveness of the therapy was proved.
Keywords: sodium, potassium, female, pregnant women, blood sample, FAES

1. INTRODUCTION

Electrolytes are important for the regulation of some essential processes in the body, among which the most important are: i) regulation of water balance and its distribution in the body, ii) regulation of osmotic equilibrium, iii) regulation of acid-alkaline balance through plasma bicarbonates management, iv) regulation of electrical potential of cell membranes and, v) impact on neuromuscular activity (Brommer and Coburn 1981; Dubose Jr 2008).

The concentration of electrolytes plays an important role not only in maintaining osmotic pressure, but in moving water in different compartments of the body (Bonardi and Deambrogio 1999). Hypertension is a universal problem at least in 10% of the pregnancies (Indumati *et al.*, 2011). The electrolytes play an important role in the pathogenesis of hypertension (Pallavi *et al.*, 2012). The hypertension, proteinuria and edema are signed as the triad of the preeclampsia that is specific to human pregnancy (Shakhmatova *et al.*, 2000; Blaustein *et al.*, 2006; Indumati *et al.*, 2011).

The study shows reduced levels of serum potassium and increased level of sodium in patients of preeclampsia as compared to the non-pregnant pregnant women (Anjum and Alka 2013). The concentrations of sodium, potassium, calcium, and magnesium ions are regulated by independent mechanisms to provide retention of these parameters within certain periods of pregnancy at the level of non-pregnant women on the background of hypoosmia (Shakhmatova *et al.*, 2000). The dietary sodium restriction is one of the prime treatments of high blood pressure (Indumati *et al.*, 2011). All these make the determination of electrolytes very important for the biological and medical sciences (Zilva and Pannall 1979; Osmond, 1987; Buzo, 1993; Kopelkaj and Buzo 2007).

1.1 *Sodium*

Sodium (Na) is the major positively-charged ion (cation) outside body cells. The total body potassium of a healthy person is 4000 mMol and is spread in the whole parts of the organism in the form of: i) the extra cellular fluids containing 45% of the total quantity of sodium or about 1800 mMol, ii) the intracellular water spaces containing approximately 10% of the total quantity of sodium or about 400 mMol / l and, iii) the reminder or 45% (1800 mMol / l) found in bone tissue, in the form of chemical bonds and unaffected by normal metabolic changes.

The everyday food and external environment uptake of Na is 4-6 grams per day, mainly in the form of sodium chloride. After the dissociation process, Na+ and Cl- ions are mainly absorbed in the digestive tract without any active control, through a mechanism similar to the sodium-potassium pump-ATP-aze. The content of sodium in the body is kept at relatively constant via renal regulation. The mechanism of re-absorption of sodium cations Na + in the kidney, check and regulate the sodium concentration in the water space plasma. This mechanisms control the Na concentration that in the normal organism varies from 135 to 145 mMol / l (Zilva and Pannall 1979; Kruse *et al.*, 1984). However, the range of normal values depends on many factors and each laboratory brings it in line with the population that covers and analytical technology of the laboratory.

Beside it, the most important regulatory and supervisory mechanism of the excretion process of sodium from the organism is the action of mineralo-corticoid hormones and especially that of aldosterone. The aldosterone is the hormone, which strongly affects the sodium-potassium exchange through the cell membranes, especially at the cellular level of the renal tubes. Aldosterone hormone is the most important factor, which operates and realizes the Na excretion (Osorio and Alon 1997).

Several factors affect the normal function of the proximal renal tubes. One among them that we should take into the consideration, is the speed of glomerular filtration (VFG). A very low glomerular filtration process may decrease the renal excretion of sodium ions, while a relatively high glomerular filtration rate (VFG), may increase the renal excretion of sodium ions. Na retention is likely due to vasoconstriction leading to reduction of glomerular filtration rate and stimulation of rennin angiotensin aldosterone mechanism. The net effect is decreased intracellular fluid and increased extracelluar fluid volume (Sunitha *et al.,* 2012).

The variation of the blood flow to the kidney and plasma osmotic pressure is usually followed by the variability of the re-absorption of sodium. The reduced concentration of sodium in the blood below 135 mMol /L, is called the hipo-sodium condition. If the plasma sodium values reach the value of 120 mMol /L, undergoing an intensive therapy would be necessary.

On the other hand, the exceedance of Na concentration in blood (over 145 mMol / l) might cause the hiper-sodium symptom due to the significant water loss which leads to the decrease of water-plasmatic spaces and increase of relative concentrations of sodium in blood.

1.2 Potassium

Potassium (K) is the most essential cation of intracellular fluids. The average concentration of potassium inside the cell environment is 140 mMol/L, while in the extracellular environment, it is more or less 4 mMol /L. Intracellular concentration of potassium differs significantly in function to its metabolic activity. Reserves of potassium in the body are smaller than those of sodium and this can change, leading to serious pathology (Fraser and Harris 1989). The most important exercise and metabolic functions of potassium are: i) activation of many enzymatic processes, ii) regulation of fibro- cells conductivity in general and those of myocarditis in particular and, iii) transmission of nerve impulses. The content of potassium in the body is more or less 3200 mMol. The everyday food intake of the potassium is 26 mMol/day. The normal potassium concentration in plasma is generally 3.5-5.3 mMol / l. As a result of this low concentration, compared to the sodium, potassium does not affect the water

balance. An important mechanism that affects the displacement process of potassium through the cell membranes is the acid-alkaline balance. The hipo-potassium condition is a clinical situation in which the amount of plasmatic potassium is below the lower limit of normal values (Fraser and Harris 1989) that is caused by several factors.

Pregnant women in the present investigation involved underwent a treatment with alimentary integrators that are the vitamins and minerals necessary to replace all the losses that women are supposed to have during pregnancy and maintain their metabolism efficient.

The content of vitamins and minerals was based on WHO recommendations (2010).

2. MATERIALS AND METHODS

2.1. Blood Sampling

Blood sampling took place from February to March 2013 following the WHO protocol (2010): i) extending the patient's arm and inspect the antecubital fossa or forearm, ii) locating a vein of a good size that is visible, straight and clear, iii) applying the tourniquet about 4-5 finger widths above the venepuncture site and re-examine the vein, iv) disinfecting the site using 70% isopropyl alcohol for 30 seconds and allow to dry completely (30 seconds), v) anchoring the vein by holding the patient's arm and placing a thumb below the venepuncture site, vi) entering the vein swiftly at a 30 degree angle, vii) once blood is sufficiently collected, tourniquet could be released before withdrawing the needle and, viii) withdrawing the needle gently and then give the patient a clean gauze or dry cotton-wool ball to apply to the site with gentle pressure.

2.2 Blood Serum Preparation

5 ml of blood obtained by venous puncture were added to the tube with gel. Blood was allowed to clot by leaving it undisturbed at room temperature for 5 min. The tube was put in thermostat with temperature 37© to accelerate the degradation of fibrinogen for 4 min. Once the tube was put in the thermostat and the degradation of fibrinogen was accelerated, the clot was removed via centrifugation at 3600 rpm/min using a refrigerated centrifuge.

At the end of this process, a light yellow blood serum was obtained (WHO, 2010). The serum samples were diluted to 1:10 ratio with de-ionized water comprising 0.01% Triton X-100 (Tabassum *et al.*, 2015).

2.3 Methods

Once measurement conditions were optimized, the flame Atomic Emission Spectroscopy (FAES) was involved to investigate the absorbance of Na and K

in serum samples. As certified samples CRM lacked, the following procedures were carried out: i) calibration method, ii) measurement of the blank sample, iii) the discontinuation of the apparatus after each measurement, iv) control of each standard every 10 measurements and, v) analysis of several parallel samples (10% of the total number of samples).

3. RESULTS AND DISCUSSIONS

The data for each element have been subject to the descriptive statistics and the results are in Table 1 and 2 reported.

Table 1 Statistical analysis (Descriptive Statistics) of Na concentration data in blood serum (N=75)

Parameters	Normal	Pregnant
Mean	140	143
Median	141	140
Mode	141	147
Standard Deviation	7	13
Sample Variance	52	162
CV%	5	9
Kurtosis	7	7
Skewness	-2	2
Range	44	62
Minimum	112	127
Maximum	155	189
Count	36	36

The difference between the values of the mean and the median of non-pregnant women is smaller than of pregnant women by indicating that the Na concentration data of non-pregant women are more or less (dC=1) normally distributed. Na has low value of the coefficient of the variance (CV% <25%) by indicating that the data vary in a small range and are more or less stable in most of the women under investigation. Na content in blood samples of non-pregnant women is characterized by a high negative value of skewness (-2) and positive values of kurtosis (7), by indicating that the Na concentration data are negatively skewed. The Na content in the blood samples of pregnant women is characterized by high positive value of skewness (2) and kurtosis (7). The high positive values of skewness (>0) and kurtosis (>3) show that the data are positively skewed and effected by different factors.

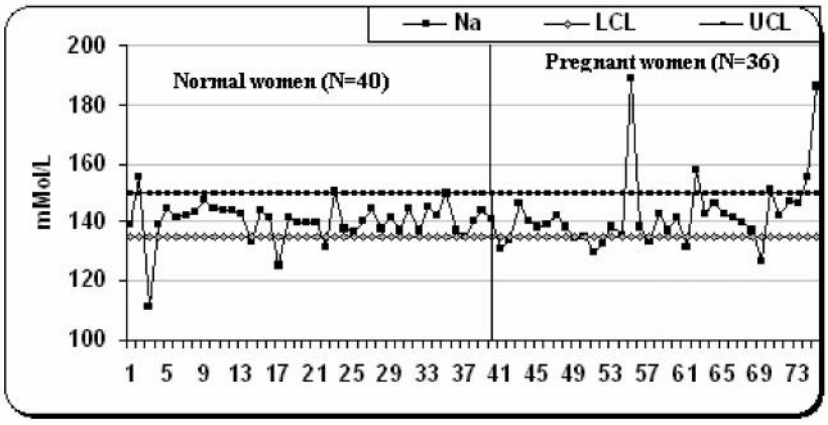

Fig. 1 The diagram of Na concentration in blood serum of non-pregnant women (N=40) and pregnant women (N=36)

Proving that Na content in blood samples is within the permitted levels, results reported that Na content is higher than the permitted levels only in 6.6 % of the cases and K content close to the lower limit of Na content in blood in only 9.2% of the cases.

Table 2 Statistical analysis (Descriptive Statistics) of K concentration data in blood serum (N=76)

Parameters	Non-pregnant	Pregnant
Mean	3.85	3.97
Median	3.70	3.66
Mode	3.75	3.66
Standard Deviation	0.71	0.84
Sample Variance	0.51	0.71
CV%	18	21
Kurtosis	3.79	-0.65
Skewness	1.24	0.59
Range	4.06	3.10
Minimum	2.33	2.33
Maximum	6.39	5.42
Count	40	36

The small difference between the mean and median values of K proves that the data are more or less normally distributed for the two groups. K has a low value of variance coefficient (CV% <25%), but lower than the CV% value of

Na, proving that the data of potassium vary in a lower range of concentration compared with Na concentration in blood samples. The K content in blood samples was characterized by positive values of skewness (1.24) and kurtosis (3.79) for normal women. The K content in blood samples of pregnant women were characterized by negative values of skewness (-0.65) and small value of kurtosis (0.59) by indicating the K data are negatively skewed, while the Na data of this group of women are positively skewed (skewness= 2, kurtosis=7). It shows that as Na concentration in blood samples of pregnant women increases, of K concentration decreases.

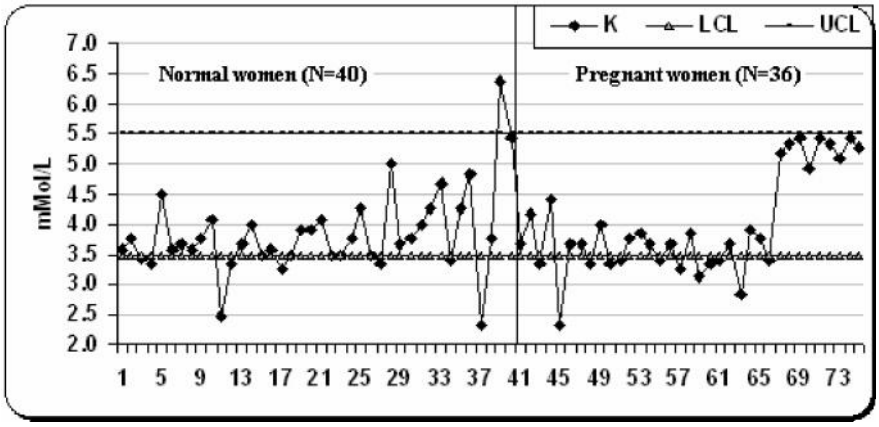

Fig. 2: The diagram of K concentration in blood serum of non-pregnant (N=40) and pregnant women (N=36)

Proving a normal concentration of K, results reported a lower K content than the permitted levels in only 5.3 % of the case and a higher level K content than the permitted level in only 1 case.

4. CONCLUSIONS

The results reported that most of the samples had a normal range of Na and K concentration in blood serum of the investigated women. Only a small group of blood samples reported higher values of Na and K than the permitted levels.

The concentrations of the two elements in pregnant women are comparable with those of non-pregnant women showing the effectiveness of prenatal vitamin supplements. It was found that the increase of Na concentration in blood samples of pregnant women is followed by the decrease of K concentration.

REFERENCES

Anjum K Sayyed, Alka N Sonttake. 2013. Electrolyte Status in Preeclampsia, Online International Interdisciplinary Research Journal, {Bi-Monthly}, ISSN 2249-9598, Volume-**III**, Issue-III, May-June 2013.

Blaustein MP, Zhang J, Chen L, Hamilton BP. 2006. How does salt retention raise blood pressure? *American Journal of Physiology - Regulatory, Integrative and Comparative Physiology*. **290**: 514-523.

Bonardi R, Deambrogio V, OliaroA. 1999. Interpretazione dei dati di Laboratorio, Torino.

Brommer F, Coburn JW. 1981. Disorders of mineral metabolism. New York. Academic Press.

Buzo S. 1993. Studimi eksperimental klinik i ekuilibrit acido-bazik, oksimetrisë dhe balancit elektrolitik, Dezertacion Universiteti i Tiranës, Fakulteti Mjekësisë, Katedra Farmakologji, Fiziologji, Biokimi. Tiranë.

DuBose TD Jr. 2008. Disorders of acid-base balance. In: Brenner BM, ed. Brenner and Rector's The Kidney.8th ed. Philadelphia, Pa: Saunders Elsevier; Chap **14.**

Fraser CG, Harris EK. 1989. Generation and application of data on biological variation in clinical chemistry. *Critical Reviews in Clinical Laboratory Sciences*, **27**:409-437.

Indumati K, Kodliwadmath MV, Sheela MK. 2011. The Role of serum Electrolytes in Pregnancy induced hypertension. *Journal of Clinical and Diagnostic Research.* 2011; **5(1)**: 66-69.

Kolpepaj R, Buzo S. 2007. Biokimia Klinike. Tiranë, :76- 106.

Kruse K, Kracht U, Kruse U. 1984. Reference values for urinary calcium excretion and screening for hypercalciuria in children and adolescents. *European Journal of Pediatrics*: **143**: 25-31.

Osmond MF. 1987. Calcium assay and reagents therefore. US 3771961 A Soc. Chim. **47**:745.

Osorio AV, Alon US. 1997. The relationship between urinary calcium, sodium, and potassium excretion and the role of potassium in treating idiopathic hypercalciuria. *Pediatrics*, **100**: 675-681.

Pallavi PC, Pranay AJ, Jasmin HJ. 2012. Changes in serum calcium and Magnesium level in preeclampsia vs normal pregnancy. *International Journal of Biomedical and Advance Research;* **3(6)**: 511-513.

Shakhmatova EI, Osipova NA, Natochin YV. 2000. Changes in osmolality and blood serum ion concentrations in pregnancy, *Human Physiology*, **26, (1)**, 92-95.

Sunitha T, Sameera K, Umaramani G. 2012. Study of Biochemical changes in Preeclamptic women. International Journal of Biological & Medical Research. 2012; **3 (3)**: 2025-2028.

Tabassum H, Al-Jameil N, Ali NM, Al-Rashed F. 2015. Status of serum electrolytes in preeclamptic pregnant women of Riyadh, Saudi Arabia. *Biomedical Research*; **26 (2):** 219-224 ISSN 0970-938X www.biomedres.info

World Health Organization (WHO). 2010. *WHO guidelines on drawing blood.* http://whqlibdoc.who.int/publications/2010/9789241599221_eng.pdf

Zilva JF, Pannall PR. 1979. Calcium, Phosphate and Magnesium metabolism in Clinical Chemistry in Diagnosis and Treatment. Lloyd-Luke 1979; Chap **X1**:253-4.

ASSESSMENT OF TRACE METALS LEVEL USING LIGUSTRUM LUCIDUM, FAM: OLEACEAE AS VASCULAR PLANT

Rudina TRIKSHIQI and **Mimoza REXHA**
Dept. of Chemistry, Faculty of Natural Sciences,
University of Tirana, Albania

ABSTRACT

Ligustrum lucidum, Fam: Oleaceae is in the present investigation used as bio-indicator to monitor the level of trace metal in Tirana, Albania. Eleven leaves samples were collected from different urban areas with different anthropogenic impact in March 2013. Heavy metals (Cu, Pb, Zn, Mn, Fe, Na, K, Mg, Ca and Hg) concentrations in the leaves' samples were determined via atomic absorption spectrometry (AAS). Wet digestion technique was applied for sample digestion in half pressure Teflon tubes. Correlation analysis was carried out on the data set of heavy metals to describe their behaviour and association. Results reported a weak correlation ($R2<0.45$, $p<0.05$) between Cu-Fe and a high correlation between Cu-K. The source is the dust particles. The correlation between Pb- Ca and the high correlation between Zn – Mn, Mg and Ca relates to traffic emission. Multivariate analysis (Cluster Analysis) helped identify similar patterns of groups of elements. Plant species and their location affect trace metals distribution. The principal component analysis (PCA) helped identify the main source categories of contamination and elements' distribution.
Keywords: *Ligustrum lucidum Fam: Oleaceae*, vascular plant, heavy metal, furnace AAS, urban environment, Air Pollution.

1. INTRODUCTION

Air pollution relates to the substances that unload in environment by human activities and natural process, causing harmful effects in human health and environment. Population growth in large urban areas such as Tirana has resulted in air pollution. Life quality is directly related to the quality of the environment. It is important to raise people awareness (Mills *et al.,* 1985) making in evidence their role in environmental pollution, which is equivalent to their role in solving environmental problems (Dako *et al,* 2010). Researches in the field detection of pollutants compounds (in air, water and soil) help us to relate them to the

diseases, which are caused from different pollution sources (Kukkonen *et al*, 2005). The individual reaction of pollutants depends on exposure level, individual activity, and kind of pollution (Brodribb and McAdam 2010). In addition to the heavy metals in air, other elements such as particles with diameters below 10 microns (PM10), and particularly 2.5 microns (PM2.5) can penetrate deeply into the airways of respiratory tract and deposit predominantly in certain areas where absorption efficiency for trace elements is higher, potentially damaging the human health.

The areas with highest number of vascular plants in Europe are located in the Mediterranean region (Melanie *et al.*, 2011). These plants are used as bio-indicator, because they are stationary, practical and reflect conditional sites (Brodribb and McAdam 2010). Also, they can absorb heavy metal from the ground and air (Banks and Nishiyama, 2011). In the present investigation the *Ligustrum lucidum* from the family of *Oleaceae* was used as a bio-indicator to monitor the level of trace metal in Tirana, Albania. The leaves of the plant are dark green in colour, 6–17 centimetres long and 3–8 centimetres wide (Stroh *et al.,* 2014). They are a residential street plants, that grow in urban areas where air pollution, poor drainage, compacted soil are common (Mills *et al*, 1985; Baker *et al*, 2013). *Ligustrum* plant can grow in full sun or partial shade on various soil types, and is moderately salt-tolerant. Clay soil and high pH cannot cause any problem as long as water drains away from the roots. They are planted along boulevards where regular mowing will kill germinating seedlings and in locations with limited overhead space. Mature specimens will require only light pruning to maintain shape (Muchuweti *et al,* 2006). In addition, it has appropriate surface roots and it is called winter flowers. Moreover, it has a long-term health, unaffected by pests.

The present paper aims to investigate the level of metal contaminants (Cu, Pb, Zn, Mn, Fe, Na, K, Mg, Ca and Hg) using one vascular plant species able to accumulate heavy metals in the air. The most toxic metals for vascular plant are Hg, Cu, Pb, Cd (Kabata-Pendias and Pendias, 1984). The toxic level is related with methylation process of heavy metals in the environment (Dako and Mankolli 2010). Hg can be methylated in environment through the action of enzymes secreted by microorganisms and also by abiotic chemical reactions (Akosy and Sahin 1999). The bacteria, which are associated with methylation process of these elements, are found in the sediments at bottom of coastal waters and the digestive tracts of humans. This methylation radically affects the behaviour of these elements in the components of the environment, their bioavailability and their toxicology. In this case we have mono methyl mercury (CH3Hg+), the most toxic form of Hg, which is lipophilic and therefore, accumulates in body fats (Ferguson *et al*, 1990; Muchuweti *et al*, 2006). In the present investigation results reported that the atmosphere is one of the

most important pathways for the transport of heavy metals (Langard, 1980; Brodribb and McAdam, 2010). According to their different physical and chemical properties, the size and composition of the source particles these pollutants are partitioned between liquid and vapour phases and are subsequently transported in to the air (Alloway and Ayres 1997; Baker and De Salas, 1997; Caille *et al*.,2005; Lika *et al*., 2012).

2. MATERIAL AND METHODS

Sampling

In the present investigation, the vascular plant *Ligustrum lucidum and Fam: Oleaceae plants* was used to monitor air pollution in Tirana city. Sampling took place in the last 10 days of March 2013, once a week, after rainy days. Samples were collected from 11 stations in Tirana, along the main streets. Figure 1 depicts the leaves of the plant during the drying process.

Fig.1 Drying process of leaf sample (Ligustrum, lucidum).

The stations' distribution is in the Figure 2 depicted.

Fig. 2: Map of Tirana city. Sampling stations: Sample 1- close to the National Museum; Sample 2 – close to the University Hospital Centre Mother Teresa.; Sample 3- close to Brryli area; Sample 4- at the Dëshmorët e Kombit Bulevard; Sample 5- at Sheshi Shqiponja; Sample 6- Rr e Dibrës; Sample 7- at the Kombinat area; Sample 8- close to the Polytechnic University of Tirana, Albania; Sample 9- at 21 Dhjetori; Sample 10- at Zogu i Zi; Sample 11- Elbasani Street.

Preliminary treatment of the samples

Once transported at the laboratory, the leaves samples were dried at ambient air on sheet papers until a constant weight was reached. Once dried, the leave samples were homogenized to a fine material and crushed by hand, wearing laboratory polyethylene gloves without powder.

Sample digestion

The dried plant samples were digested with nitric acid (ultra pure, 65%) and deionised water (9:1) in half pressure Teflon tubes. The experiment dishes were cleaned using dilute nitric acid and washed with distilled water. Elements standard solutions used for calibration curves were prepared by diluting the base standard liquids of 1000 mg / L. 0.5 g dry leaves of each sample were digested with 10 mL of nitric acid HNO3 (9:1). Teflon tubes were closed and left at room temperature for 48 h. Samples were subsequently digested for 3 hours at 80-90° C and temperature increased to 200° C for 1 hour for full

digestion. Once cooled, the Teflon tubes were opened and left for the evaporation of nitric acid to small volumes. Once nitric acid, was evaporated to small volumes, the samples were diluted with deionised water to a total volume of 50 mL.

The vascular plant digests were analysed for Cu, Zn, Mn, Fe, Na, K, Mg, Ca and Hg using the flame Atomic Absorption Spectrophotometry (AAS) involving air-acetylene flame. Pb metal was determined by using the AAS equipped with electro-thermal atomiser with graphite furnace.

Calibration method

The linear calibration method which is a means to address the relationship between the analytical signal and concentration was applied to obtain the calibration curves of each element. Blank solution of each element was used to identify the source of contamination in the sample. The concentration of heavy metals in samples was calculated based on their analytical signal (value of absorbance and the relevant equations of calibration curves).

3. RESULT AND DISCUSSION

Table 1 reports the descriptive statistic analysis on the data sets. The analytical data were subject to the statistical analysis. The data were statistically analysed using EXCEL and MINITAB-15 Package Programs.

Table 1: Results of statistical data processing (EXCEL, Descriptive Statistic) (mg/kg, DW)

Paramters	Hg	Pb	Cu	Zn	Na	Mn	Fe	K Fe	Mg	Mg
Mean	0.35	4.58	9.09	41.08	32.50	107.79	415.27	1510.67	4164.	6516
Median	0.36	3.18	8.43	42.42	24.66	84.76	375.00	1465.22	4123	6354
Minimum	0.11	2.15	4.82	19.87	5.48	44.76	255.43	665.22	2278	4064
Maximum	0.58	13.60	15.66	73.06	91.10	172.38	758.15	2169.57	6121	8759

Figure 3 reports distribution tendency of the elements listed in an increasing order of accumulation.

Heavy metals were detected in increasing order: Hg< Pb< Cu< Zn< Na< Mn< Fe< K< Mg< Ca. Here, the changes in concentration of the elements in various monitoring points are clear.

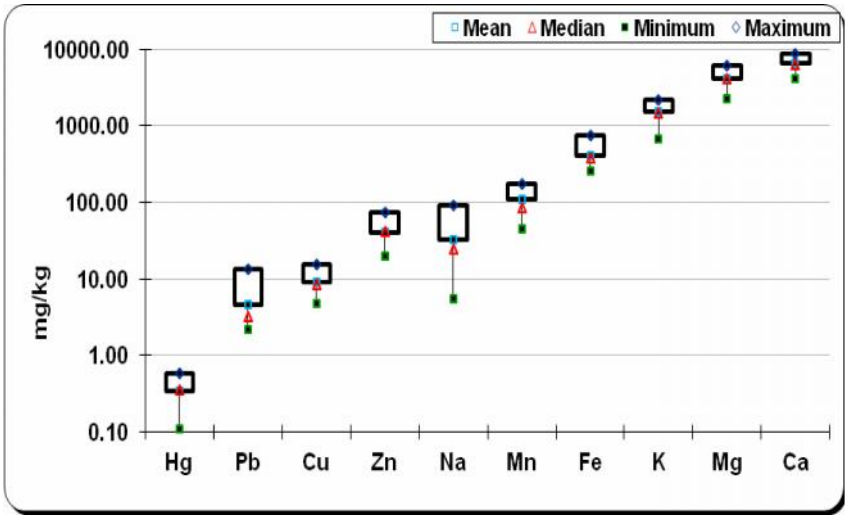

Fig. 3 The box-plot of the distribution of the elements (log-normal scale) (mg/kg, DW).

Table 2: The Mean/Median and Max/Min ratios

Element	Hg	Pb	Cu	Zn	Na	Mn	Fe	K	Mg	Ca
Mean/Med Ratio	0.98	1.44	1.08	0.97	1.32	1.27	1.11	1.03	1.01	1.03
Mean/Med Ratio	5.20	6.34	3.25	3.68	**16.63**	3.85	2.97	3.26	2.69	2.15

Natural in origin, Natrium (Na) has the highest Max/Min ratio (Tab 3). As a natural element, Na is an important nutrient for the *Ligustrum lucidum* plants. Correlation analysis and cluster analysis (analysis of elements in groups) were carried out to identify the origin of heavy metals in the leaves.

Correlation analysis ($p<0.05$) was carried out on the data set of heavy metals in order to describe their behaviour and the association is reported as follows:

	Cu	*Pb*	*Cd*	*Zn*	*Hg*	*Na*	*Mn*	*Fe*	*K*	*Mg*	*Ca*
Cu	1.000										
Pb	-0.226	1.000									
Cd	0.546	-0.096	1.000								
Zn	-0.088	0.461	-0.042	1.000							
Hg	0.036	0.016	0.232	-0.139	1.000						
Na	0.179	0.228	0.672	-0.020	0.230	1.000					
Mn	0.140	0.025	0.489	**0.584**	0.005	0.471	1.000				
Fe	**0.582**	-0.312	-0.045	0.055	-0.100	-0.022	0.217	1.000			
K	**0.688**	-0.073	0.290	-0.437	0.140	0.137	-0.020	0.454	1.000		
Mg	0.017	0.047	0.207	**0.614**	0.447	0.062	0.407	0.138	-0.416	1.000	
Ca	-0.160	**0.651**	0.065	**0.688**	0.350	0.329	0.450	-0.234	-0.212	0.383	1.000

The results reported: i) a weak correlation ($R2<0.45$, $p<0.05$) between Cu-Fe and a high correlation between Cu-K due to dust particles, ii) the correlation between Pb- Ca and the high correlation between Zn – Mn, Mg and Ca due to traffic emission.

Cluster Analysis of the observations helped identify similar patterns of element concentrations.

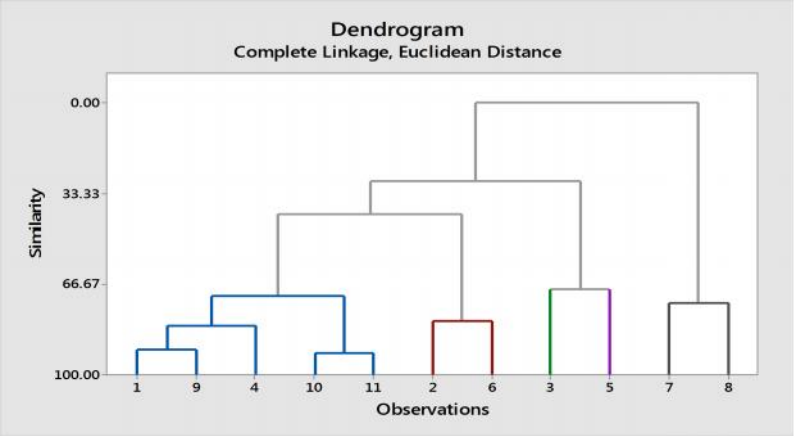

Fig. 4. The dendrogram of the distribution of the stations classified on their similarity, Euclidean Distance, Complete Linkage, Amalgamation Steps; Final Partition: Number of clusters: 5

Cluster 1 comprises station 1, 9, 4, 10 and 11 which represent an urban area characterized by a high level of air pollution. These stations have similar environmental conditions of heavy metals, as they are located close to heaviest traffic areas.

Cluster 2 comprises station 2 and 6 which represent the area close to UHC and Rr e Dibrës. Samples were collected during roadwork, reporting high values of heavy metal in this area.

Station 3 is in the **Cluster 3** included. This station shows high values of heavy metals due to traffic emission as it is located because close to the crossroad at Brryli area.

The station 5 is in the **Cluster 4** included. This station represents the street along the Sheshi Shqiponja. It shows high level of pollutions due to traffic emission.

Cluster 5 comprises station 7 and 8, which represent the area close to Dëshmorët e Kombit Boulevard. These stations show high level of pollution due to traffic emission and the building of fabric of wheat.

The dendogram of the correlation coefficients distance of the elements with similarity and distance values obtained from Cluster Analysis is depicted in Figure 5.

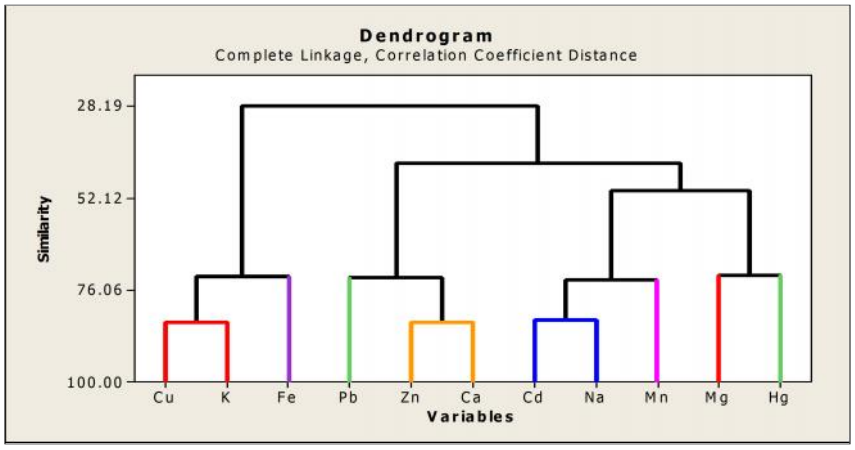

Fig. 5 The dendrogram of the distribution of the elements classified on their similarity, Euclidean Distance, Complete Linkage, Amalgamation Steps; Final Partition: Number of clusters: 4; Cluster 1: Cu, Fe, K; Cluster 2: Pb, Zn, Ca; Cluster 3: Cd, Na, Mn; Cluster 4: Hg, Mg.

Cluster 4 comprises the station 5 which represents Sheshi Shqiponja characterized by a high level of pollutions from traffic emission.

Cluster 5 comprises station 7 and 8 which represent the area close to the UPT and the Kombinat area with high level of pollution, caused by traffic emission and old fabric that are not used anymore.

The distribution of the elements classified on their similarity via Cluster Analysis are as following:

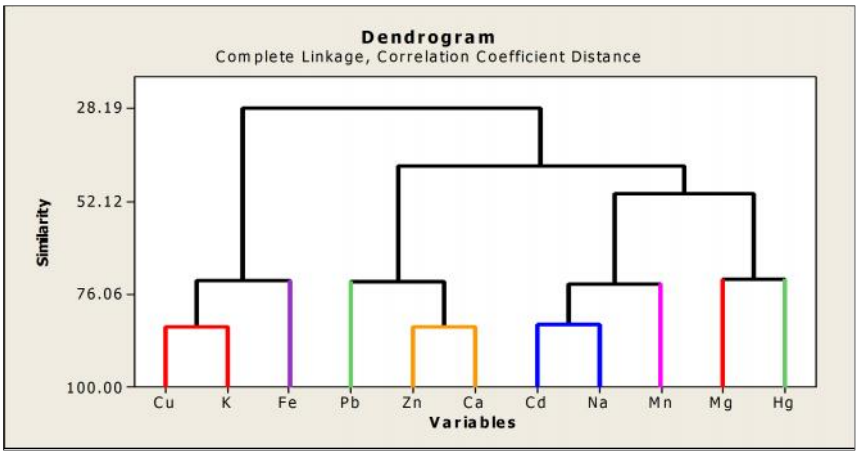

Fig. 6: The dendrogram of the distribution of the elements classified on their similarity, Euclidean Distance, Complete Linkage, Amalgamation Steps; Final Partition: Number of clusters: 4; Cluster 1: Cu, Fe, K; Cluster 2: Pb, Zn, Ca; Cluster 3: Cd, Na, Mn; Cluster 4: Hg, Mg.

Cluster 1 contains Cu, K and Fe due to anthropogenic activities such as brake lining, tire wear particle, cars brake and soil dust. K has been transported to the leaves from the roots.

Cluster 2 contains Pb, Zn and Ca. The source is traffic emission. Pb element acts as the marker element for motor vehicle emissions. Ca has been transported to the leaves from the roots.

Cluster 3 contains Cd, Na and Mn. The presence of these elements is due to anthropogenic activities (traffic emissions) and transportation by wind soil dusts and roots' system, respectively. As a natural element, Na is a very important nutrient for Ligustrum lucidum plants.

Cluster 4 contains Mg and Hg. Anthropogenic Hg and Mg emissions (from small plants located in Tirana and the burning of urban wastes) characterise this site. As a natural element, Mg is an important nutrient for Ligustrum lucidum plants.

PC analysis was a means to address an accurate interpretation of the results as follows:

Principal Component Analysis: Cu, Pb, Cd, Zn, Hg, Na, Mn, Fe, K, Mg, Ca

Eigenanalysis of the Correlation Matrix

Eigenvalue **3.178 2.732 1.579 1.257 1.083** 0.540 0.402 0.201 0.016 0.010

Proportion **0.289 0.248 0.144 0.114 0.098** 0.049 0.037 0.018 0.001 0.001

Variable	PC1	PC2	PC3	PC4	PC5
Cu	-0.113	**-0.507**	-0.162	0.113	0.181
Pb	**0.311**	0.147	0.259	0.486	0.348
Cd	0.137	**-0.469**	0.245	-0.101	-0.346
Zn	**0.459**	0.078	-0.388	0.198	0.027
Hg	0.156	-0.151	0.308	-0.581	0.487
Na	0.226	**-0.338**	0.393	0.107	-0.269
Mn	**0.361**	-0.281	-0.206	0.100	-0.341
Fe	-0.119	**-0.322**	-0.534	0.087	0.243
K	-0.244	**-0.413**	0.116	0.265	0.385
Mg	**0.379**	-0.066	-0.300	-0.490	0.105
Ca	**0.487**	0.027	0.126	0.156	0.284

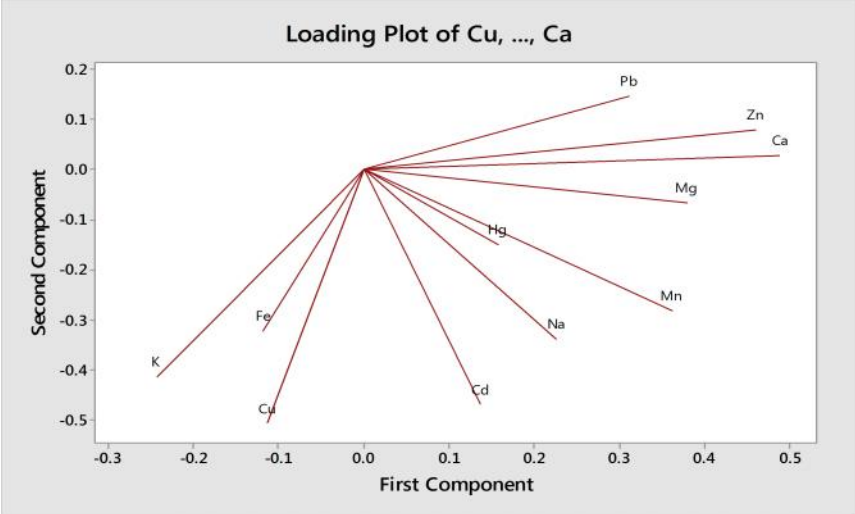

Fig.7: The dendrogram of Principal Component Analysis of the Correlation Matrix.

The following five principal components (PC's with Eigenvalue>1) that affect differences in trace metals distribution in vascular plant species have been selected:

PC 1 is the strongest PC characterized by high loadings of Ca, Zn and Mg. Anthropogenic sources are tire wear particle, car brake and soil dust. As a natural element, it is a very important nutrient for *Ligustrum lucidum* plants.

PC 2 is another strong PC characterized by high loadings of the elements Pb and Zn due to traffic emission. Pb acts as the marker element for motor vehicle emissions.

PC 3 is another strong PC characterized by high loading of Na. As a natural element, Na is an important nutrient for plants.

PC 4 is another strong PC characterized by high loadings Pb due to traffic emissions. Pb acts as the marker element for motor vehicle emissions (Caille *et al*., 2005).

PC 5 is the less strong PC characterized high loading of the element Hg due to various plants located in Tirana and by burning urban waste.

4. CONCLUSION

Ligustrum lucidum, Fam: Oleaceae is in the present investigation used as bio-indicator to monitor the level of metal contaminants (Cu, Pb, Zn, Mn, Fe, Na, K, Mg, Ca and Hg) in Tirana, Albania. Heavy metals were detected in increasing order: Hg< Pb< Cu< Zn< Na< Mn< Fe< K< Mg< Ca. The trend of

the distribution for each element is: Hg< Pb< Cu< Zn< Na< Mn< Fe< K< Mg< Ca. Results reported that calcium (Ca) has the highest level of concentration at Dëshmorët e Kombit Bulevard due to: i) tire wear particle, ii) car brake and, iii) soil dust.

Crossroads and roads with heavy traffic reported high concentration rate of heavy metals. In addition, results reported the correlation ($R2<0.45$, $p<0.05$) between Cu- Fe and a high correlation between Cu – K due to dust particles which are transported by the winds. In addition to the correlation Pb - Ca, the high correlation between Zn – Mn, Mg and Ca occurred due to traffic emission.

Statistical analysis showed high values of Max/Min values of Natrium (Na) concentration. As a natural element, Na is a very important nutrient for the plant. Cluster Analysis showed similar accumulation abilities under similar environmental conditions of heavy metals in *Ligustrum lucidum* plant. Traffic emission is the main source of pollution.

REFERENCES:

Alloway BJ, Ayres DC. 1997. Chemical principles of environmental pollution. Blackie Academic and Professional, an imprint of Chapman & Hall, 2-6 Boundary Row, London UK. **2:**196-199**.**

Akosy A, Sahin U. 1999. *Elaeagnus angustifolia* L. as a biomonitor of heavy metal pollution. *Turkish Journal of Botany*, **23(2):** 83-87.

Baker ML, De Salas MF. 2013. A Census of the Vascular plants of Tasmania. Published by the Tasmanian Herbarium, Tasmanian Museum and Art Gallery. pp: 2:323; 2:353.

Banks JA, Nishiyama T. 2011. The *Selaginella* Genome Identifies Genetic Changes Associated with the Evolution oh Vascular Plants. Published 20 may. **332 (6032):** 960-963.

Brodribb TJ, McAdam SAM. 2010. Passive origins of stomatal control in vascular plants. *Published Science*, **331 (6017):** 582-585.

Caille N, Zhao FJ, McGrath, SP. 2005. Comparison of root absorption, translocation and tolerance of arsenic in the hyperaccumulator *Pteris vittata* and then hyperaccumulator *Pteris tremula*, *New Phytologist***, 165(3):** 755-761.

Dako A, Lika M, Mankolli, H. 2010. Monitoring Aspects of Air Quality in Urban Areas of Tirana and Durres city. Podgorica, **7(2):** 549-557.

Fergunson JE. 1990. The heavy elements: chemistry, Environment Impact and Health Effect. Pergamon Press, Oxford.: 200-211.

Kabata – Pendias, A, Pendias H 1984. Trace elements in soil and plants. CRC Press, Boca raton, FL. pp: 207-209

Kukkonen J, Pohjola M, Sokhi SR, Luhana L, Kitwiroon N, Fragkou L, Rantamaki M, Berge E, Odegaard V, Slordal HL, Denby B, Finardi S. 2005. Analysis and evaluation of selected local-scale PM10 air pollution episodes in four European cities: Helsinki, London, Milan and Olso. Atmospheric Environment, **39(15):** 2759-2773.

Langard S. 1980. In Metals in the Environment.(ed. H. A. Waldron). Academic Press, London. Commission of the European Communities, Directorate-General Information Market and Innovation, Luxembourg. **Vol 4**:115,119-123.

Lika M, Coku A, Nelaj E. 2012. Health Impact Assessment of Air Pollution in Some Regions in Albania. Journal of life Sciences, **6**: 1028-1033.

Melanie B, Shelagh PK, Nigel M, Richard VL. 2011. European red list of vascular plants. Publications Office of the European Union.

Mills WB, Porcella DB, Ungs MJ, Gherini SA, Summers KV. 1985. A Screening Procedure for Toxic and Conventional Pollutants. U.S. Environmental Protection Agency, Washington DC. **1 and 2**: 38-78

Muchuweti M, Birkett JW, Chinyanga E, Zvauya R, Scrimshaw MD, Lester JN. 2006. Heavy metal content of vegetables irrigated with mixtures of wastewater and sewage sludge in Zimbabwe: Implications for human health. Agriculture, Ecosystems and Environment **112(1):** 41-48

Stroh PA, Leach SJ, August TA. 2014. A Vascular Plant Red List for England. Published by the Botanical Society of Britain and Ireland 57 Walton Road, Shirehampton, Bristol: 3-4, 21.

VENTILATOR ASSOCIATED PNEUMONIA IN THE PEDIATRIC CARE UNIT OF UNIVERSITY HOSPITAL CENTER IN ALBANIA

Irena KASMI, Sashenka SALLABANDA, Iliriana BAKALLI
Pediatric Department University Hospital Center, Tirana, Albania
Gentian KASMI
Laboratory Department University Hospital Center, Tirana, Albania
Eliana IBRAHIMI
Department of Biology, Faculty of Natural Sciences, University of Tirana, Albania.

ABSTRACT

The present paper aims to describe the rate, risk factors, and the outcome of ventilator associated pneumonia (VAP) in the Paediatric Intensive Care Unit (PICU) of University Hospital Center (UHC), Tirana, Albania. We performed a prospective study on the incidence of VAP from May 2011 to December 2012 in a single15 bed-PICU. Among six hundred and fifteen patients admitted to PICU, those who received Mechanical Ventilation (VM) for 48 hours or more were enrolled and monitored for VAP till discharge from PICU or death. VAP was defined as per CDC criteria. Data of patients with VAP was compared with those without VAP. Outcome was measured as length of PICU stay (LOS) and survival or death. During the study the use of devices (endotracheal tube [ETT], central venous catheter [CVC] and urinary catheter [UC]), enteral feeding, the use of antacids, parenteral nutrition were recorded to calculate the device associated infection rate (DAR), incidence density and device utilization ratio (DUR) and risk factors. There were 42 episodes of VAP among 270 ventilated patients, with an incidence rate 6.8 per 100 admissions or VAP rate 16 per 1000 patients-days. The incidence, incidence density, DAR and DUR among patients using ET/MV was as follows: 15.5%, 1.8 %, 34.4 per 1000 VM- days, 0.52, respectively. The group age mostly affected by VAP was children under one year old followed by other age groups ($p=0.019$). The mean duration of mechanical ventilation was 10.5 days for VAP patients and 3.5 days for non-VAP patients ($p=0.001$). The predominant isolates were gram negative (n=30, 71.4%) of which Pseudomonas aeruginosae was the most common, followed by gram positive (n=12, 28.5%) of which Staphylococcus aureus was the most encountered. Higher frequency and duration of device utilization of ETT, continuous enteral feeding, use of parenteral nutrition, primary surgical diagnosis, CVC use, CU use, were risk

factors for VAP on univariate analysis. The median LOS was longer in patients with VAP with those without (16.6 vs.7.2, *p=0.001*). The presence of VAP, was associated with a raise in mortality rate in patients with VAP compared without VAP respectively (57.1% vs. 32.9%, *p = 0.01*). In the present study the VAP rate was consistent with that reported by other similar studies in developing countries. The device associated VAP was higher than international standards. The present paper is a benchmark for further studies of VAP in the pediatric intensive care population for future comparisons. The surveillance and guidelines must become a priority to lower this studied baseline rate.
Keywords: ventilator associated pneumonia, children

1. INTRODUCTION

VAP is defined as nosocomial pneumonia in patients receiving MV that develops 48 hours or more after the initiation of ventilation. It is the second most common nosocomial infection in PICUs, with bloodstream infection being the first. It accounts for 20% of all nosocomial infections in this population (Alumneef *et al*., 2004). Such infection adversely affects patient outcome and results in considerable morbidity and mortality. It also significantly increases medical costs by prolonging PICU and hospital stay (Raymon and Aujard 2000; Stover *et al*., 2001; Urrea *et al*., 2003). The value of surveillance as an initial step toward controlling nosocomial infections was documented in the landmark Study on the Efficacy of Nosocomial Infection Control, which demonstrated that surveillance coupled with a well-run infection control program can decrease nosocomial infections by 32% (Haley *et al*., 1985; CDCP, 1997).

Given the importance of the problem, this study would help giving us initial data on incidence, risk factors, etiological organisms and outcome of this complication of intensive care. The data here provided are a means to address a better estimation of the rate and identification of the risk factors so that preventive measures and guidelines could be initiated. In Albania until now no similar studies are performed. Although consolidated data on the prevalence of NI in Albanian hospitals is lacking, it is estimated to be in the range of 10-19.1% (Faria *et al*., 2007). National Nosocomial Infections Surveillance (NNIS) System standards and definitions were used to compare results with those from developed and developing countries.

2. METHODS

Setting

The study was performed in the single 15-bed combined medical–surgical PICU of UHC, from May 2011 to December 2012. The unit admits approximately 500 patients per year and it is staffed by 5 critical care physicians

and 2-3 pediatric residents. The nurse patient ratio is 2:1 during the day and 3:1 during the night shifts.

Patients

All patients who were admitted to the PICU from May 2011 to December 2012 and who received mechanical ventilation for 48 hours or more are in the present study involved. Patients were observed daily while receiving mechanical ventilation and until 48 hours after extubation, discharge from the unit, or death, whichever came first.

Data Collection

Patients' demographics, underlying disease, duration of VM, and length of stay in the PICU were recorded prospectively by one critical care physician in charge. The potential risk factors for VAP were recorded on enrollment and were updated prospectively, as required. They included underlying diseases, continuous nasogastric feeding, parenteral nutrition and use of prophylaxis for stress ulcer. Laboratory results, radiographic reports, and microbiologic reports on the tracheal aspirate and blood cultures, were recorded for all suspected VAP patients. The diagnosis of VAP was confirmed as per CDC criteria (Garner *et al*., 1996), if there was agreement between two of the three physicians using clinical/radiological criteria. On the same day, the critical care physician also provided a description of the appearance (purulence) of the tracheal secretions. Endotracheal secretions were collected using a standard procedure after tracheal instillation of 5 ml saline and endotracheal aspirates samples were sent into a sterile container for qualitative culture. All samples were collected on the day of clinical and radiologic evaluation. No bronchoschopy, protected specimen brush or lung biopsy were performed, not being a routine in this institution.

Statistical Analysis

We used IBM SPSS version 20.0 for statistical analysis. The continuous variables were expressed as means (± standard deviation [SD]). Student's *t* test was used to compare continuous variables and chi-square was used to compare proportions. All statistical tests were two-tailed. Logistic regression analysis was used to find the independent risk factors associated with ventilator-associated pneumonia.

3. RESULTS

From May 2011 to December 2012, a total of 615 patients were admitted to the PICU and 270 (44%) who had mechanical ventilation for 48 hours or more are in the present study involved. The age patients ranged from 1 month to 14 years (mean± SD, 19.4 ±33.6 months; median, 6 months) and their demographics, underlying disease and potential risk factors are in Table 1reported. Of the 270 enrolled patients, 42 (15.5%) had VAP. The mean rate of ventilator-associated pneumonia was 34.4 per1000 ventilation-days with a ventilator utilization rate of 52%. The most common organisms causing ventilator-associated pneumonia among patients in the PICU was *Pseudomonas aeruginosae* (20, 47.6%) followed by *Staphylococcus aureus* (7; 18.9%). Nine (24.3%) of the patients had other gram-negative bacilli (Table 2).

Table 1. Characteristics of the patients in the pediatric intensive care unit receiving mechanical ventilation for 48 hours or more with and without vap

Characteristics VAP	All patients (n=270)	With VAP (n=42)	Without (n=228)
Age (months) Mean ±SD	17.9(±33.8)	21.9(±42.5)	17.2(±32.1)
Age group, n(%)			
1mo- <1 year	175(64.8)	29(69)	146(64)
2-5 years	74(26.7)	7(16.7)	65(28.5)
5-12 years	14(5.2)	4 (9.5)	10(4.4)
>12 years	9(3.3)	2 (4.8)	7(3.1)
Primary diagnosis at admission, n (%)			
Medical	106(39.3)	23(54.8)	83(36.4)
Surgical	164(60.7)	19(45.2)	19(45.2)
Emergency department	158(58.5)	28(66.7)	130(57)
Others wards	112(41.5)	14(33.3)	98(43)
Device utilization ETT, n(%)	270(100)	42(15.6)	228(84.4)
Antiacide	101(37.4)	27(64.3)	74(32.5)
Enteral feeding	230(85.2)	40(95.2)	190(83.3)
CVC n (%)	92(34.1)	20(47.6)	7(31.6)
Parenteral nutrition, n(%)	83(30.7)	29(69)	54(23.7)
CU, n(%)	240(88.9)	41(97.6)	199(87.3)
Outcome Death n, (%)	99(36.7)	24(57.1)	75(32.9)
Device duration(days), mean ±SD	4.5(±4.4)	10.5(±4.7)	3.5(±3.5)
PICU stay(days), mean ±SD	8.6(± 7.5)	16.6(±9.1)	7.2(±6.2)

Table 2.Etiological organisms for VAP (n=42)

Pseudomonas aeruginosae	20(47.6)
Staphylococcus aureus	7(16.6)
Acainetobacter baumani	5(11.9)
Klebsiella pneumoniae	4(9.5)
Enterococcus spp.	3(7.2)
Streptococcus pneumoniae	2(4.8)
Escherichia coli	1(2.4)

Results of patients receiving MV and having VAP with those receiving mechanical ventilation and not having VAP are in Table 1 reported. An association was reported between VAP and underlying diagnosis; ventilator-associated pneumonia was more common in surgical patients than in patients with medical diagnoses (Table 3). Patients with VAP had a mean duration of MV of 10.5 (±4.7) days for VAP patients and 3.5(3.5) days for non-VAP patients *(P=0.001).* The median LOS was longer in patients with VAP 16.6(±9.1) days with those without 7.2 days (±6.2) (*P=0.001*). The presence of VAP was associated with a raise in mortality rate in patients with VAP compared without respectively (57.1% vs. 32.9%; *P = 0.01*). Risk factors associated with VAP included the continuous enteral feeding (P = .001) and the use of H2-blocker *(P=0.001),* parenteral feeding *(P=0.001)* the use of CVC *(P=0.04),* the use of CU *(P=0.001).* Variables significant on univariate testing (*P* <0 .05) were entered in multiple logistic regression analysis; only parenteral nutrition (OR=3.3; 95% Cl: 1.15-9.5; p=0.04), continuous enteral feeding (OR= 1.34; 95% CI: 1.01-1.78; p=0.03), surgical status (OR=4.2; 95% Cl: 1.3-12.7; P=0.01) (Table 3) resulted risk factors.

Table 3.Logistic regression analysis of risk factors associated with vap among patients in the PICU

Risk Factor	**OR**	**CI 95**	P*
Time of ETT usage	1.32	1.18-1.48	0.001
Surgical condition	4.2	1.4-12.7	0.01
Parenteral nutrition	3.3	1.15-9.5	0.04
Continuous enteral feeding	1.34	1.01-1.78	0.03
OR = odds ratio; CI95 = 95% confidence interval. **P* < .05 considered to be significant at 5%.			

4. DISCUSSION

This prospective study is the first from the single Albanian PICU to have evaluated the rate and risk factors of VAP among pediatric patients using the NNIS System standards and definitions. Studies such as this provide a benchmark for future studies from developing countries and the region and allow for comparison of international and national data. The mean rate of VAP in this PICU was 34.4 per 1,000 ventilation-days, much higher than that reported by NNIS System surveillance of PICUs (mean 4.9 per 1,000 ventilation-days). Our rate is higher than the 90th percentile of the NNIS System, which is 11.1 per 1000 ventilation-days (NNIS, 2001).

Our rate is similar to those reported from some developing countries. Kanafani *et al*., (2003) from Lebanon reported a VAP rate in an adult ICU of 30 per 1000 ventilation-days. Khuri-Bulos *et al*., (1999) from Jordan reported a VAP rate of 19.08 per 1,000 ventilation-days in an adult medical–surgical ICU, which is also higher than the 90th percentile of the NNIS System (1999). Citak *et al*., (2000) from Turkey reported a nosocomial infection rate in a PICU of 45%; ventilator-associated pneumonia accounted for most (67%) of these nosocomial infections. In consecutive studies conducted in Egypt in ICU and PICU of different health care facilities during the period 2008-2010, were reported very high VAP rates 31.7 and 36.5 per 1000 device days, which are from the highest figures reported in the literature (Rasslan *et al*., 2012; El-Kholi *et al*., 2012).

The reasons for our high rate compared with that of the NNIS System are difficult to ascertain. The first reason is that this is an individual study performed only in one PICU. Previous individual studies from hospitals in the United States that were not participating in the NNIS System also showed a higher rate (Richards *et al*., 1999; Bauer *et al*., 2000; Elward *et al*., 2002). Elward *et al*., (2002) reported a mean VAP rate in a PICU of 11.6 per 1000 ventilation- days while Richards *et al*., (1999) reported a rate of 5.9 per 1,000 ventilation-days. This difference in the rate of VAP could have resulted from the type of patients admitted to each unit. A recent report demonstrated that rates of nosocomial infections including VAP differed by the type of patients in PICUs. It showed that PICUs that serve mainly cardiothoracic surgery patients have lower rates than do other PICUs (Epps *et al*., 2002). Therefore, the type of patients admitted to our unit being 60% surgical and 65% age group 1 month-1 year could have influenced our higher VAP rate. In the future, more stratification by type of patient and age group may be required. Another reason of the high rate of VAP registered in the study is the way used to collect specimen and the etiological agent identification method. The open endotracheal aspiration is routine in our PICU because is easy to perform, safe for the patient, requires little technical

expertise and no specialized equipment. Confirmation of VAP is difficult; confirmation of etiology usually requires a lower respiratory tract culture, including bronchoalveolar lavage, or protected specimen brush, so tracheal aspirate culture can over diagnosis VAP compared with lower tract specimen invasively obtained of clinically suspected cases. Although an etiological diagnosis is made from a respiratory tract culture, colonization of the trachea precedes development of pneumonia in almost all cases of VAP, and therefore a positive culture cannot always distinguish between pathogen and a colonizing organism. However, a sterile culture from the lower respiratory tract in an intubated patient, in the absence of a recent change in antibiotic therapy, is strong evidence that pneumonia is not present, and an extra pulmonary site of infection should be considered. The etiological cause of pneumonia can be defined by semi quantitative cultures of tracheal aspirates or sputum. Tracheal aspirate cultures consistently grow more micro-organisms than do invasive quantitative cultures, and most microbiology laboratories report the findings in a semi quantitative manner to avoid this disadvantage of the qualitative culture (Luna and Chirino 2004).

The risk factors associated with VAP in our population were not different from those cited in previous reports (Beck-Sague, 1996; Elward 2002). In our study mechanical ventilation, continuous enteral feeding, the use of nasogastric tube, the H2-blocker use, parenteral nutrition, the presence of CVC, CU were associated with VAP in univariate analysis. Continuous enteral feeding is associated with a higher gastric pH and increased gastric colonization with gram-negative organisms. Intermittent feeding is associated with a lower gastric pH. Intervention to prevent VAP by controlling the gastric pH through the use of prophylaxis for stress ulcers has been assessed in adults and, more recently, in children (Yildizdas *et al*., 2002; Lopriore *et. al*., 2002). In our study, the H2-blocker ranitidine was used in 37% of the patients receiving ventilation resulting to be a risk factor for VAP. The role of H2-blocker is still controversial, with some studies showing protection and others showing no difference. Randomized, controlled trials in children comparing continuous enteral feeding with intermittent feeding with or without prophylaxis for stress ulcers are needed to institute appropriate preventive measures. Alexis *et al*., (2009) showed that administering parenteral nutrition supplements can also increase the rate of VAP in ventilated pediatric patients. They also considered CVC to be a risk factor for VAP.

The results showed that patients with VAP have a median LOS longer than those without, a greater mortality rate than do patients without VAP which compiles with similar studies (Alexis *et al*., 2009; Ramya *et al*., 2009).

The most common organisms observed in our study were *Pseudomonas aeruginosa*e and *Stafilocccus aureus*. Therefore, empiric antibiotics should

be used for all possible Pseudomonas aeruginosae and Stafilococcus spp. cases in pediatric ventilated patients if VAP occurs.

Alexis *et al*., (2009) showed that Pseudomonas aeruginosa was the most common VAP pathogen in pediatric patients, whereas Ramya *et al*., (2009) reported that Staphylococcus aureus was the most common. *Hina et al*., (2010) also showed that Pseudomonas aeruginosa was the most common pathogen in adult ICUs.

Prior antibiotic therapy was not studied as a risk factor for VAP in our study, although it has been mentioned in studies of adults (Beck-Sague 1996; Bauer 2000; Gruson 2003). In our study, approximately 98% of the patients in VM and 100% of them with VAP were taking antibiotics prior to its development. Treatment with antibiotics may affect the ecology of colonization with gram-positive or gram-negative organisms. Also, antibiotic treatment selects for resistant organisms already present in the respiratory tract in small inocula. This study couldn‘t demonstrated the role of antibiotic use in developing VAP in the PICU. A recent study demonstrated that rotation of antibiotics could improve the susceptibilities of the antibiotic-resistant, gram-negative bacilli responsible for VAP in adult ICUs resulting in a decrease in the incidence of VAP (Bonten, 2000). Such strategies coupled with reasonable use of antibiotics predicting when their coverage is necessary for multiple-drug-resistant pathogens, in order to avoid under-treatment of these serious infections, are recommended and should be considered in our PICU, as an effort to decrease the rate of VAP.

The major limitation of our study is that it is a relatively small one center study, which poses difficulties to generalize the results. Numerous factors, including PRISM scores, nutritional status, narcotics use, corticosteroids use, genetic syndrome, witnessed aspiration, head position, re-intubation, known to be risk factors for VAP should be taken in consideration for future studies.

5. CONCLUSIONS

In the present study, a benchmark for VAP in the pediatric intensive care population of Albania, allowing for better comparison of national and international data and for future comparison is established. Independent risk factors for ventilator-associated pneumonia were identified and based on these risk factors, interventions should be applied.

REFERENCES

Alexis ME, David KW, Victoria JF. 2002. Ventilator Associated Pneumonia in Pediatric Intensive Care Unit Patients: Risk Factors and Outcomes. *Pediatrics*. **109**:758-764.

Almuneef M, Memish ZA, Balkhy HH, Alalem H, Abutaleb A.2004. Ventilator associated pneumonia in a pediatric intensive care unit on Saudi Arabia: a 30 month period prospective surveillance. *Infection Control and Hospital Epidemiology*. Sep; **25(9)**:7538.

Bauer TT, Ferrer R, Angrill J, Schultze-Werninghaus G, Torres A. 2000.Ventilator-associated pneumonia: incidence, risk factors, and microbiology. *Seminars in Respiratory Infections*; **15**:272-279. 20.

Beck-Sague CM, Sinkowitz RL, Chinn RY, Vergo J, Kaler W, Jarvis WR. 1996. Risk factors for ventilator-associated pneumonia in surgical intensive- care-unit patients. *Infection Control and Hospital Epidemiology*, **17**:374-376.

Bonten MJ, Weinstein RA. 2000. Infection control in intensive care units and prevention of ventilator-associated pneumonia. *Seminars in Respiratory Infections*; **15**:327-335. doi:10.1053/srin.2000.20936. PubMed: 11220415

Centers for Disease Control and Prevention. 1997. Guidelines for prevention of nosocomial pneumonia. *Morbidity and mortality weekly report*; **46(RR-1)**:1-79.

Citak A, Karabocuoglu M, Ucsel R, Uger-Baysal S, Uzel N. **2000**. Bacterial nosocomial infections in mechanically ventilated children. *Turkish Journal of Pediatrics*; **42**:39-42.

El-Kholy A, Saied T, Gaber M, Younan MA, Haleim M, El-Sayed H, et al.., **2012**. Device-associated nosocomial infection rates in intensive care units at Cairo University hospitals: First step toward initiating surveillance programs in a resource-limited country. American Journal of Infection Control.; **40(6)**: e216-e20.

Elward AM, Warren DK, Fraser VJ. **2002**. Ventilator-associated pneumonia in pediatric intensive care unit patients: risk factors and outcomes *Pediatrics*; 109:758-764.

Epps B, Edwards JR, Sohn AH, Horan TC, Gaynes RP. 2002.Improving benchmarks for surveillance by defining types of pediatric intensive care units. *American Journal of Infection Control*; **30**:68-70

Faria S, Sodano L, Gjata A, Dauri M, Sabato AF, Bilaj A, Mertiraj O, Llazo E, Kodra Y, Schinaia N. **2007.**The first prevalence survey of nosocomial infections in the University Hospital Centre 'Mother Teresa' of Tirana, Albania. *Journal of Hospital Infection*, **65**:244–250.

Garner JS, Jarvis WR, Emori TG, Horan TC, Hughes JM. 1996. CDC definitions for nosocomial infections. In: Olmsted RN, ed.: APIC Infection Control and Applied Epidemiology: Principles and Practice. St. Louis: Mosby;: pp. A-1—A-20.

Gruson D, Hilbert G, Vargas F, ValentinoR, Bui N, Pereyre S, Bebear C, Bebear CM, Gbikpi-Benissan G. 2003. Strategy of antibiotic rotation: long-term effect on incidence and susceptibilities of gram-negative bacilli responsible for ventilator-associated pneumonia. *Critical Care Medicine*; **31**: 1908-1914.

Haley RW, Culver DH, White JW, Morgan WM, Emori TG, Munn VP, Hooton TM 1985.The efficacy of infection surveillance and control programs in preventing nosocomial infection in US hospitals. *American Journal of Epidemiology*, **121**:182-205.

Hina G, Arun V, Akhya KK. 2010. A study of ventilator associated pneumonia: Incidence, outcome, risk factors and measures to be taken for prevention. *Indian Journal of Anaesthesia*, **54**:535-540.

Kanafani ZA, Kara L, Hayek S, Kanj SS. 2003. Ventilator-associated pneumonia at a tertiary-care center in a developing country: incidence, microbiology, and susceptibility patterns of isolated microorganisms. *Infection Control and Hospital Epidemiology*, **24**:864-869.

Khuri-Bulos N, Shennak M, Agabi S, Saleh S, Al Rawashdeh S, Al Ghanem S, Al Adham M, Faori I, Abu Khader I. 1999. Nosocomial infections in the intensive care units at a university hospital in a developing country: comparison with National Nosocomial Infections Surveillance intensive care unit rates. *American Journal of Infection Control*; **27**:547-552.

Lopriore E, Markhorst DG, Gemke RJ. 2002. Ventilator-associated pneumonia and upper airway colonisation with gram negative bacilli: the role of stress ulcer prophylaxis in children. *Intensive Care Medicine*, **28**:763- 767.

Luna C, Chirino Al. 2004.Qualitative cultures in ventilator-associated pneumonia – can they be used with confidence? *Critical Care*. **8(6)**: 425–426.

National Nosocomial Infections Surveillance (NNIS) System. **2001**.National Nosocomial Infections Surveillance (NNIS) System report: data summary from January 1992-June 2001, issued August. *American Journal of Infection Control*, **29**:404-421.

Rasslan O, Seliem ZS, Ghazi IA, El Sabour MA, El Kholy AA, Sadeq FM, Kalil M, Abdel-Aziz D, Sharaf HY, Saeed A, Agha H, El-Abdeen SA, El Gafarey M, El Tantawy A, Fouad L, Abel-Haleim MM, Muhamed T, Saeed H, Rosenthal VD. **2012**. Device-associated infection rates in adult and pediatric intensive care units of hospitals in Egypt. International Nosocomial Infection Control Consortium (INICC) findings. *Journal of Infection and Public Health*. Dec, **5(6)**:394-402.

Ramya S, Jeanette A, Ginny G, Wiener-Kronish J, Flori HR.2009. A Prospective Study of Ventilator Associated Pneumonia in Children. Pediatrics; 123:1108-1115.

Raymond J, Aujard Y. **2000**. Nosocomial infection in pediatric patients: a European, multicenter prospective study. *Infection Control and Hospital Epidemiology*, **21**: 260-263.

Richards MJ, Edwards JR, Culver DH, Gaynes RP.1999. Nosocomial infections in pediatric intensive care units in the United States. *Pediatrics*; 103:e39.

Stover BH, Shulman ST, Bratcher DF, Brady MT, Levine GL, Jarvis WR. 2001. Nosocomial infection rates in US children's hospitals' neonatal and pediatric intensive care units. *American Journal of Infection Control*, **29**:152-157.

Urrea M, Pons M Serra M, Latorre C, Palomeque A. 2003. Prospective incidence study of nosocomial infections in a pediatric intensive care unit. *Pediatric Infectious Disease Journal*; **22**:490-493.

Yildizdas D, Yapicioglu H, Yilmaz HL. 2002. Occurrence of ventilator-associated pneumonia in mechanically ventilated pediatric intensive care patients during stress ulcer prophylaxis with sucralfate, ranitidine, and omeprazole. *Journal of Critical Care*, **17**:240-245.

EVOLUTION OF KRUJA CARBONATE PLATFORM IN THE SOUTH OF ELBASAN-DIBËR TRANSVERSE (TOMORRI AND DAJTI SUBZONES)

Pëllumb SADUSHI
National Scientific Center of Hydrocarbours, Tirana, Albania
Shyqyri ALIAJ
Institute of Seismology, Tirana, Albania
Vangjel SYLARI
National Geological Survey, Tirana, Albania

ABSTRACT

The present investigation is based on a biostratigraphic study carried out by Koroveshi *et al*., (1999) which provides information about marked changes of Cretaceous carbonate facies in the Kruja zone, south of Elbasan-Dibër transverse. The Kruja zone consists of two subzones with typical structural and paleogeographical evolution features: a) the Tomorri subzone which includes Tomorri, Kulmaka and Qeshibeshi brachyanticline structures, has evolutional features of an internal carbonate platform up to the Lower Cretaceous (Albian), and an external platform with plunging tendency towards the Ionian basin from the Late Albian-Early Cenomanian to the Eocene age and, b) Dajti subzone which includes Valesh and Tërvolli crest anticlines, represented an internal carbonate platform from Cretaceous up to Eocene age. The Kruja zone structures during the Pliocene-Quaternary neotectonic stage were affected by an extensional tectonics that caused its fracturing via longitudinal and transversal normal faults.
Keywords: Kruja zone: Tomorri and Dajti subzones, structure, stratigraphy, paleogeographic and geodynamic evolution

1. INTRODUCTION

The Kruja zone is considered a unique tectonic zone over all its extension (Biçoku *et al*., 1970; Shehu *et al*., 1990; Meço *et al*., 2000). Only the biostratigraphical investigation concerning the carbonate deposits of this zone in the south of Elbasan-Diber transverse, carried out by Koroveshi *et al*., (1999), reported some new data about the marked changes of Cretaceous carbonate facies: i) shallow carbonate facies in Renc, Kakariq, Makaresh, Dajt, Letan,

Valesh and Tërvoll anticline structures that form its eastern part and, ii) transitional carbonate facies that has benthic and planktonic faunal associations - a mixed facies in Ishm, Tomorr, Kulmak and Qeshibesh anticline structures composing the western part of Kruja zone.

Based on the aforementioned data, Xhomo *et al*., (2002) reported that the Kruja zone is divided into: i) the Dajti subzone extending from Renc and Kakariq structures in the north to the Tërvolli one in the south and, ii) the Tomorri subzone that includes the Tomorri, Kulmaka, Qeshibeshi and Ishmi structures.

Based on a stratigraphic study involving the Tomorri anticline section, Kondo *et al*., (1971) identified the Kruja external subzone due to the alternation of neritic and pelagic facies. Here, neritic facies prevailed.

In a subsequent investigation, Heba (2008) reported that the Kruja platform consists of: i) the Eastern part (from Renc and Kakariq to Tërvoll) which during the Cretaceous and Paleocene was characterized by sedimentation of internal platform and external platform sedimentation during the Middle and Upper Eocene age. These two sedimentation regimens were separated by a sedimentation break, proving the emersion episodes with continental erosions, at times associated with bauxites and, ii) the western part (Kulmak, Qeshibesh and Ishm) characterized by internal platform sedimentation from Albian (Lower Cretaceous) to Lower Maastrichtian (CsB6) and a differentiated sedimentation from the Upper Maastrichtian (CsB7) to the Middle-Upper Eocene: the external platform type and the basin type. The large stratigraphic breaks in the carbonate series and the polygenic breccias in Kulmaka and Qeshibeshi structures prove that the synsedimentary tectonics is of great impact.

The present paper provides information about the Tomorri and Dajti subzones based on the geological data concerning the Tomorri and Kulmaka anticlines (Tomorri subzone) and Tërvolli anticline (Dajti subzone).

2. THE GEOLOGIC STRUCTURE OF TOMORRI AND DAJTI SUBZONES

2.1 TOMORRI SUBZONE

Rich in transitional carbonate facies, the structure of Tomorri subzone is geologically represented by the Tomorri-Kulmaka anticline chain where two positive structural lines could be distinguished: i) Tomorr-Çorovodë-Lemnicë-Lengaticë-Melesin anticlinal line and, ii) Kerpicë-Kulmakë-Qeshibesh anticlinal line. In the west, the Tomorr-Kulmaka anticlinal chain is associated by a regional thrust fault. Investigating the Tomorri and Kulmaka structures is of great interest for the Kruja carbonate platform.

2.1.1 Tomorri Anticline

Brachyanticline in shape, the Tomorri anticline represents the largest structure of the region. Referring to the transitional marly packet, it has a north-north east extension 22 km long and 5.5 km wide. Its core comprises the Lower Cretaceous dolomites, dolomitic limestones and Upper Cretaceous limestones. The flanks and the south pericline consist of the Eocene limestones and Lower and Middle Oligocene flysch (Figure 1). At the summit (2379 m), Tomorri Mountain is represented by Eocene limestones of the eastern flank that go parallel with the structural ridge. Along its extension, Tomorri anticline is associated in the western flank by a thrust fault, which dipping plane angle becomes softer at the depth (Figure 1). The pericline in the north is more abruptly plunged due to the normal transverse faults. Consequently, a graded dipping toward the north was created. In the south, the pericline has a gradual dipping that creates a separation pass with Çorovoda anticline, which core consists of Eocene limestones.

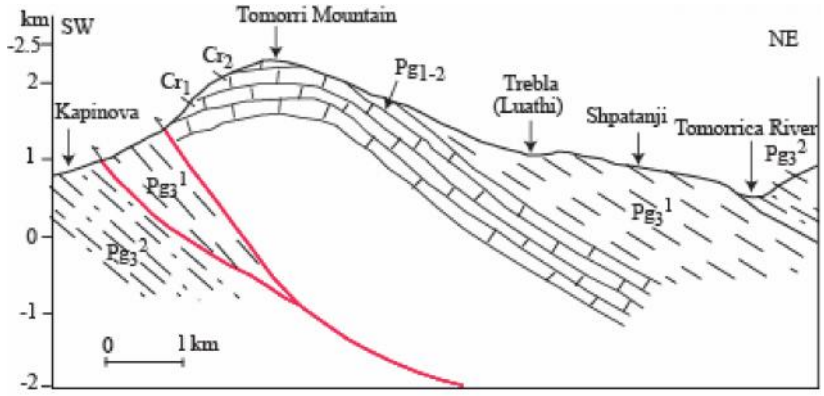

Fig. 1: Geological cross-section through Tomorri anticline.

2.1.2 Kulmaka Anticline

Based on the Upper Cretaceous limestones' data, the Kulmaka anticline is a brachyanticline fold (15 x 5.6 km) with an altitude of 2174 m and a stepwise coextension with the Tomorri structure. In addition, it consists mostly of Cretaceous limestones and less by Paleocene-Eocene bioclastic limestones. In the north, it meets the southern Tomorri pericline at the Kulmaka Pass and overlays it southwards. The two structures are separated from each other at Kulmaka Pass by Lower Oligocene flysch deposits delimited in their both sides by normal faults of Y type (Figure 2). A structure apex could be noted near the

Devri Pass. The eastern flank consists of Upper Cretaceous limestones dipping towards the east with the angle varying from 15° to 30°-40°. In addition, these limestones are covered by transgressive Eocene limestones, transitional marly packet and the first three packets of Lower Oligocene age. Lower Cretaceous limestones could be met at the western flank (Heba, 2008). Kulmaka structure is fractured by three longitudinal normal faults and some transversal ones (Shteto *et al*., 1982). Westwards, the carbonate complex is covered discordantly by Oligocene flysch. Cretaceous limestones are cut in the east by a normal fault setting them in direct contact with the younger packets of Lower Oligocene flysch deposits. The latter are covered generally by the Middle Oligocene flysch deposits (Figure 2).

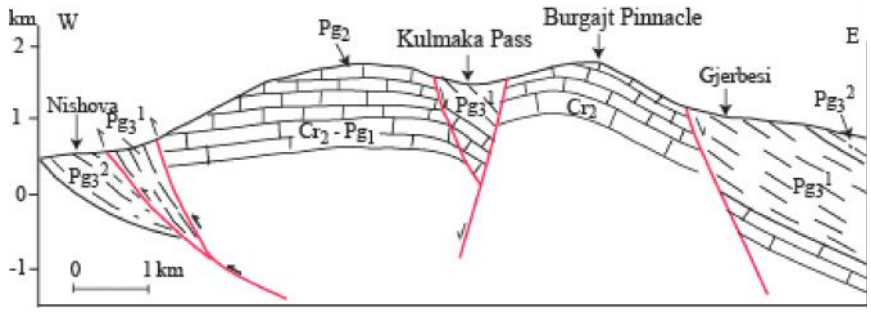

Fig. 2: Geological cross-section through southern pericline of Tomorri anticline and Kulmaka anticline.

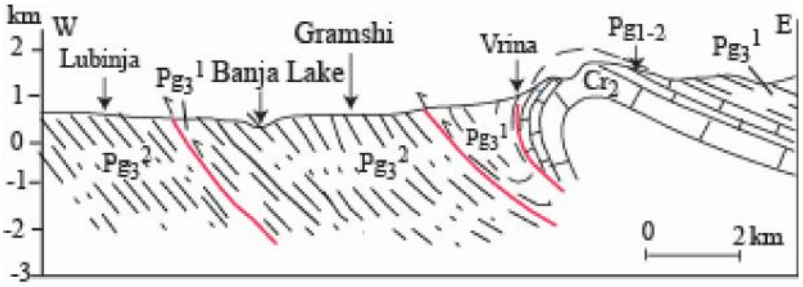

Fig. 3: Geological cross-section through Tervolli anticline.

2.2 DAJTI SUBZONE

Part of the Valesh-Tervoll anticlinal chain and with a southeast extention, Tervolli anticline structure lays in the northeast of Tomorri and Kulmaka structures as a continuation of the Dajt-Letan anticlinal chain.

Valesh-Tervoll chain is represented by Valesh and Tervoll anticlines that are

separated between them by a relatively deep pass. The Valesh anticline stucture has been complicated due to longitudinal and transversal normal faults.

2.2.1 Tervolli Anticline

Figure 3 depicts the Tervolli anticline which has a crest anticline structure, western abrupt flank with dipping angles up to 60°-70° and a soft eastern flank with dipping angles 25°-30°. Its core is consisted of Upper Cretaceous carbonate deposits and Paleocene and Middle Eocene limestones (Lower Lutetian), subsequently followed by Middle Eocene (Upper Lutetian) and Upper Eocene deposits, after sedimentation hiatus of Middle Lutetian marked by the presence of bauxites. The carbonate sequence is covered in both flanks by Lower Oligocene flysch deposits. Tervolli anticline is affected by a thrust fault along which flysch deposits of Lower Oligocene of western flank are thrusting over those of Middle Oligocene. The eastern flank of the structure is affected by some normal transversal faults. The repetition for three times of carbonate Paleocene-Eocene deposits in the Holte section proves that Tervolli anticline was affected during the neotectonics stage also by longitudinal normal faults.

Transgressive Lower Miocene deposits rich in numerous rock-forming microforaminifera could be met at both structures. Southwards, continuation of this anticlinal chain is not seen due to Devolli ultrabasic massive and Krasta zone overthrusts.

3. STRATIGRAPHY OF CARBONATE DEPOSITS

Investigations have been carried out in the stratigraphic sections of Tomorri and Dajti subzones (Dalipi *et al*., 1964; Dalipi *et al*., 1966; Peza, 1968; Kondo *et al*., 1971; Shteto *et al*., 1982; Peza and Marishta 1993; Koroveshi *et al*., 1999; Sadushi, 2000; Yzeiraj *et al*., 2002; Heba 2008). The present investigation is based on biostratigraphic studies carried out in the Tomorri, Kulmaka, Qeshibeshi and Holte anticlines by Koroveshi *et al*., (1999). The reminder provides information about the lithologic and biostratigraphic profile of each section. The structures' surface of both Tomorri and Dajti subzones comprise the carbonate formation dating from Lower Cretaceous to Upper Eocene age and flysch formation dating from Lower Oligocene to Middle Oligocene. In the present paper carbonate stratigraphic formation is reported.

3.1 TOMORRI SUBZONE

Situated in the South of Elbasani-Dibër transverse, Tomorri subzone consists of the Tomorri, Kulmaka and Qeshibeshi structures.

3.1.1 Tomorri Section (Tomorri Anticline)

Figure 4 depicts the Tomorri stratigraphic section where four lithologic bed packets could be distinguished from the bottom to the top: i) dolomitic packet, ii) the packet of clastic and organogenous limestones with cherts, iii) detritic, micritic and biomicritic skeletal limestones with dolomite concretions and, iv) the packet of micritic, clastic-organogenous limestones with cherts.

1. Dolomitic packet

The dolomitic packet is 400 m thick and represented by crystalline dolomites alternated with thick bedded and massive dolomites which in the upper part are replaced by middle bedded and thin bedded dolomites with banded and shaly structures. Here, the dolomites are not fossil-bearing rocks. Their age is Lower Cretaceous because they underlay the Aptian-Albian limestones.

2. The packet of clastic-organogenous limestones with cherts

The lower part of this packet is 55 m thick. The first layer of this packet consists of sparite, microsparite and crystalline limestones and the second layer consists of thick-middle and thin bedded bioclastic limestones with chert concretions consisting of microfacies rich in *Miliolidae, Pseudonummoloculina sp., Textularidae, Orbitolinidae, Orbitolina* (*Mezoorbitolina*) *texana, Orbitolina (conicoorbitolina) conica, Orbitolinopsis capuensis, Debarina hahounerensis, Pseudochrysaldina infracretacea, Cuneolina sp., C. pavonia, Ovalveolina sp., O. crassa, Nezzazata simplex, Bacinella irregularis, Thaumathoporella parvovesiculifera, Codiacea, Cayexia sp., Rudistae* (*Caprinidae* and *Radiolitidae)* and *Gastropoda*. Upwards, the benthic foraminifera: *Orbitolina* (*conicoorbitolina*) *cuwillieri, Nezzazatinella picardi, Cuneolina pavonia, Neoiraqia insolita, Hemicyclaminna sigali* and the planktonic foraminifera: *Hedbergella, Ticinella, Heterohelicidae* and *incertaesedis Pithonella ovalis* and *Calcispherulidae, Caprinida* and broken Rudistae could be met which prove that the lower part of the packet dates since Aptian-Cenomanian.

120 m thick, the upper part of the packet lies along a stratigraphic lacuna, on the Albian-Cenomanian deposits where the benthic foraminifera like *Acordiella conica, Montcharmontia appenninica, Scandonea sammnitica, Dicyclina schlumbergeri, Rotalia skourensis, Miliolidae, Textularidae, Pseudocyclamina sphaeroidea* and planktonic foraminifera like *Globotruncana arca, G. bulloides, Globotruncana (Marginotruncana) coronata, Globotruncana (Marginotruncana) pseudolinneiana, Globotruncana (Dicarinella) concavata, Globotruncana*

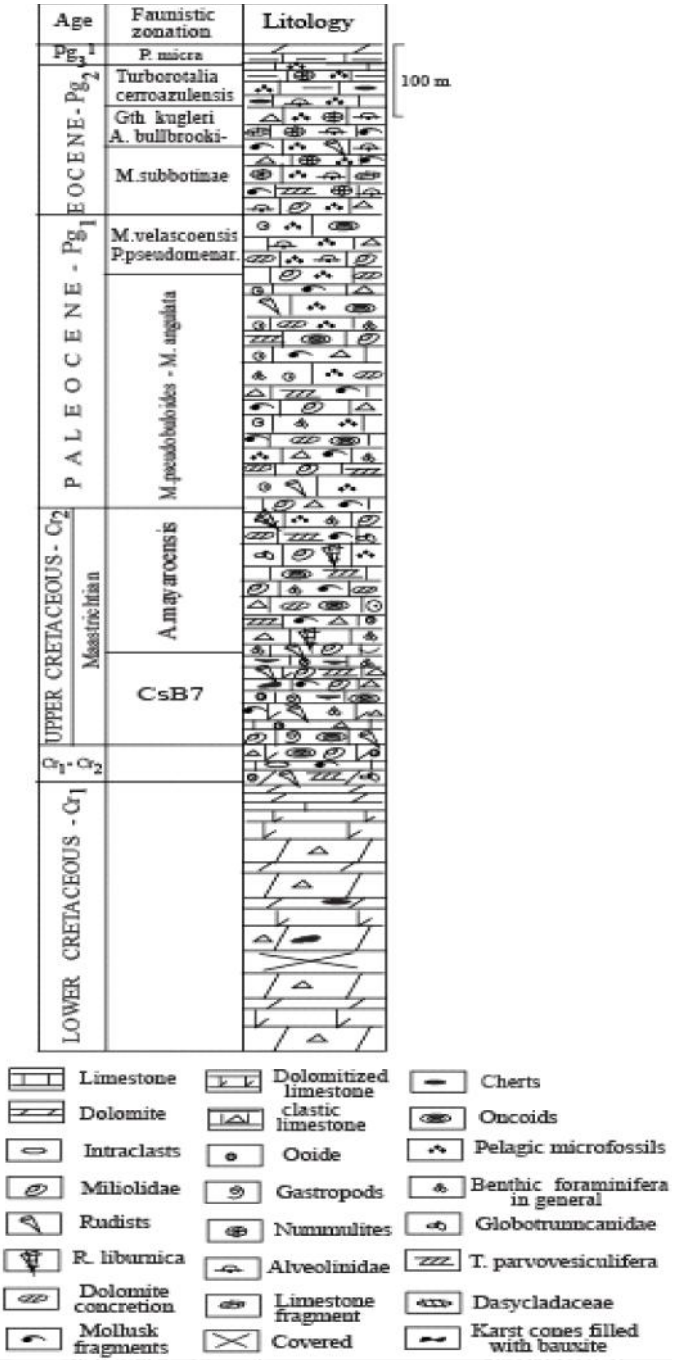

Fig. 4: Tomorri stratigraphic section (Tomorri anticline).

(Globotruncanita) stuartiformis and *Rudistae* could be met proving that the respective age is Coniacian – Lower Maastrichtian.

3. The packet of detritic and microsparitic limestones with dolomitic concretions

The lower part is represented by biomicritic, crystalline, thick-middle bedded, bioclastic limestones with oncolites and oolites (182 m thick). The latter normally overlay biomicritic and bioclastic limestones with cherts rich in *Miliolidae, Textularidae, Rotalidae, Sulcoperculina sp., Lepidorbitoides socialis, L. minor, Smoutina sp., Sirtina orbitoideus, Siderolites calcitropoides, Omphalocyclus macroporus, Orbitoides media, Rhapidionyna liburnica, Rudistae (Hipuritidae), Globotruncana arca, G. bulloides, G. lapparenti, G. (Globotruncanita) stuartiformis, G. (Globotruncanita) stuarti, G. (Rossita) contusa, Gansserina gansseri, Apathomphalus mayaroeni,* which prove that the packet dates since Middle-Upper Maastrichtian age.

The upper part of the packet is 345 m thick and represented by oolitic, oncolite-micritic, detritic limestones that either lay or are associated by a stratigraphic lacuna. *Miscellanea miscella, Glomalveolina primaeva, Discocyclina seunesi* and many planktonic foraminifera such as *Globigerina eugubina, Morozovella angulata, M. pseudobulloides, M. velascoensis, Planorotalites pseudomenardii, P. compressa, Globigerina triloculinoides* could be met confirming that it dates since Paleocene age. In these deposits, *Globigerina eugubina* planktonic zone of Danian age and the zone *Morozovella pseudobulliodes, M. angulate, Planorotalites pseudomenardii e Morozovella velascoensis* of the Middle-Upper Paleocene age have been separated. In the Paleocene turbiditic bioclastic limestones benthic and planktonic foraminifera reworked from the Upper Cretaceous deposits such as *Globotruncana, Orbitoides, Lepidorbitoides, Siderolites* and *Rudistae* could be met (Sadushi 2000).

4. The packet with bioclastic, biomicritic and micritic limestones with cherts

Here, deposits dating between Upper Paleocene and Upper Eocene could be met. The Eocene deposits are successively laying on Paleocene ones and occasionally associated with a stratigraphic lacuna. The upper part of the packet is represented by turbiditic, bioclastic, biomicritic and micritic limestones, where the following microfacies rich in planktonic foraminifera could be met: *Morozovella subbotinae, M. aqua, M., gracilis, M. formosa, M. aragonensis, M. spinulosa, M. lehneri, Acarinina bullbrooki, Truncorotaloides topilensis, Globigerina senni, Globigerinatheka kugleri, Turborotalia cerroazulensis, T. centralis, Pseudohastigerina micra,* and

Hantkenina alabamensis, along with benthic foraminifera such as *Nummulites, Discocyclina, Assilina, Alveolina, Pellatispira, Spiroclypeus and Heterostegina*. Here, zones rich in planktonic foraminifera such as *Morozovella subbotinae* dating since Lower Eocene age; the zone with *Acarinina bullbrooki* and *Globigerinatheka kugleri* of Middle Eocene age and the zone with *Turborotalia cerroazulensis of Upper Eocene* age have been separated (Sadushi, 2000).

3.1.2 Devri Section (Kulmaka Anticline)

Figure 5 depicts the Devri section where bed packets such organogenous-clastic limestones with a massive structure and bioclastic limestones and thick bedded, skeletal, micritic, oncolite limestones could be met.

1. The packet of clastic-organogenous limestones with massive structure

136 m thick, the lower part is represented by an alternation between massive bioclastic and biomicritic limestones and biosparitic and biomicritic limestones where microfacies with benthic foraminifera like *Orbitolinidae, Orbitolina (conicoorbitolina) cuwillieri, Orbitolina (conicoorbitolina) conica, Hemicyclamina sigali, Neoiraqia insolita, Cisalveolina fraasi, Ovalveolina crassa, Praealveolina gr. cretacea, Nezzazatinella picardii, Miliolidae, Textularidae, Bacinella irregularis, Thaumathoporella parvovesiculifera* and *Rudistae*, *Gastropoda* could be met. In addition, planktonic foraminifera could be sporadically met: *Hedbergella, Ticinella, Globigerinidae, Heterohelicidae and Pithonella ovalis, Calcisphaerulidae*. This assemblage dates the Albian-Cenomanian age (Koroveshi *et al*., 1999).

360 m thick, bioclastic, biomicritic and micritic limestones overlay the lower part of the packet. Here, benthic foraminifera such as *Nezzazata simplex, N. conica, Chrysaldina gradata, Biconcava bentori, Pseudonummoloculina dubia, Cuneolina pavonia, Acordiella conica, Montcharmontia appenninica, Scandonea samnitica, Rotalia skourensis, Cisalveolina fraasi, Dicyclina schlumbergeri, Pseudolituonella reicheli* and *Rudistae, Gastropoda, Thaumathoporella parvovesiculifera* could be met. In the bioclastic (turbiditic) limestones, planktonic foraminifera such as *Hedbergella, Globigerinidae, Heterohelicidae, Globotruncana arca, G. bulloides, Globotruncana (Marginotruncana) coronata, Globotruncana (Dicarinella) concavata, Globotruncana (Rossita) fornicata, Globotruncana (Globotruncanita) stuatiformis, Pithonella ovalis, Stomiosphaera sphaerica* could be met. This assemblage proves that CsB -CsB6 dates Cenomanian-Lower Maastrichtian age.

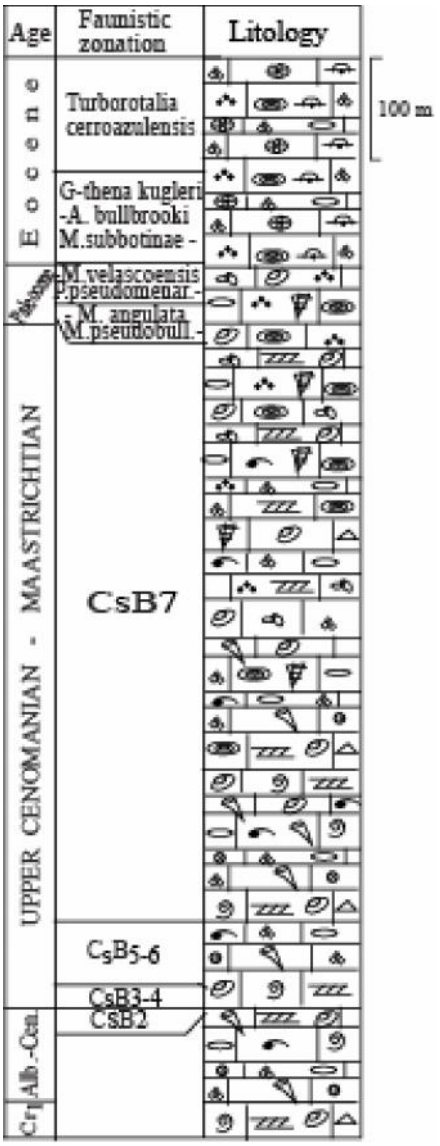

Fig. 5: Devri stratigraphic section (Kulmaka anticline).

2. The packet of bioclastic limestones and oncolite-micritic-skeletal, thick bedded limestomes

The lower part is represented by bioclastic (turbiditic) limestones and rarer by micritic and biomicritic limestones where benthic foraminifera *Miliolidae, Textularidae, Acordiella conica, Montcharmontia appenninica, Orbitoides media, Lepidorbitoides socialis, L. minor, Sirtina orbitoideus, Omphalocyclus macroporus, Siderolites calcitropoides, S. vidali, Rhapydionina liburnica* and *Rudistae (Hippuritidae), Thaumathoporella parvovesiculifera, oncoids, oolite* could be met. In addition to the benthic foraminifera, in the turbiditic limestones, planktonic foraminifera *Globotruncana bulloides, G. conica, Globotruncana (Globotruncanita) stuarti, Globotruncana (Rossita) contusa, Gansserina gansseri, Abathomphalus mayaroensis* could be met. The aforementioned assemblage proves that the benthic zone CsB7-equivalent of planktonic zones *Gansserina gansseri* and *Abathomphalus mayaroensis*- dates between Middle and Upper Maastrichtian (Sadushi, 2000).

The upper part of this packet is represented by bioclastic, biosparite, sparite, biomicrite, micritic limestones where microfacies rich in planktonic foraminifera *Globigerina eugubina, Morozovella angulata, M. pseudobulloides, M. velascoensis, Planorotalites pseudomenardii, P. compressa* and benthic foraminifera: *Miscellanea miscella, Discocyclina seunessi* and *Ethelia alba* could be met proving that planktonic zones *Globigerina eugubina, Morozovella pseudobulloides, M. angulata, M. velascoensis, Planorotalites pseudomenardi* date the Paleocene (Sadushi, 2000).

The Eocene deposits comprise the uppermost part of the packet and are represented by biomicritic and micritic limestones and less by bioclastic limestones, mainly in the lower part of the deposits. Here, facies rich in planktonic and benthic foraminifera *Morozovella aragonensis, M. aequa, M. gracilis, M. formosa, M. lehneri, M. crassata, M. subbotinae, M, spinulosa, Globigerina senni, G. linaperta, Pseudohastigerina micra, Hantkenina alabamensis, Truncorotaloides topilensis, Acarinina bullbrooki, Globigerinetheka kugleri, Turborotalia centralis, T. gr. cerroazulensis, T, cerroanzulensis cunialensis, T. cerroazulensis cocoansis, T. cerroazulensis cerroazulensis* could be met. In addition to the planktonic foraminifera, in the biomicritic limestones, benthic foraminifera: *Nummulites* and *Discocyclina, Assilina, Asterodiscus, Actinocyclina, Alveolina, Pellatispira, Spiroclypeus granulosus, Operculina, Chapmanina gassinensis, Fabiana cassi*, and *Orbitoides complanata* could be met. The zone rich in *Morozovella subbotinae* dating since Lower Eocene age, the zone rich in *Acarinina bullbrooki* and *Globigerinatheka kugleri* dating since Middle Eocene age

and the zone rich in *Turborotalia cerroazulensis* dating since Upper Eocene age have been separated (Sadushi 2000).

3.2 DAJTI SUBZONE

The Dajti subzone comprises the Valesh and Tërvoll anticliens; both located in the south of Elbasani-Dibër transverse. The Holte section is in the Tërvolli anticline included.

3.2.1 Holte Section (Tërvolli Anticline)

Figure 6 depicts the Holte section comprising the dolomite packet, packet of organogenous limestones and spathic massive limestones and, biomicritic, skeletal, oncoid, organogenous-clastic limestones (Koroveshi *et al*., 1999).

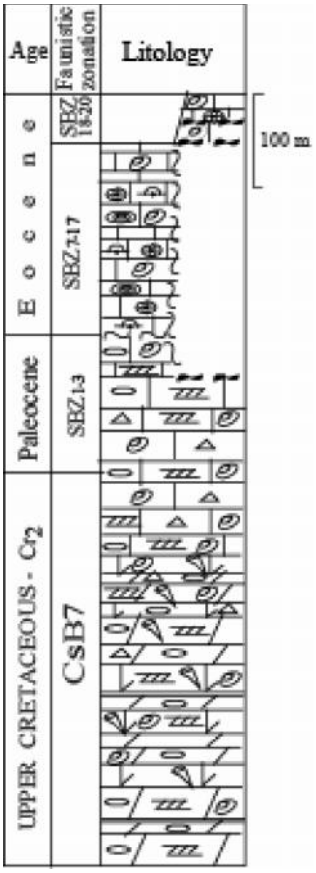

Fig. 6: Holte stratigraphic section (Tervolli anticline). The legend see Figure 5

1. Dolomite packet

290 m thick, the dolomite packet is represented by dolomites and less by calcareous dolomites, clastic dolomites, dolomitic limestones and dolomitized limestones. In dolomitic and dolomitized limestones *Acordiella conica, Scandonea samnitica, Monchtarmontia appenninica, Rotalia skourensis, Rotorbinella scarsellai, Cribrogrosella sp., Dicyclina schlumbergeri, Miliolidae, Textularidae, Minouxia sp.,* and *Rudistae (Hippuritidae), Gastropoda and Thaumathoporella parvovesiculifera* could be met proving that the packet dates since Coniacian-Campaniane age.

2. The packet of organogenous limestones and spathic massive limestones

This packet is characterized by the alternation of algal, miliolidic, biomicritic limestones with biosparitic and crystalline limestones where *Acordiella conica, Moncharmontia appenninica, Cribrogrosella sp., Minouxia sp., Rotorbinella scarselli, Thaumathoporella parvovesiculifera, Charophyta, Prochara stacheana, Stensioina surentina, Radshovenia salenitana, Aeolisacus kotorri, Scandonea samnitiac* and *Rudistae,* dating since the Upper Senonian age could be met.

3. The packet of biomicritic-skeletal- oncolite-clastic- organogenous limestones

This packet is characterized by an alternation of biomicritic and crystalline limestones. Benthic foraminifera: *Laffitteina sp., Glomalveolina primaeva, Coscinon rajkae, Fallotella alvensis, Ranikothalia sp., Microcodium elegans, Mischellanea miscella, Periloculina sllovenica* and *Idalina sinjarica* could be met at the lower part of the packet.

In the lower part of this packet have been encountered benthic foraminifera: *Laffitteina sp., Glomalveolina primaeva, Coscinon rajkae, Fallotella alvensis, Ranikothalia sp., Microcodium elegans, Mischellanea miscella, Periloculina sllovenica* and *Idalina sinjarica,* that belong to Paleocene, Upper Solandian and Thanetian, which belong to benthic zones SBZ 2-4 (Sadushi 2000). Benthic foraminifera: *Coscinolina liburnica, Alveolina cremae, A. levantina, A. violae, Discocyclina archiaci archiaci, Nummulites partschi, Cuwillierina cuwillieri, Miliolidae and Textularidae* of the Ylerdian age have been encountered in the biomicritic limestones.

In the upper part of this packet, within the limestone bedding, the bauxite levels overlay the biomicritic limestones dating since Upper Lutetian-Priabonian. These limestones correspond to the benthic zone SBZ 17-20 rich in *Miliolidae, Textularidae, Alveolina fusiformis, A. elongatae, Nummulites fabianii, N. incrasatus, N. perforatus, Heterostegina sp., Spiroclypeus granulosus,*

Asilina exponens, Asterocyclina gr. stella, Discocyclina pratti-pratti, D. nummulitica, Pellatispira madaraszi, Lituonella roberti, Dendridina, Eorupertia, Austrotrillina, Chapmanina gassinensis, Fabiana sp., Turborotalia gr. cerroazulensis, and *Pseudohastigerina micra*. The Paleocene and Eocene deposits are 517 m thick.

4. PALEOGEOGRAPHIC AND GEODYNAMIC EVOLUTION OF THE KRUJA CARBONATE PLATFORM IN THE SOUTH OF ELBASANI-DIBËR TRANSVERSE

In the present investigation, faunal and floral collections from the carbonate deposits in the Tomorri subzone were a means to address sedimentation and paleogeographic characteristics.

During the Lower Cretaceous, the Tomorri subzone represented a ridge where dolomites, dolomitic limestones, clastic-organogeneous (bioclastic) thick bedded limestones, micritic and thin-middle bedded biomicritic limestones and less oolitic and oncolite limestones of very shallow littoral facies (typical of a shallow internal platform) were deposited. Microfacies rich in benthic foraminifera such as *Orbitolinidae, Orbitolinopsis, Ovalveolina, Miliolidae, Cuneolina, Cisalveolina, Algae* like *Thaumathoporella parvovesiculifera, Aeolisacus kotorri, Codiceae, Rudistae* and *Gastropoda* could be here met. Mikrofacies rich in rock-forming *Oolits* and *Oncolites* are less met.

The benthic foraminifera, macrofossils, algae, and ooids prove the formation of these deposits in shallow sea under normal temperatures and salinity, in an internal platform and unrelated with the offshore. Formation conditions remain the same up to the Albian age (See Figure 7).

From the Late Albian and Early Cenomanian, in the Tomorri subzone (Tomorri, Kulmaka, Qeshibeshi stratigraphic sections), with the exception of neritic shallow facies, there are also limestones of mixed facies, related to the continental slope. Together with microfacies rich in benthic foraminifera of the genera *Miliolidae, Textularidae, Cuneolina, Ovalveolina* as well as abundant macrofossils as Rudistae, Gastropoda and Algae, there are planktonic foraminifera like *Heldbergella, Globigerinidae, Globotruncanidae*, Heterohelicidae and incertasedis like Pithonella and Calcisphaerula.

Planctonic foraminifera reports the sedimentation conditions in the offshore environment of an external platform continuously plunging via the continental slope towards the basin.

In the Late Albian and Early Cenomanian, Tomorri subzone (specifically, Tomorri, Kulmaka, Qeshibeshi structures) represented an external platform with plunging tendency via the continental slope towards the basin. Consequently, it could be distinguished from the easternmost part of Kruja zone, i.e., the Dajti

subzone comprising Renci, Kakariqi and Tërvolli structures. The Dajti subzone remained a ridge with a neritic sedimentation, an internal platform up to the end of the Upper Eocene. Planktonic foraminifera of the genera *Globigineridae, Turborotalia, Morozovella, Acarinina, Pseudohastigerina* appeared for the first time. The transitional marly packet sedimentation conditions show that the Kruja platform plunged into the basin conditions. Consequently, it was unified with the Ionian zone.

Sedimentation conditions remained the same throughout the Upper Cretaceous Turonian-Maastrichtian, in the Tomorri subzone, i.e., is offshore external neritic – continental slope. Thin-middle bedded, organogenous-clastic turbiditic bioclastic, biomicritic, micritic limestones whose microfacies are rich in benthic foraminifera: *Miliolidae, Textularidae, Cuneolina, Acordiella, Dicyclina, Orbitoides, Lepidorbitoides, Omphalocyclus, Rhapydionina* as well as *Rudistae, Gastropoda* and *Algae* have been deposited. In the majority of cases, Rudistae have been fragmented, as they moved and glided along the continental slope. In addition to the benthic foraminifera, planktonic foraminifera, namely the genera: *Globotruncana, Globigerinidae, Heterohelicidae* and also incertasedis *Pithonella ovalis, Calcispherula innomminata* could be met. The Senonian turbiditic and orgonogenous-clastic limestones are characterized by a great number of planktonic foraminifera; both in genera and species.

In the Paleocene, an offshore basin laid between the external neritic and continental slope where organogenous-clastic (bioclastic, turbiditic), biomicritic, micritic limestones could be met. The first small globigerina like Globigerina eugubina of Danian could be met at the micritic and biomicritic limestones. In addition to the planktonic foraminifera *Globigerina, Morozovella, Planorotalites and* benthic foraminifera as well: *Miscellanea miscella* and *Alveolina primaeva, Orbitoides, Omphalocyclus, Lepidorbitoides, Siderolites, fragmented Rudistae* and Upper Cretaceous reworked *Globotruncana* could be met.

The Tomorri subzone was found at the same conditions of deposition: biomicritic, micritic and less bioclastic turbiditic (organogenous-clastic) limestones. The Lower-Middle-Upper Eocene microfacies rich in planktonic foraminifera like *Globigerinidae, Morozovella, Acarinina, Truncorotalia, Globigerinatheka, Turborotalia, Pseudohastigerina, Chilogumbelina* could be met together with benthic foraminifera and, particularly macroforaminifera of the genera *Discyclina, Alveolina, Nummulites, Asterodiscus, Spiroclypeus, Heterostegina, Chapmanina, Assilina and Operculina* prove a sea space between external neritic and continental slope.

Geodynamic evolution of Kruja carbonate platform relates to subduction-collision mechanism. The latter is a means to address both folding and thrusting: on one side, Dajti subzone thrusts Tomorri subzone and, on the other side, Tomorri subzone thrusts the internal Ionian subzone.

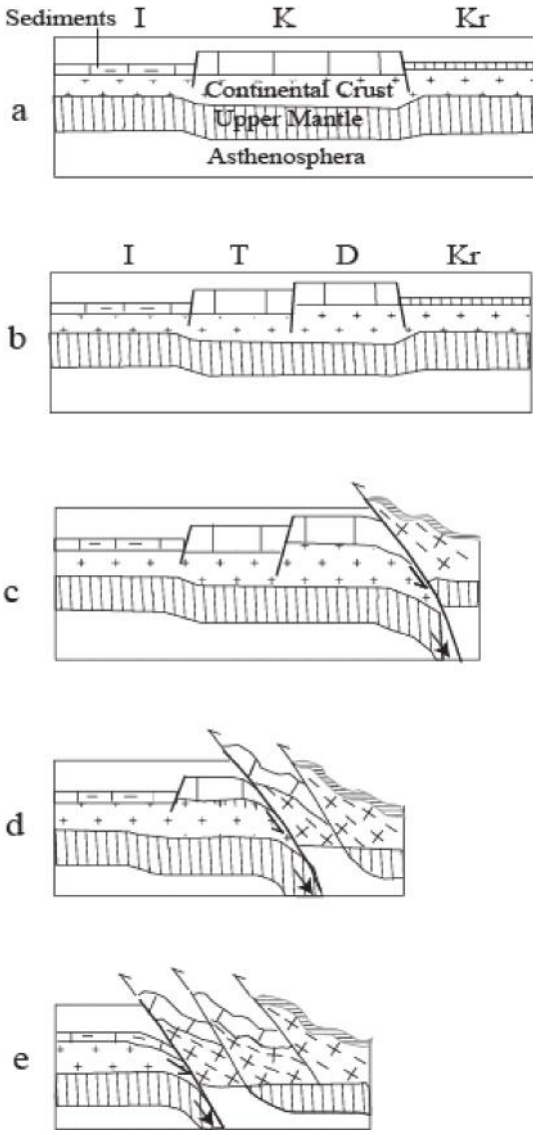

Figure 7: Evolution of Kruja carbonate platform in the south of Elbasan-Diber transverse**: a) Early Cretaceous (Albian)**: Kruja carbonate platform (K) differentiated as a neritic platform between Ionian basin (I) in the west and Krasta basin (Kr) in the east. b) **End of Albian (end of Early Cretaceous)-Cenomanian-Maastrichtian till Late Eocene**: Kruja neritic platform was broken up into two parts: Tomorri (T) external platform in the west with deepening towards the open sea of Ionian basin, and Dajti (D) internal neritic platform in the east. c) **Beginning of Early Oligocene**: Krasta basin closed and folded, meanwhile Dajti platform started subduction. d) **End of Early Oligocene:** Dajti platform folded, meanwhile Tomorri platform began subduction.e) **End of Middle Oligocene**: Tomorri platform folded, meanwhile internal Ionian basin started subduction.

Synsedimentary normal faults that broke and differentiated the Kruja platform and the basins along its sides, turned into thrusts due to compressive deformations.

The flysch formations are considered as orogenic reflection. The beginning of the flysch accumulation registers the compressive tectonic phase of the neighboring eastern unit, while the end of the flysch accumulation expresses the orogeny of the same unit where it was accumulated. Hence, in, the Kruja platform, the flysch beginning dates since the Lower Oligocene. In the Dajti subzone, the accumulation of the flysch finished at the end of Lower Oligocene. In the Tomorri subzone, it ended at the end of Middle Oligocene.

At the beginning of Early Oligocene, Krasta basin closed and folded, as the Dajti platform began its subduction underneath the Krasta thrust (Figure 7). The folding and thrusting of Dajti platform occurred as the Tomorri platform subducted at the end of Early Oligocene. The folding and thrusting of the Tomorri platform occurred at the end of Middle Oligocene, when internal Ionian basin (Berati belt) subducted. The latter folded at the end of Late Oligocene.

The Kruja zone structures were affected by an extensional tectonics during the Pliocene-Quaternary neotectonic stage that caused its fracturing by the longitudinal and transversal normal faults. Thermal waters sources met along normal faults, especially related with transversal ones in Kruja zone, testify their today's activity.

5. CONCLUSIONS

The following conclusions could be drawn: i) the Kruja zone consists of two subzones with typical structural and paleogeographical evolution features: a) the Tomorri subzone including Tomorri, Kulmaka and Qeshibeshi brachyanticline structures, with evolutional features of an internal carbonate platform up to the Lower Cretaceous (Albian), and an external platform with plunging tendency towards the Ionian basin from the Late Albian-Early Cenomanian to the Eocene age and, b) Dajti subzone including Valesh and Tërvolli crest anticlines represented an internal carbonate platform from Cretaceous up to Eocene, ii) Kruja carbonate platform evolved geodynamically due to the subduction-collision mechanism—a means to address both folding and thrusting. Kruja subzones have been structured through subduction-collision mechanism as following: i) the folding and thrusting occurred in Dajti subzone as Tomorri platform subducted at the end Early Oligocene, ii) the folding and thrusting of Tomorri subzone occurred as the internal Ionian subzone (Berati belt) subducted at the end of Middle Oligocene. The latter folded at the end of Late Oligocene and, iii) the structures in the Kruja zone were affected during the Pliocene-Quaternary neotectonic stage by an extensional tectonics that caused its fracturing by the longitudinal and transversal normal faults.

REFERENCES

Biçoku T, Pumo E, Papa A, Spiro A, Çili P, Dede S. 1970. Gjeologjia e Shqipërisë. Monografi, 343.Shtëpia Botuese "Naim Frashëri" Tiranë.

Dalipi H, Kondo A, Pejo I, Konomi J. 1964. Stratigrafia e Mesozoikut në Shqipërinë Jugore dhe Perendimore. Fondi i Institutit të Naftës dhe Gazit Fier.

Dalipi H, Kondo A, Meçaj B, Pejo I. 1966. Mbi ekzistencën e një njësie tektonike midis Zonës Jonike dhe asaj të Krujës në Shqipëri. Referat në Sesionin e II-të Shkencor të Industrisë së Naftës, Kuçovë.

Heba G. 2008. Évolution de la plate-forme carbonatée de Kruja en Albanie, du Crétacé a l'Éocène. Thèse de doctorat à l' Université de Québec, 19ç5 pp.

Kondo A, Meçaj B, Dalipi H, Pejo I. 1971. Mbi praninë e një njësie tektonike (facialo-strukturore) midis zonës Jonike dhe zonës së Krujës. Përmbledhje Studimesh. **4**, 77-90.

Koroveshi T, Sadushi P, Meçaj B. 1999. Stratigrafia e depozitimeve karbonatike të Kretë-Paleogjenit të zonës Kruja dhe brezit të Tomorrit.Fondi i Institutit të Naftës dhe Gazit Fier.

Meço S, Aliaj Sh, Turku I. 2000. Geology of Albania. Gebruder Borntraeger ser. 28, 246 pp. Berlin – Stuttgart.

Peza L. 1968. Disa të dhëna mbi stratigrafinë e strukturës të Tërvollit (Gramsh). Bul. USHT, ser. shk. nat. Nr.3, 31-40.

Peza L, Marishta S. 1983. Saktësime të mëtejshme stratigrafike lidhur me suitën gëlqerore të Holtës. Buletini i Shkencave Gjeologjike **4**, 37-71.

Sadushi P. 2000. Unifikimi i nëndarjeve biostratigrafike në faciet e cekta dhe të thella karbonatike në zonat Sazani, Jonike, Kruja dhe Krasta.Ambientet e sedimentimit dhe bashkëlidhja me zonat analoge të Mesdheut bazuar në rishikimin e materialeve ekzistuese. Fondi i Institutit të Naftës dhe Gazit Fier.

Shehu R, Shallo M, Kodra A, Vranai A, Gjata K, Gjata Th., Melo V, Yzeiri D, Bakiaj H, Xhomo A, Aliaj Sh, Pirdeni A, Pashko P. 1990. Gjeologjia e Shqipërisë. Shtëpia Botuese "8 Nëntori" Tiranë, 306.

Shteto Th, Nurçe L, Iljazi F. 1982. Ndërtimi gjeologjik dhe perspektiva naftë-gazmbajtëse e rajonit Potom-Kulmakë. Fondi i Institutit të Naftës dhe Gazit Fier.

Yzeiraj D, Fejzullahu F, Nazaj Sh, Duro P, Sadushi P, Nishani P, Prifti I. 2002. Studim gjeologjik për pjesën jugore të zonës Kruja. Fondi i Institutit të Naftes dhe Gazit Fier.

Xhomo A, Kodra A, Dimo Ll, Xhafa Z, Nazaj Sh, Nakuçi V, Yzeiraj D, Lula F, Sadushi P, Shallo M, Vranai A, Melo V. 2002. Gjeologjia e Shqipërisë. Tekst shpjegues i Hartës Gjeologjike të Shqipërisë në shkallë 1:200.000. Fondi Qendror i Gjeologjisë Tiranë, 475.

VALBONA SUBZONE, THE POSITION AND RELATION WITH MALËSI E MADHE SUBZONE

Shyqyri ALIAJ
Institute of Seismology, Tirana, Albania

ABSTRACT

The Albanian Alps zone comprises the Malësi e Madhe and Valbona subzones. Xhomo *et al*., (2002b) said that the Valbona Subzone is divided into two sectors: i) the first sector consisting of the Budaçe block and, ii) the second sector extending from north-east to south-west and consisting of Valbona, Thethi and Bishkaz-Shale tectonic blocs. As a result, the Valbona Subzone has been considered to surround the Malësi e Madhe Subzone from north, east and north-east, and interpreted as a linking slope of Malësi e Madhe platform with the Vermoshi basin, as well as with Cukali basin too (Xhomo *et al*., 2002b). The position and relation of the Valbona Subzone with the Malësi e Madhe Subzone are in the present paper re-investigated through geologic cross-sections of the Albanian Alps Zone. The facial characteristics and location of the Bishkaz-Shale block, overthrusting the Cukali-Budva Zone, prove that it belongs to the Malësi e Madhe Subzone. The Valbona Subzone is located north-east of Malësi e Madhe subzone and comprises the Budaçe block overthrusting towards the south-west Kelmendi block of Malësi e Madhe Subzone, and Valbona block that together with Thethi block overthrust towards the south-west Bishkaz-Shale block of the Malësi e Madhe Subzone. The latter overthrusts Cukali-Budva Zone for about 40 km, from north and north-west of Cukali Mountain up to Taraboshi Mountain foots, while the Valbona Subzone overthrusts the Malesi e Madhe Subzone at fronts of Budaçe and Thethi blocks. The Valbona Subzone represented throughout its paleogeographic evolution a linking slope between Malësi e Madhe neritic platform and Vermoshi pelagic basin.
Keywords: Albanian Alps zone, Valbona subzone, position and relation with Malësi e Madhe subzone.

1. INTRODUCTION

The Albanian Alps Zone (Papa and Biçoku, 1965; Biçoku *et al*., 1967; Peza, 1967) has been previously addressed to the Northern Albanian Plate or the Albanian Alps Nappe (Nopcsa, 1929) and its continuation in Montenegro has been called the Nappe of High Karst (Petković, 1961) or the Dalmatian-Hercegovian Zone (Dimitrijević, 1995).

Albanian Alps is extended between the Cukali-Budva Zone and the Gashi Zone. In Tropoja region it contacts the Mirdita Zone and in the Vermosh area the Vermoshi Zone. The Albanian Alps zone comprises the Malesi e Madhe subzone and Valbona subzone (Xhomo *et al*., 1969; Biçoku *et al*., 1970; Shehu *et al*., 1983, 1990; Xhomo *et al*., 2002b).

The Malesi e Madhe Subzone is characterized by : i) a terrigenous formation dating from the Permian to the Middle Triassic, ii) a neritic carbonate formation dating from the Middle Triassic to the Late Cretaceous where limestones rich in Globotruncana could be met and, iii) flysch dating from Paleocene to Lower Eocene.

The Valbona Subzone had stratigraphic similarities with the Malësi e Madhe Subzone up to Early Jurassic, and especially from the Dogger-Malm to the Cretaceous inclusive it was characterized by the pelagic facies, thin-bedded and siliceous limestones, and then by the Maastrichtian flysch (Meço *et al*., 2000).

Xhomo *et al*., (2002b) said that the Valbona Subzone is divided in the two sectors: i) the first sector is extended from Greca through Golishti Mountain up to Vajusha Mountain and consists of Triassic and Cretaceous deposits thrusting towards the south the Paleocene-Eocene flysch and Senonian limestones of Malësi e Madhe Subzone and, ii) the second sector is extended from Jezerca, Valbona Valleys up to Padesh and consists of Trassic-Jurassic-Cretaceous deposits, and further towards the southwest from Thethi and Curraj i Epërm to Drishti and consists of Permian-Triassic deposits thrusting towards Cukali unit in the south-east.

The first sector consists of the Budaçe block and the second sector which has a north-east to south-west extension consists of the Valbona, Thethi and Bishkaz-Shalë tectonic blocs (see Figure 1). Consequently, the Valbona Subzone has been interpreted as a linking slope of the Malësi e Madhe platform with the Vermoshi basin and the Cukali basin (Xhomo *et al*., 2002b) showing that Valbona subzone surrounds the Malësi e Madhe subzone from north-east, east, south-east and south-west. Figure 1 depicts the Valbona subzone overthrusting the Malësi e Madhe subzone from north-east, and the Cukali unit from south-east, and finally underlying the Malësi e Madhe subzone from south-east.

Such position of the Valbona subzone has been of great interest for the author who thinks that the Albanian Alps Zone comprises the Malësi e Madhe subzone and Valbona subzone in the south-west and north-east, respectively. The Valbona subzone represents a linking slope from the neritic platform of the Albanian Alps (Malësi e Madhe subzone) to the Vermoshi pelagic basin (Aliaj, 1996; 2003; 2012; Meço *et al*., 2000).

The position of the Valbona subzone is in the present paper investigated along with its relation with Malësi e Madhe Subzone based on the geologic cross-sections of the Albanian Alps Zone. The forthcoming paragraph reports the relation between the Bishkaz-Shale tectonic block and Malësi e Madhe Subzone.

The tectonic and neo-tectonic structure of Albania in the whole and its separate parts and the nappe structures widely developed in the eastern part of the country have been of great interest for the author during its fifty year work in the field of Seismology and Geology. Investigations have been time to time carried out throughout the country, results of which were presented in publications of different works and papers (Shehu *et al*., 1983; Shehu *et al*., 1990; Aliaj, 1996, 1998; Meço *et. al*., 2000; Aliaj *et al*., 2010; Aliaj, 2012 etc.).

2. GEOLOGIC SETTING OF VALBONA AND MALESI E MADHE SUBZONES

The geologic section of the Albanian Alps Zone overthrusting on the Cukali Zone begins with the terrigenous and carbonates deposits of Upper Permian - Lower Anisian and continues with Anisian siliceous and tuffites limestones and mainly platform limestones dating up to the Late Triassic. With different facial characteristics, both the Malësi e Madhe subzone and Valbona subzone have been distinguished since Jurassic time.

2.1. Valbona Subzone

The Valbona Subzone was first investigated by Xhomo *et al*., (1969). Xhomo *et al*., (2002b) said that the Albanian Alps Zone is divided into A_1 – Malësi e Madhe Subzone and A_2 – Valbona Subzone. The latter surrounds from north, east and north-east the Malësi e Madhe Subzone (Fig. 1).

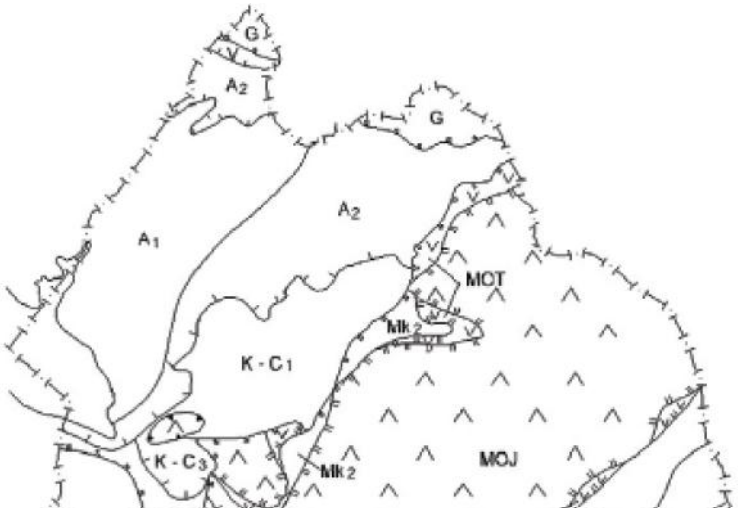

Fig. 1: Tectonic Scheme of Albania, Northern part of Albania (Xhomo *et al*., 2002).

The Budaçe, Valbona, Bishkaz-Shale and Thethi tectonic blocks could be met in Valbona Subzone (Xhomo *et al*., 2002b). Only the Budaçe and Valbona blocks have the facial characteristics of Valbona Subzone. The geologic section of Valbona Subzone is characterized by condensed Jurassic and Cretaceous carbonates of small thickness and limited extension. In Budaçe block the Cretaceous limestones overlay through a stratigraphic lacuna the Upper Triassic deposits, while in Valbona block the Cretaceous deposits normally overlay the Jurassic ones.

The Budaçe block consists of Upper Triassic and Cretaceous carbonates, Maastrichtian flysch and the Tithonian-Cenomanian flysch of Vermoshi Zone overthrusting the Budaçe block deposits. The Triassic deposits in Greca-Golisht locations overthrust towards the south the Paleogene flysch of Kelmendi block of Malësi e Madhe Subzone. The Valbona block consists mainly of Triassic deposits and less by Jurassic and Cretaceous deposits. These last two latter are characterized by condensed pelagic facies. This block shows an anticline structure with west-east extension and Jurassic-Cretaceous limestones and Maastrichtian flysch on its flanks. Bauxite layer could be met between the Middle and Upper Triassic deposits.

The Thethi block consists of Middle-Upper Triassic deposits overthrusting the Bishkaz-Shale block towards the south-west that is proved by the Zorzi Mountain klippe (Shehu *et al*., 1983; Xhomo *et al*., 2002a). The Bishkaz-Shalë block consists of Permian and Triassic deposits of low dipping towards the north-west. Here, it meets the Reç-Mardom block via a normal fault. The facial characteristics and the location of the Bishkaz-Shale block overthrusting on the Cukali Zone prove that it belongs to the Malësi e Madhe Subzone.

2.2 Malësi e Madhe Subzone

The Malësi e Madhe Subzone is characterized mainly by a monocline structure with small folding near the tectonic faults. Limited by faults, the Kelmendi, Kastrati and Reç-Mardom could be here met (Xhomo *et al*., 2002b).

Representing a monocline plate of low dipping towards north-east, the Kelmendi block consists of Jurassic-Cretaceous carbonates and Paleocene-Eocene flysch. In addition to the Kelmendi block, the Kastrati block consists of Jurassic and Cretaceous deposits of low dipping towards the south-west. The Reç-Mardom block borders from north-west with the Kastrati block and from south-east with the Bishkaze-Shalë block.

2.2.1 Bishkaz-Shalë block – an integral part of Malësi e Madhe Subzone

The Bishkaz-Shalë block is extended from Zogaj and Shiroka in the south-west of Shkodër Lake and consists of Triassic, Jurassic and Cretaceous deposits

with dipping angles 30-40° towards north-northeast, and further continues from Drisht to Kolshi Pass-Curraj i Eperm, consisted of the Permian and Triassic deposits with low dipping angles 20-25° towards north-west and north, overthrusting Cukali Zone (Fig. 2 and 4).

The almost complete Triassic-Jurassic-Cretaceous profile with low dipping angles 20-30° towards north-east follows in Montenegro territory, overthrusting the Budva Zone (analogue of Cukali Zone) (Kalezić *et al*., 1976).

An asymmetric syncline structure could be met at the front of Albanian Alps Zone with its south-western flank outcropped at Taraboshi Mountain (Fig. 2). An anticline structure of Cukali Zone consisting of Upper Cretaceous limestones and Maastrichtian-Eocene flysch could be met at Zues village, under the nappe front of Taraboshi Mountain (Aliaj, 1986; Melo, 2002; 2003, Aliaj 2003; 2012) (Figure 2).

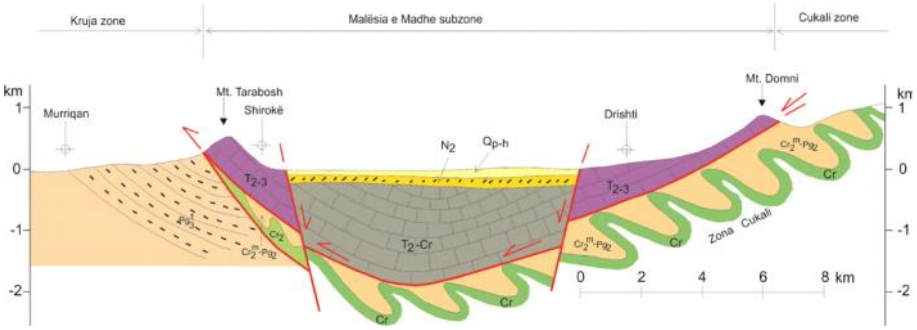

Fig. 2: Taraboshi Mountain - Domni Mountain Geologic Cross-section.

The area from the Jurassic and Cretaceous sections to pre-Late Cretaceous at Taraboshi Mountain and its prolongation in Montenegro represent characteristics of neritic facies, quite different from pelagic ones evidenced in the Valbona block.

The Kastrati, Reç-Mardom and Bishkaz-Shalë tectonic blocks represent a monocline structure with low dipping towards north-west, associated with slight positive and negative foldings, and divided by normal faults (Fig. 3). The profile of Triassic-Jurassic and Cretaceous deposits in the extension of Albanian Alps Zone is characterized by the neritic facies, proving that the Bishkaz-Shalë block is an integral part of the Malësi e Madhe subzone (Fig. 3).

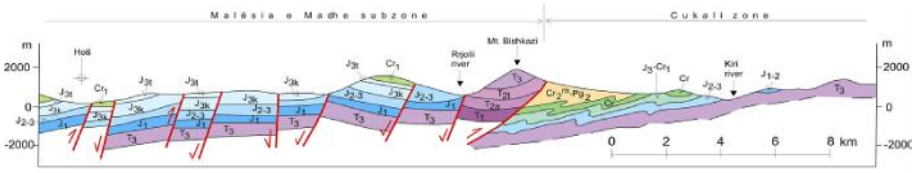

Fig. 3. Hot - Cukal Geologic Cross-Section through the extension of Albanian Alps Zone.

POSITON OF VALBONA SUBZONE IN FRAMEWORK OF ALBANIAN ALPS ZONE

The rule that the subzone differentiation can be done via the transverse profiles of tectonic zones using the contemporary criterion of tectono-stratigraphic units, i.e. tectonic subzones and zones is well known (Aliaj, 2012).

The position of Valbona Subzone and its relation with the Malësi e Madhe Subzone are here investigated via three geologic cross-sections of Albanian Alps Zone (Fig. 2, 4 and 5), and the results are compiled in the Tectonic Scheme of Albanian Alps Zone (Fig. 6).

In the Pliocen-Quaternary neotectonic stage, the Albanian Alps Zone were fractured into tectonic blocs of different dimensions by three systems of normal faults: i) the north-western system parallel with Shkoder Lake, ii) the north-eastern system parallel with Shkodër-Pejë dislocation and, iii) the little developed northern system (Aliaj, 2012).

The first two normal fault systems shows tectonic block boundaries (Xhomo *et al.*, 2002b). The third north extending system has complicated block structures, cutting and horizontally shifting also the front of tectonic subzones or zones northwards of Shkodër-Pejë transversal (Xhomo et al., 2002a).

The subzones were separated in the Albanian Alps Zone and the High Karst Zone of Montenegro by nappe boundaries

The subzones were separated in the Albanian Alps Zone and the High Karst Zone of Montenegro by nappe boundaries. The following nappe fronts in the Tarabosh Mountain-Domni Mountain and Kir-Kollate Mountain geologic cross-sections (Fig.2 and. 4) were distinguished: i) the Malësi e Madhe nappe front could be met at Taraboshi foots, Domni Mountain (Fig. 2) and the north-east of Kir village (Fig. 4 and 6), where the Albanian Alps Zone overthrust Cukali tectonic window in a saddle shape and, ii) the Valbona nappe front could be met at Thethi block front, where the Middle-Upper Triassic deposits overthrust the Upper Triassic deposits of Malesi e Madhe Subzone (Fig. 4 and 6).

The nappe front of the Valbona Subzone could be met in the south-west of Golisht Mountain, Bajzë-Vermosh geologic cross-section, overthrusting the Malësi e Madhe Subzone (Fig. 5 and 6).

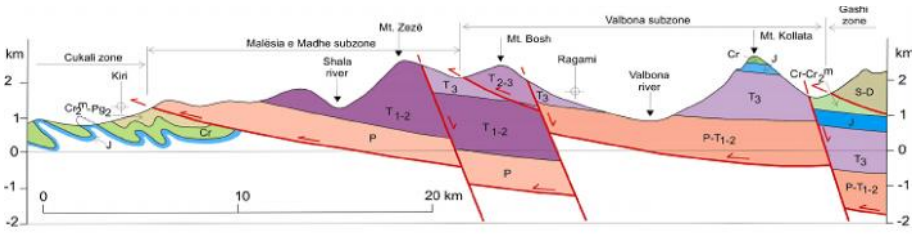

Fig. 4: Kir - Kollata Mountain Geologic Cross-section.

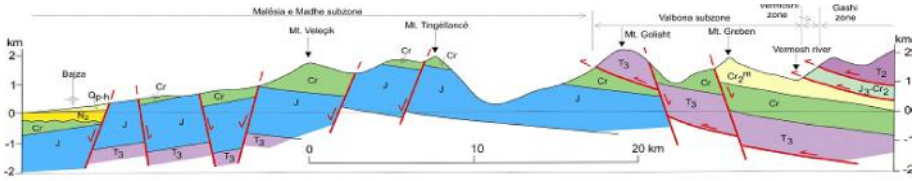

Fig. 5: Bajzë - Vermosh Geologic Cross-section.

The Tectonic Scheme of the Albanian Alps Zone with subzones was compiled based on the aforementioned differentiation of the Valbona and the Malësi e Madhe subzones in the framework of the Albanian Alps Zone, on the Scheme of tectonic blocks separated for this zone (Xhomo *et al*., 2002b) and on the role of different fault systems (Fig. 6).

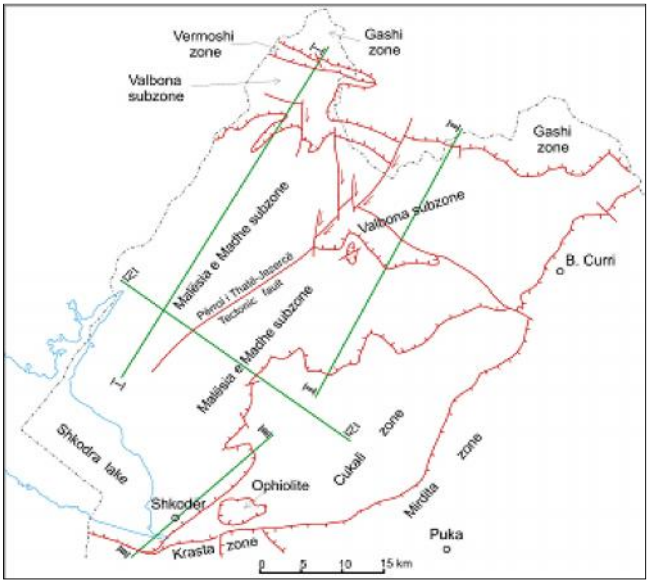

Fig. 6: Tectonic Scheme of Albanian Alps Zone with its subzones: Malësi e Madhe and Valbona. Geologic cross-sections marked on it are as following: I - I: Bajzë - Vermosh, II - II: Kir – Kollata Mountain, III - III: Taraboshi Mountain - Domni Mountain, IV - IV: Hot - Cukal.

Figure 6 depicts the Valbona nappe front from Budaçe block to Valbona one has horizontally shifted for 12-14 km towards south-west due ti the Jezerca fault segment, locating at the nappe front of Thethi block. The Jezerca fault segment of Përroi i Thatë-Jezerca fault is cut and also shifted due to some normal faults of northern system.

The Thethi block and the Valbona block divided by Ragam-Kolshi Pass fault which has a north-west extension comprise the Valbona Subzone in this sector.

4. CONCLUSIONS

The following conclusions could be drawn based on the last updated basic research work on Albanian Geology (Xhomo et al., 2002a,b) and on the analysis carried out in this paper: i) the Valbona Subzone is located in the north-east of Malësi e Madhe one and it is presented by the Budaçe block overthrusting towards south-west the Kelmendi block of Malësi e Madhe Subzone and the Valbona block together with Thethi block overthrusting towards south-west the Bishkaz-Shalë block of Malësi e Madhe Subzone, ii) the Valbona nappe front from Budaçe block to Valbona one has been fractured and horizontally shifted for 12-14 km towards south-west by the Jezerca fault segment, taking place at nappe front of Thethi block, iii) nappe fronts of Albanian Alps subzones represented by these nappe structures: the Malësi e Madhe Subzone overthrusting the Cukali-Budva Zone for about 40 km from north and north-west of Cukali Mountain up to Taraboshi Mountain foots and the Valbona Subzone overthrusting the Malësi e Madhe Subzone at fronts of Budaçe and Thethi blocks and, iv) the Valbona Subzone that represented a linking slope between the Malësi e Madhe neritic platforme and the Vermoshi pelagic basin throughout its paleogeographic evolution.

REFERENCES:

Aliaj Sh. 1986. Ndërtimi gjeologjik i zonës reth qytetit të Shkodrës Në: Koçiaj S, Sulstarova E, Aliaj Sh, Peçi V, Konomi N, Dakoli H, Kapllani L, Kozmai S, Lika M. 1986. Mikrozonimi sizmik i qytetit të Shkodrës. Instituti Sizmologjik Tiranë.

Aliaj Sh. 1996. Pozita dhe struktura gjeologjike e Shqipërisë. Në: Aliaj Sh, Melo V, Hyseni A, Skrami J, Mehillka Ll, Muço B, Sulstarova E, Prifti K, Pashko P, Prillo S. 1996. Struktura neotektonike e Shqipërisë dhe evolucioni gjeodinamik i saj. Kap. II, Instituti i Sizmologjisë Tiranë.

Aliaj Sh. 1998. Neotectonic Structure of Albania. *AJNTS*, No 4, 15-42.

Aliaj Sh. 2003. Seismic source zones in Albania. Paper presented in Albanian

Seminar, Paris June 26-28, 2003 and published in NATO Science for Peace Programme, Final Report, Project "Seismotectonics and Seismic Hazard Assessment in Albania", March 2004.

Aliaj Sh, Koçiaj S, Muço B, Sulstarova E. 2010. Sizmiciteti, sizmotektonika dhe vlerësimi i rrezikut sizmik në Shqipëri. Botim i Akademisë së Shkencave të Shqipërisë, Tiranë, 2010.

Aliaj Sh. 2012. Neotektonika e Shqipërisë, 292 f. Shtypshkronja "KLEAN".

Biçoku T, Pumo E, Xhomo A, Papa A, Spiro A, Çili P, Dede S.1967. Harta Gjeologjike e Shqipërisë në shkallë 1:200.000. Fondi Qëndror i Gjeologjisë Tiranë.

Biçoku T, Pumo E, Xhomo A, Papa A, Spiro A, Çili P, Dede S. 1970. Gjeologjia e Shqipërisë, 343 f. Monografi, Shtëpia botuese "Naim Frashëri" Tiranë.

Dimitrijević MD. 1995. Geology of Yugoslavia. Geoinstitut, Belgrade.

Kalezić M, Skuletić D, Perović Z. 1976. Geolo]ki sastav i tektonika priobalong dijela na teritoriji SR Crne Gore. Buletin Geologija, 4, 7-42.

Meço S, Aliaj Sh, Turku I. 2000. Geology of Albania. Gebruder Borntraeger ser. 28, 246 pp. Berlin – Stuttgart.

Melo V. 2002. Kap. VII – Tektonika e vonëshme dhe neotektonika. Në: Xhomo A, Kodra A, Dimo Ll, Xhafa Z, Nazaj Sh, Nakuçi V, Yzeiraj D, Lula F, Sadushi P, Shallo M, Vranaj A, Melo V. 2002b. "Gjeologjia e Shqipërisë", Tekst shpjegues i Hartës Gjeologjike të Shqipërisë shkallë 1:200.000. Monografi, Fondi Qendror i Gjeologjisë Tiranë, 475 f.

Melo V. 2003. Struktura tektonike e Shqipërisë (me të dhëna kinematike të lëvizjes dhe të fushës së sforcimeve). Studim i brendshëm, Instituti Sizmologjik.

Nopcsa F. 1929. Geographie und Geologie Nord-Albaniens. *Geologica Hungarica*, **3**, 1-620.

Papa A, Biçoku T. 1965. Mendime mbi rajonizimin tektonik të Shqipërisë. Përmbledhje Studimesh. Nr. **1**. 10-16.

Petković K. 1961. Citation from Dimitrijevic M.D., 1995. Geology of Yugoslavia. Geoinstitut, Belgrade.

Peza L. 1967. Rajonizimi gjeologo-tektonik i Shqipërisë. Botim i UT, Fakulteti Gjeologji-Miniera.

Shehu R, Shallo M, Kodra A, Vranaj A, Gjata K, Gjata Th, Melo V, Yzeiri D, Bakiaj H, Xhomo A, Aliaj Sh, Pirdeni A, Pashko P. 1983. Harta Gjeologjike e Shqipërisë në shkallë 1:200.000. NMMSK "Hamid Shijaku" Tiranë. Fondi Qendror i Gjeologjisë Tiranë.

Shehu R, Shallo M, Kodra A, Vranaj A, Gjata K, Gjata Th, Melo V, Yzeiri D, Bakiaj H, Xhomo A, Aliaj Sh, Pirdeni A, Pashko P. **1990**. Gjeologjia e Shqipërisë. Monografi. Shtëpia botuese "8 Nëntori" Tiranë, 306.

Xhomo A, Peza LH, Theodhori P. 1969. Disa facie pelagjke të Jurasikut

dhe Kretakut në Zonën e Alpeve Shqiptare. Përmbledhje Studimesh, **11**, 55-66.

Xhomo A, Kodra A, Dimo Ll, Xhafa Z, Nazaj Sh, Nakuçi V, Yzeiraj D, Lula F, Sadushi P, Shallo M, Vranaj A, Melo V. 2002a. Harta Gjeologjike e Shqipërisë në shkallë 1:200.000. Fondi Qendror i Gjeologjisë Tiranë.

Xhomo A, Kodra A, Dimo Ll, Xhafa Z, Nazaj Sh, Nakuçi V, Yzeiraj D, Lula F, Sadushi P, Shallo M, Vranaj A, Melo V. 2002b. Gjeologjia e Shqipërisë, tekst shpjegues i Hartës Gjeologjike të Shqipërisë shkallë 1:200.000. Monografi, Fondi Qëndror i Gjeologjisë Tiranë, 475.

THE EFFECTS OF CROSSOVER AND MUTATION RATES ON CHEMOTAXIS DIFFERENTIAL EVOLUTION OPTIMIZATION ALGORITHM

Yunus Emre YILDIZ
Epoka University, Tirana, Albania
Özgun ALTUN
Yildiz Technical University, Istanbul, Turkey
Ali Osman TOPAL
Epoka University, Tirana, Albania

ABSTRACT

Nature inspired, bacterial foraging optimization algorithm (BFOA), and bio inspired, differential evolution (DE), have been employed to solve complex search optimization problems. Researchers have been investigating the performance of different DE parameters (crossover rate and mutation factor) in solving optimization problems. In the present paper, the performance of a hybrid technique called Chemotaxis Differential Evolution Optimization Algorithm (CDEOA) which hybridizes BFOA with DE using different crossovers and mutation rates is reported along with the impact their combinations have on CDEOA in terms of exploration and exploitation of the population. In the present investigation, 6 unimodal and multimodal benchmark functions were involved.
***Keywords*:** bacterial foraging optimization algorithm (BFOA), nature-inspired algorithm, differential algorithm (DE), chemotaxis differential evolution optimization algorithm (CDEOA)

1. INTRODUCTION

Differential Evolution (DE) and its variants with adapted parameters have been employed to solve the real-world optimization problems. Recent studies (Zaharie 2002; Jingqiao and Sanderson, 2009; Qin *et a*l., 2009) have fostered the fine-tuning the parameters of DE. So far, Bacterial Foraging Optimization Algorithm (BFOA) has been successfully applied in the area of optimal control design (Passino, 2002), harmonic estimation (Mishra, 2005), transmission loss reduction (Tripathy *et al*, 2006).

The CDEOA's (hybrid technique of BFOA) behavior on different DE

parameter pairs such as mutation and crossover rate has been reported (Yildiz and Altun, 2015). BFOA mimics the chemotaxis behaviors of a bacterium, whereas DE employs the evolutionary operators, i.e. mutation, crossover, and selection. CDEOA hybridizes the aforementioned techniques in such a way that if a bacterium fails to explore the food, the behavior of the algorithm turns out to be explorative and, if it discover the nutrient-rich areas, the algorithm acts as an exploitative fashion.

The remainder of the paper introduces the related processes of classical BFOA (section 2), outlines the operators of the DE algorithm in sufficient details (section 3), provides information about CDEOA (section 4), summarizes the simulation results and performance comparison (section 5) and, conclusions.

Bacterial foraging optimization algorithm (BFOA)

The mechanism of Passino (2002) consisting of chemotaxis, reproduction, and elimination-dispersal is here introduced briefly. Figure 1 depicts a flowchart of BFOA adapted from (Dasgupta, 2009). A pseudo code of BFOA is embedded in the Algorithm 1.

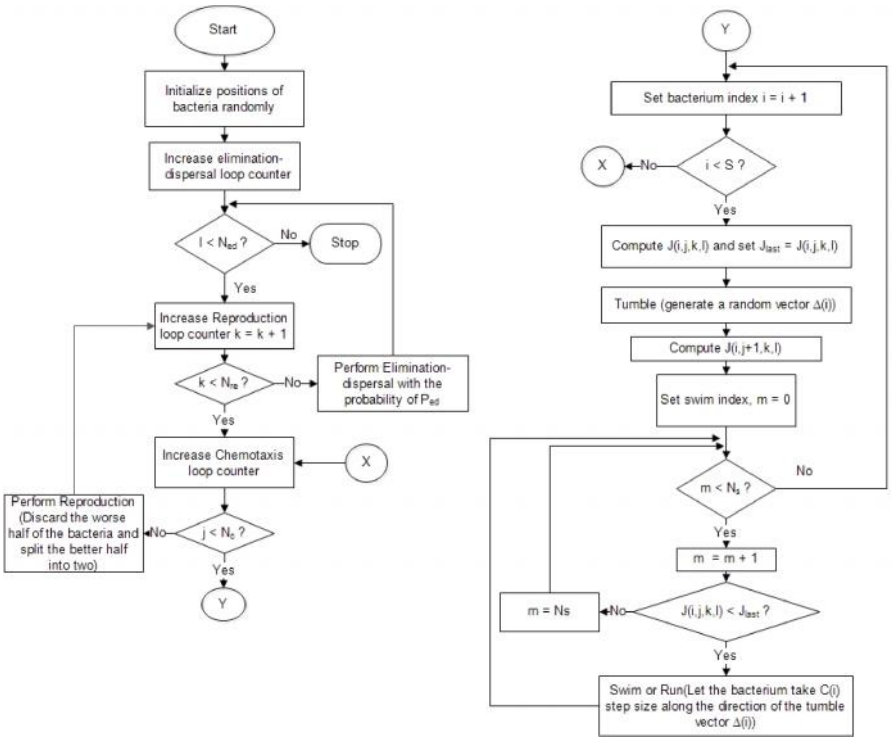

Fig. 1: A flowchart of BFOA.

Chemotaxis

An *E.coli* bacterium makes *tumble* and *run* steps in succession via flagella in its lifetime. The *tumble* is the random direction of a swim, whereas *swim* is the successive step in the same direction. θ(*i*,*j*,*k*,*l*) represents the position of the *i*-th bacterium at *j*th chemotactic, *k*th reproductive, and *l*th elimination-dispersal step. Eq. 1 and 2 refer to the position of a bacterium in the following steps:

$$\vec{t}(j) = \frac{\Delta(i)}{\sqrt{\Delta^T(i) * \Delta(i)}} \tag{1}$$

$$\bar{}(i, j+1, k, l) = \bar{}(i, j, k, l) + C(i) * \vec{t}(j) \tag{2}$$

where *C(i)* is a constant, $\vec{t}(j)$, Eq. 1 refers to the direction of the *j*th step, and $\Delta(i)$ is a random vector whose elements vary from [-1, 1].

Reproduction

The cost function values, health of a bacterium are accumulated in the life-time of a bacterium. Based on each bacterium's health, the bacteria in the swarm were classified from the lowest (the healthiest ones) to highest cost. The population members, which have lowest health, were split into two bacteria and placed at the same positions while the other bacteria were not considered.

Elimination and dispersal

In case of gradual or sudden changes such as significant rise of temperature or sudden flow of water in the environment, elimination and dispersal events may occur. BFOA mimics these events by liquidating some bacteria randomly with a predetermined probability and substituting new bacteria that are randomly launched over the search space.

Differential evolution (DE)

Differential evolution (DE) is a bio-inspired optimization method employing mutation, crossover and selection operators to solve complex problems. For each generation *G*, a new population is generated from the current population $x_{i,G}, i = 1, 2, ..., N$ where *N* is the size of the population. The initial population is randomly generated in the search space according to a uniform distribution. Once population is initialized, DE enters loop of evolutionary operations: mutation, crossover, and selection operators (Storn and Price, 1995).

Mutation

At each generation *G*, a mutant vector is generated for each target vector $x_{i,G}, i = 1, 2, ..., N$ in the current population. Some of the mutation strategies in the literature are as follows (Eq. 3- 5):

- "DE/rand/1"

$$v_{i,G} = x_{r_1,G} + F * (x_{r_2,G} - x_{r_3,G}) \quad (3)$$

- "DE/best/1"

$$v_{i,G} = x_{best,G} + F * (x_{r_1,G} - x_{r_2,G}) \quad (4)$$

- "DE/rand-to-best/1"

$$v_{i,G} = x_{i,G} + F * (x_{best,G} - x_{i,G}) + F * (x_{r_1,G} - x_{r_2,G}) \quad (5)$$

where $x_{best,G}$ is the best vector in the current generation *G*, r_1,r_2 and r_3 are different integers from each other which are selected at random out of the current population and are different from *i*th index, and *F* is the mutation scaling factor which usually ranges in [0,1+].

Crossover

Once mutation process is carried out, the target vector $x_{i,G}$ combines with the mutated vector $v_{i,G}$, and a new trial vector $u_1(i,G) = [u_1(i,1,G), u_1(i,2,G), u_1(i,D,G)]$ is generated by Eq. 6:

$$u_1(i,G) = \begin{cases} v_{1,j,G} \; if R_j(0,1) \le CR \quad \text{or } j = j_{rand} \\ v_{1,j,G} \; if R_j(0,1) > CR \end{cases} \quad (6)$$

where $j=1,2,...,D, j_{rand}$, is a randomly chosen integer within the range of [1,D]. $R_j(0,1)$ is a uniform random number between 0 and 1. For each *j*, $CR \in [0,1]$ is the predetermined crossover rate parameter.

Selection

The selection operator chooses the healthier of the parent vector $x_{i,G}$ and the trial vector $u_{j,G}$. If we have a minimization problem, the selected parent vector in the next generation is given by Eq. 7:

$$x_{i,G+1} = \begin{cases} u_{i,G} & \text{if } f(u_{i,G}) < f(x_{i,G}) \\ x_{i,G} & \text{otherwise} \end{cases} \quad (7)$$

where $f(\bullet)$ is the function for minimization. If trial vector $u_{i,G}$ yields a better fitness value than that of $x_{i,G}$, it substitutes its parent in the next generation; or the parent is retained in the search space.

Chemotaxis differential evolution optimization algorithm (CDEOA)

CDEOA is a hybrid population-based nature inspired optimization technique whose driving forces rely on the operators of chemotaxis, reproduction, mutation, crossover, and selection. It employs the local search operator (chemotaxis) from BFOA and global search operators (mutation and crossover) from DE. CDEOA works on the "weak" bacteria to make the algorithm explorative where "weak" bacteria are the individuals in positions with nutrients-poor medium and "strong" bacteria to make the algorithm exploitative where "strong" bacteria are the individuals in positions with nutrients-rich medium (`Yildiz` and Altun 2015).

Algorithm (1) Detailed pseudo-code of CDEOA

1: Parameters:
2: $p \leftarrow$ dimension of the search space
3: $S \leftarrow$ total number of bacteria in the population
4: $N_c \leftarrow$ number of chemotaxis steps
5: $N_s \leftarrow$ swimming steps
6: $N_r \leftarrow$ reproduction steps
7: $C(i) \leftarrow$ the run length unit
8: $M_t \leftarrow$ maximum number of tumble steps
9: $M_r \leftarrow$ maximum number of run steps
10: $f \leftarrow$ objective function to be minimized
11: // Initialize some local variables
12: $E_t \leftarrow 0$ // bacterium's unsuccessful tumble step
13: $E_r \leftarrow 0$ // bacterium's successful run step
14: $\theta_{best} \leftarrow$ random position in the search space
15: $f_{best} \leftarrow f(\theta_{best})$
16: $M_{fes} \leftarrow$ maximum number of FEs allowed
17: $N_{fes} \leftarrow 0$ // current number of function evaluations
18: // Define a helper function J that will call the actual objective function f. This helper function also updates the N_{fes}, θ_{best}, and f_{best} variables.
19: function $J(\theta)$:
20: $v \leftarrow f(\theta)$
21: $N_{fes} \leftarrow N_{fes} + 1$ // update number of FEs
22: if $v < f_{best}$ then
23: $\theta_{best} \leftarrow \theta$ // update global best position
24: $f_{best} \leftarrow v$ // update global best function value
25: return v
26: end // function
27: while $N_{fes} < M_{fes}$ do // FEs control loop
28: for k from 1 to N_r do // Reproduction loop
29: for j from 1 to N_c do // Chemotaxis loop
30: for i from 1 to S do // Tumble-Swim loop
31: $J_{last} \leftarrow J(\theta(i,j,k))$ // $J(.)$ computes the fitness
32: $\Delta(i) \leftarrow$ random vector within $[-1,1]$ // Tumble
33: $\theta(i,j+1,k) \leftarrow \theta(i,j,k) + C(i) * \frac{\Delta(i)}{\sqrt{\Delta^T(i)*\Delta(i)}}$
34: if $J(\theta(i,j+1,k)) > J(\theta(i,j,k))$ then
35: $E_t \leftarrow E_t + 1$
36: // Swim:
37: for m from 1 to N_s do // Swim loop
38: if $J(\theta(i,j+1,k)) < J_{last}$ then
39: $J_{last} = J(\theta(i,j+1,k))$
40: $\theta(i,j+1,k) = \theta(i,j,k) + C(i) * \frac{\Delta(i)}{\sqrt{\Delta^T(i)*\Delta(i)}}$
41: $E_r \leftarrow E_r + 1$
42: else
43: $m = N_s$ // Break from swim loop
44: end // If
45: end // Swim loop
46: end // Tumble-Swim loop
47: // Exploration loop
48: for i from 1 to S do // Exploration loop
49: // Take an exploration step for bacterium i
50: if $E_t = M_t$ then
51: $\theta(i,j+1,k) \leftarrow$ random position
52: $J_{last} = J(\theta(i,j+1,k))$
53: if $J_{last} < J(i,j,k)$ then
54: $J(i,j+1,k) \leftarrow J_{last}$
55: end // If
56: $E_t = 0$
57: end // If
58: end // Exploration loop
59: // Exploitation loop
60: for i from 1 to S do // Exploitation loop
61: if $E_r = M_r$ then let bacterium undergo:
62: DE mutation, crossover, selection
63: end // If
64: end // Exploitation loop
65: end // Chemotaxis loop
66: //Reproduction
67: $J^i_{health} = \sum_{j=1}^{N_c+1} J(i,j,k)$
68: Sort bacteria cost J_{health} in ascending order. Let bacteria with the highest J_{health} values die and the remaining bacteria with the best values reproduce.
69: end // Reproduction loop
70: end // FES control loop
71: Return θ_{best}

Algorithm 1 Detailed pseudo-code of CDEOA

If the bacterium explores a nutrient-rich medium and carries on running for a predetermined M_r number of consecutive generations, this bacterium will enter exploitation state which is the use of the mutation, crossover, and selection operators of DE (line 60 in Algorithm 1). If the bacterium's current cost remains fixed for a predefined number M_t of consecutive generations, then this bacterium will enter exploration state which is its liquidation (line 48 in Algorithm 1). Yýldýz and Altun (2015) reported that the balance between exploration and exploitation of search space is established due to these two strategies. The pseudocode of CDEOA is presented in Algorithm 1.

Experimental study

The performance of CDEOA on different mutation and crossover rate pairs were tested using a set of 6 standard benchmark functions. Functions 1 and 2 are unimodal and functions from 3 to 6 are multimodal functions. Table 1 describes the benchmark functions used in the experiments. CDEOA/rand/1 implies the algorithm which employs DE/rand/1 mutation strategy (Eq. 3) whereas CDEOA/best/1 implies DE/best/1 (Eq. 4).

Tab. 1 Description of benchmark functions used. D: dimensionality of the functions

No	Name	Formula	Search space
f_1	Sphere	$f_1(x) = \sum_{i=1}^{D} x_i^2$	(-2,2)
f_2	Schwefel 2.21	$f_2(x) = max\{\|x_i\|, 1 < i < D\}$	(-2,2)
f_3	Rosenbrock	$f_3(x) = \sum_{i=1}^{D-1} \left[100\left(x_{i+1} - x_i^2\right)^2 + (x_i - 2)^2\right]$	(-2,2)
f_4	Ackley	$-0.2\sqrt{\frac{1}{D}\sum_{i=1}^{D} x_i^2} - \exp\left(\frac{1}{D}\sum_{i=1}^{D}\cos[(2\pi x_i])\right)$	(-2,2)
f_5	Rastrigin	$f_5(x) = 10D + \sum_{i=1}^{D}\left[x_i^2 - 10\cos[(2\pi x_i])\right]$	(-2,2)
f_6	Griewank	$f_6(x) = \sum_{i=1}^{D}\frac{x_i^2}{4000} - \prod_{1}^{D}\cos(\square][\frac{x_i}{\sqrt{i}}) + 1$	(-2,2)

For both CDEOA/rand/1 and CDEOA/best/1, the control parameters *F* (scaling factor) and *CR* (crossover rate) pair were set: [F:0.5, CR:0.9], [F:0.5, CR:0.5], [F:0.1, CR:0.1], [F:0.1, CR:0.9], and [F:0.2, CR:0.8]. In DE related studies, we see that the most effective range of *F* value is to be [0.4, 1.0]. Since a smaller *F* which is close to 0 has a tendency of helping the individuals have strong exploitative ability, we used $F = 0{,}1$ in two cases of our experiments. *CR* is generally to be used within the range of [0.1, 0.9] in the literature of DE. In contrast, Ronkkonen *et al*., (2005) reported that *CR* should vary between 0 and 0.2 for separable functions and between 0.9 and 1.0 for multimodal and non-separable functions. From this perspective, we can clearly understand that researchers agreed on *F* to be in the range [0.4, 1.0] and *CR* to be either close to 1.0 or 0.0, depending on the type of the problems.

The present paper investigates the quality of final solution and the convergence speed at the end of a fixed number of function evaluations (FEs). The algorithm-problem pair was launched from the same initial population to make the comparison fair. All functions were tested in 30 dimensions with $3x10^5$ FEs. For the CDEOA, following parameter values of classical BFOA were chosen: $N_c=100$, $N_s=16$, $N_{re}=8$, $C(i)=0.1$. Each method was run 25 times with a suite of functions and the statistics are in Table 2 and 3 reported. The convergence graph was plotted in Fig. 2 and 3. The horizontal axis of these graphs is the number of function evaluations, and the vertical axis is the mean of function values.

Comparison of five mutation and crossover rate paired techniques based on DE/rand/1 mutation strategy

DE/rand/1 (Eq. 3), one of the most used mutation strategy, is characterized by a slow convergence speed. In addition, it exhibits much stronger exploration ability as three individuals acting in distinct search space information out of the current population are randomly chosen. Here, the aforementioned mutation strategy empowers the exploitation ability. In contrast, it slows down the exploitation ability of an individual (Qin, *et al*., 2009).

Table 2 Compares CDEOA/rand/1 mutation and crossover rate pairs over 6 benchmark functions of 30 dimensions using 300000 function evaluations. “Mean error” indicates the average of the error function values in 25 trials, respectively

Tab. 2: Comparison of CDEOA/rand/1 mutation and crossover rate pairs over 6 benchmark functions of 30 dimensions using 300000 function evaluations.

	Functions	[F:0.5, CR:0.9] Mean Error	[F:0.5, CR:0.5] Mean Error	[F:0.1, CR:0.1] Mean Error	[F:0.1, CR:0.9] Mean Error	[F:0.8, CR:0.2] Mean Error
f_1	Sphere	9.27E-09	9.02E-09	1.77E-06	3.31E-03	9.09E-09
f_2	Schwefel 2.21	1.59E-02	1.03E-02	4.29E+00	2.53E+01	9.41E+00
f_3	Rosenbrock	2.57E+01	2.37E+01	2.15E+01	3.68E+01	2.23E+01
f_4	Ackley	1.66E+00	1.66E+00	1.66E+00	1.67E+00	1.66E+00
f_5	Rastrigin	1.69E+01	3.22E+00	1.75E+00	4.00E+01	3.30E+00
f_6	Griewank	4.93E-04	8.89E-09	4.19E-08	6.54E-03	8.91E-09

Unimodal functions

In these two unimodal functions in Table 2, [0.5, 0.9] and [0.5, 0.5] exhibit superior performance to the other [*F*,*CR*] pairs. Even though the *CRs* are different in each pair, they end up with the similar results. We can infer that $F = 0.5$ and *CR* which is within the range of [0.5, 0.9] yield better results in terms of quality of final solution. [0.1, 0.9] is unable to perform well in two unimodal problems because *F* which is close to 0.0 has tendency to lead less exploration ability in searching the search space.

Multimodal functions

In these four multimodal functions in Table 2, [0.5, 0.5] and [0.8, 0.2] pairs exhibit similar performance and outperform the others. [0.1, 0.1] is the second best pair although its *F* value is close to 0.0. We can also observe that [0.1, 0.1] and [0.8, 0.2] are the best in Rosenbrock due to its characteristics. In addition, a similar performance regardless the different *F* values could be shown.

Comparison of five mutation and crossover rate paired techniques based on DE/best/1 mutation strategy

Strategies based on the best solution such as “DE/best/1”, “DE/best/2” and “DE/rand-to-best/1” possess the fast convergence rate and are efficient in unimodal problems. On the other hand, they can tend to get stuck at a local minima. Consequently, they could converge to the global optimum prematurely (Qin *et al.*, 2009). Table 3 compares CDEOA/best/1 mutation and crossover rate pairs over 6 benchmark functions of 30 dimensions using 300000 function evaluations. “Mean error” indicates the average of the error function values in 25 trials, respectively. Figure 2 depicts the convergence behaviors of six functions to the global optimum.

Tab. 3: Comparison of CDEOA/best/1 mutation and crossover rate pairs over 6 benchmark functions of 30 dimensions using 300000 function evaluations.

Functions		[F:0.5, CR:0.9]	[F:0.5, CR:0.5]	[F:0.1, CR:0.1]	[F:0.1, CR:0.9]	[F:0.8, CR:0.2]
		Mean Error	Mean Error	Mean Error	Mean Error	Mean Error
f_1	Sphere	7.87E-09	8.48E-09	2.38E-04	2.49E-03	9.31E-09
f_2	Schwefel 2.21	5.71E-01	7.46E-01	1.01E+01	2.24E+01	3.54E+00
f_3	Rosenbrock	7.97E-01	6.25E+00	2.77E+01	2.87E+01	2.15E+01
f_4	Ackley	1.66E+00	1.66E+00	1.66E+00	1.66E+00	1.66E+00
f_5	Rastrigin	4.14E+01	1.32E+01	1.75E+01	1.25E+02	6.17E+00
f_6	Griewank	5.51E-03	4.92E-03	2.91E-05	7.50E-03	9.12E-09

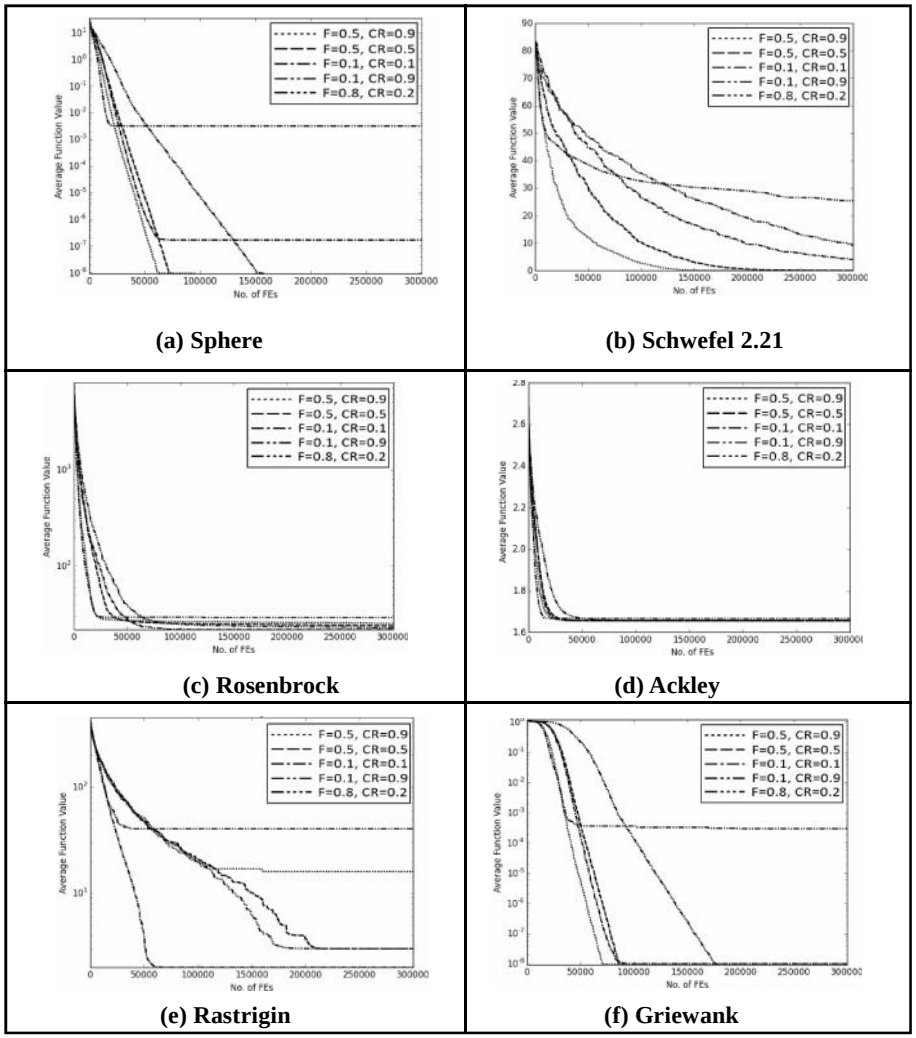

Fig. 2 Convergence behaviours of six functions to the global optimum.

Unimodal functions

In these two unimodal functions in Table 3, we can observe similarities as opposed to the CDEOA/rand/1 simulation results in Sphere function. [0.1, 0.9] does not perform due to its small *F* value. On the other hand, [0.5, 0.9] performs better than that of the others, since *F*=0.5 keeps the individual's exploration and exploitation abilities and *CR*=0.9 inherits most of the information from mutated vector (Eq. 6). Figure 3 depicts the convergence behaviours of six functions to the global optimum.

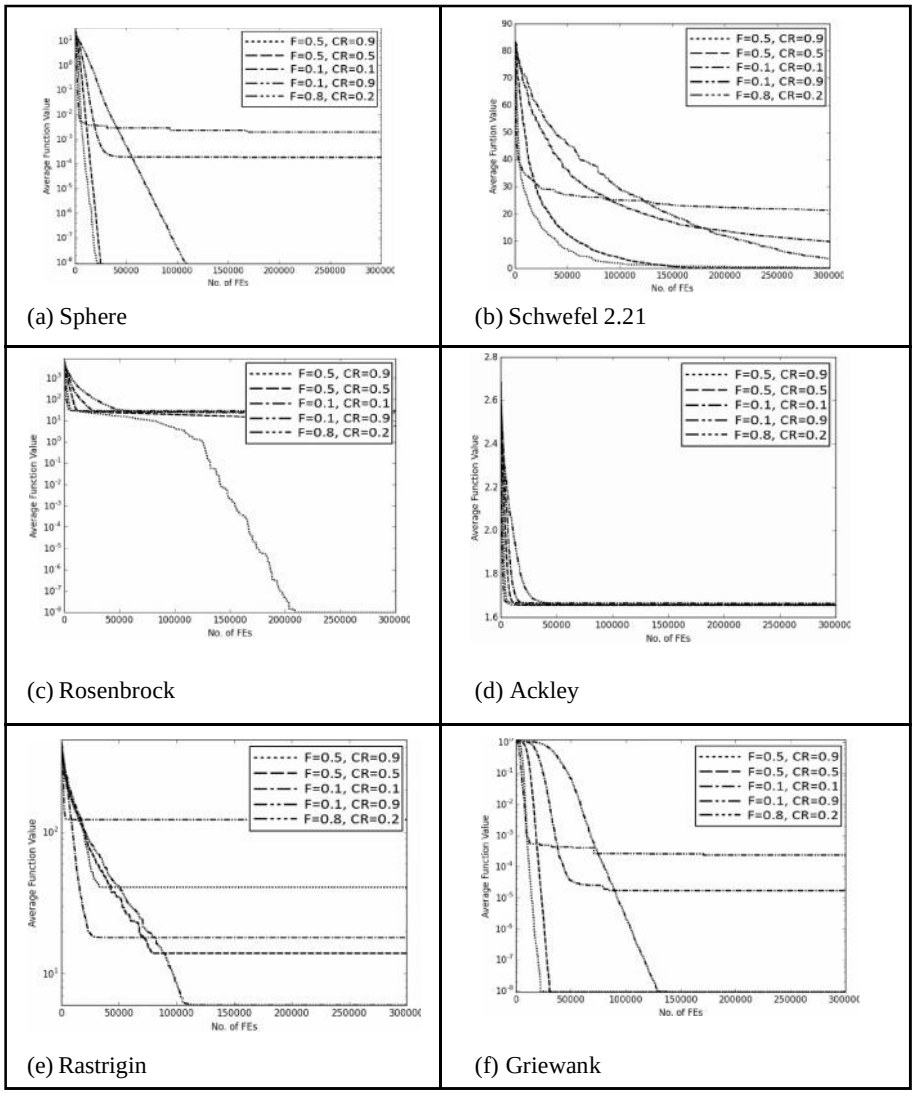

Fig. 3: Convergence behaviours of six functions to the global optimum.

Multimodal functions

In these four multimodal functions in Table 3, [0.5, 0.9] exhibits great performance in Rosenbrock. The pairs in both CDEOA/rand/1 and CDEOA/best/1 simulation results of Ackley show identical performances. It is obvious that [0.8, 0.2] outperforms the other pairs in Griewank and Rastrigin.

The convergence maps of [0.5, 0.9], [0.5, 0.5], [0.1, 0.1], [0.1, 0.9], and [0.8, 0.2] are reported in Fig. 2a-2f and Fig. 3a-3f. [0.8, 0.2] converges better than the others in Rastrigin (Fig. 2e, Fig. 3e) in both CDEOA/rand/1 and CDEOA/best/1 simulations. It is clear that each pair in both tests converged to the global optimum in Ackley (Fig. 2d, Fig. 3d) prematurely. Due to the use of the DE/best/1 (Eq. 4) strategy in CDEOA/best/1, we observe faster convergence than the others. [0.5, 0.9] possesses premature convergence in Rosenbrock (Fig. 3c) CDEOA/rand/1 simulation like the others. However, it exhibits great convergence performance in Rosenrock's CDEOA/rand/1 (Fig. 2c) while the rest of the pairs fail.

2. CONCLUSIONS

CDEOA/best/1 exhibits better performance than CDEOA/rand/1 in sphere. CDEOA/rand/1 outperforms the CDEOA/best/1 in Shwefel 2.21 showing that the behavior of CDEOA depends on unimodal functions. In multimodal functions, CDEOA/best/1 is generally better than CDEOA/rand/1 in Rosenbrock with the exception of [0.1, 0.1] and [0.8, 0.2] pairs, so these exceptions have a great impact in the success of CDEOA/best/1. Regardless the different [*F, CR*] pairs, both CDEOA/rand/1 and CDEOA/best/1 possess identical results in Ackley. CDEOA/rand/1 exhibits in Rastrigin and Griewank better performance than CDEOA/best/1. We can infer that the results are problem specific. In particular, $F \in [0.1, 0.5]$ tends to yield better performance while *CR* is equal to 0.5. Generally speaking, there are no common parameter settings for all the problems. Rather, there is an optimum parameter values for each problem after fine-tuning experiments. The Python source code of the CDEOA can be found in (https://sites.google.com/site/yeyildiz12/).

REFERENCES

Dasgupta S, Das S, Abraham A, Biswas A. 2009. Adaptive Computational Chemotaxis in Bacterial Foraging Optimization: An Analysis. IEEE Transactions on Evolutionary Computation 13:919–941. doi: 10.1109/TEVC.2009.2021982.

Jingqiao Z, Sanderson AC. 2009. JADE: Adaptive Differential Evolution with Optional External Archive. IEEE Transactions on Evolutionary Computation 13:945–958. doi: 10.1109/TEVC.2009.2014613

Mishra S. 2005. A hybrid least square-fuzzy bacterial foraging strategy for harmonic estimation. Evolutionary Computation, IEEE Transactions on 9, 61–73.

Passino KM. 2002. Biomimicry of bacterial foraging for distributed optimization and control. Control Systems, IEEE 22:52–67.

Qin AK, Huang VL, Suganthan PN. 2009. Differential Evolution Algorithm with Strategy Adaptation for Global Numerical Optimization. IEEE Transactions on Evolutionary Computation 13:398–417. doi: 10.1109/TEVC.2008.927706

Ronkkonen J, Kukkonen S, Price KV. 2005. Real-parameter optimization with differential evolution. In: The 2005 IEEE Congress on Evolutionary Computation, **1:** 506–513.

Storn R, Price K. 1995. Differential evolution-a simple and efficient adaptive scheme for global optimization over continuous spaces. ICSI Berkeley.

Tripathy M, Mishra S, Lai LL, Zhang QP. 2006. Transmission loss reduction based on FACTS and bacteria foraging algorithm, in: Parallel Problem Solving from Nature-PPSN IX. Springer, 222–231.

Yildiz YE, Altun O. 2015. Hybrid achievement oriented computational chemotaxis in bacterial foraging optimization: a comparative study on numerical benchmark. Soft Computing 1–17. doi: 10.1007/s00500-015-1687-4.

Zaharie D. 2002. Critical values for the control parameters of differential evolution algorithms. In: Proceedings of MENDEL.

THE STRATIGRAPHIC AND PALEOECOLOGICAL SIGNIFICANCE OF THE BENTHIC MICROFAUNA IN THE MIDDLE AND LATE MIOCENE OF CENTRAL PART OF EXTERNAL ALBANIDES INCLUDING DURRËS REGION

Simo PRILLO
Geological Institute of Oil and Gas, Fier, Albania

ABSTRACT

Middle and Late Miocene foraminifera from various surface and subsurface sections inside and outside the Peri-Adriatic Foredeep (PAF) have been investigated and the results reported that bolivinitids and *Ammonia* genus became abundant and diverse in the Lower Miocene. Consequently, in different regions foraminiferal assemblages have different characteristics. Likely, these different lithostratigraphic units (biofacies) developed due to: i) the eustatic changes of sea level during both transgressive and regressive cycles and, ii) the presence in time and space of the different restricted and open sea paleoenvironments. The vertical and lateral migration of biofacies makes them of great interest for paleoecologic studies. The separation of two neighbouring areas within the External Albanides (EA) could be distinguished not only by their different tectono-sedimentary regimes but also by the presence or absence of keeled globorotalids taxa and the vertical migration of most of the biofacies.
Keywords: microfauna, biofacies, paleoecology, migration, stratigraphy, Miocene, External Albanides.

1. INTRODUCTION

The present investigation is based on foraminifera samples collected from surface sections, outcrops and boreholes in the last thirty years during oil and gas drillings carried out in the south of the Peri-Adriatic Foredeep (PAF) and outside it (Fig. 1). The samples are here used to address the differences in foraminiferal content between Serravallian sediments inside and outside the PAF. In Serravallian and particularly in Late Serravallian, different regions were characterized by different foraminiferal assemblages' features.

It must be emphasized the presence of Serravallian layers (likely due to Paratethys) without species or subspecies of the *Globorotalia menardii*'s evolutionary lineage, or any other taxon with keel (carina) of planktonic

foraminifera, similarly to Ros-2 borehole, the area from Roskovec to Ballshi region and the area close Patos and Turbull section. Dalipi *et al*., (1974) reported that these regions comprise the PAF because of its eastern boundary determined based on *Orbulina* genus distribution. Ballshi 1 and Ballshi 2 borehole is characterized by the Helvetian deposits overlaying transgressively the Late Oligocene deposits (Dalipi *et al*., 1974). Prillo *et al*., (1994) re-examined the Helvetian's faunal content proving the presence of the following planktons: *Globigerina falconensis* Blow, *Orbulina suturalis* Bronnimann, *Orbulina universa* d'Orbigny and *Globorotalia peripheroronda* (Blow & Banner). Consequently, these assemblages could be aged the Early Serravallian. The Serravallian Age developed due to Tethys could be distinguished by the presence of *Globorotalia menardii* (d'Orbigny) evolutionary lineage such as *G. menardii*-2,3 and *G. menardii*-4 (Tjalsma, 1971) or *Globorotalia miozea*, and *Globorotalia praemenardii* (Cushman & Stainforth). It appears that the PAF area corresponds with Tethys in External Albanides (EA), whereas outside its eastern boundary it is analogue with Paratethys. The boundary between Early and Late Serravallian is marked by the Last Occurrence Datum (LOD) of *G. peripheroronda* within and outside the PAF area, corresponding also with the boundary rich in *Globorotalia siakensis* Le Roy in the upper part and *G. peripheroronda / Orbulina suturalis* in the lower part (Iaccarino, 1985). The Albanian Geological Service-(1983; 2002) considered the boundary between Tortonian and upper Burdigalian sediments of the Thartor section as an unconformable geological one. In Lushnja section, which represents the south-eastern part of the region here investigated, the Serravallian deposits are not exposed and the section starts with *Ammonia inflata* (Seguenza) frequent biofacies followed by *Ammonia beccarii beccarii* (Linne). Biofacies dating since Late Tortonian Age prevail. In spite of that, 3 wells drilled in Karbunara-2 (Dalipi *et al*., 1974; Prillo et al. 1994), reported the presence of the Serravallian sediments without any species of *G. menardii* s.l. On the other hand, Prillo and Hasanaj (1990) reported that the geological age of deposits rich in *Ammonia beccarii* from Karbunara-2 to Ngjeqar, in Lushnja section is not the same and shifted from Late Serravallian to Early Messinian due to stratigraphical unconformity.

In the Middle and Late Miocene sediments Bolivinitidae species disappeared since the top of Miocene sequence. Consequently, the ecological data on recent taxa could not be entirely used for paleoecological interpretation of the assemblages. Here, characteristics of the benthic foraminiferal assemblages such as species dominance or species frequency in their associations, or characteristics of other groups of fossils and on other stratigraphical and sedimentological detailed data are the only means the address such an interpretation.

The present investigation was carried out in the Centre External Abanides including Durrës region where changes in the frequency of benthonic foraminifera, especially within the Bolivinitidae, occurring both laterally and vertically (from the Serravallian up to the end of the Miocene sequence) have been reported. As a result, several dominant and frequent biofacies of Bolivinitidae and *Ammonia*'s species could be distinguished and used to explain the reasons of their development and for paleoecological interpretation.

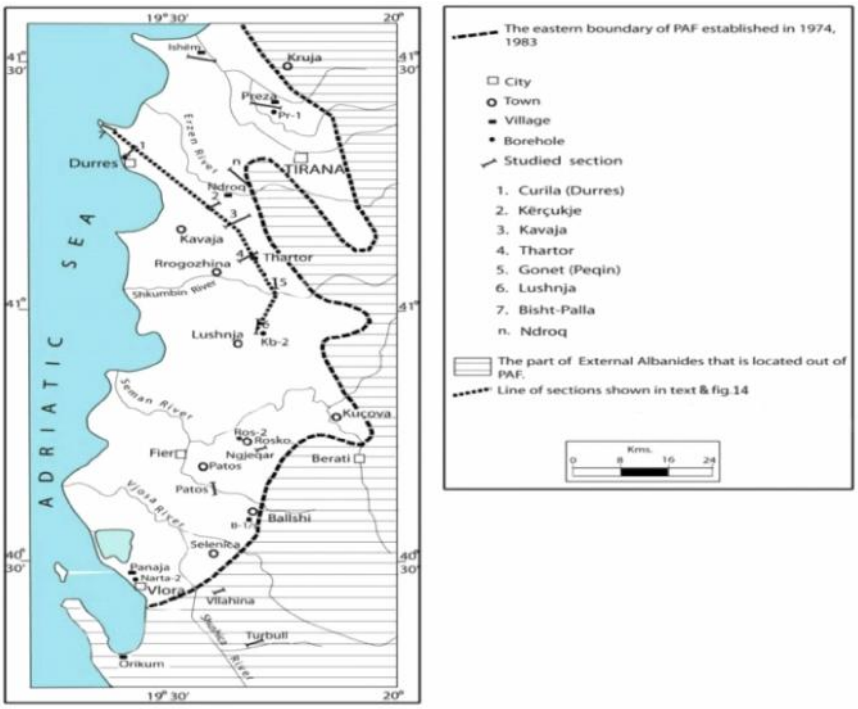

Fig. 1: Location map of study area and studied sections and boreholes.

The frequent and dominant patterns of species

During the Middle Miocene Epoch, the benthic fauna became frequent and dominant and for the first time it was reported that different areas in the Serravallian stage consisted of different composition in planktonic foraminifera. The differences in plankton content appeared since the Early Serravallian of EA because several regions that belong to the PAF area such as Ndroq, Durrës, Kavaja, Thartor, Vlora (Narta-2) are rich in plankton with carina such as *G. menardii*-2, 3, *Globorotalia miozea* Finlay. In other regions such as Roskovec, Ngjeqar, Ballsh, Vllahine and Turbull comprising the area originated from Paratethys or outside the PAF, plankton with carina never occurred as in Serravalian and in younger ages of this area. *Spiroplectammina carinata*

(*d*'Orbigny) is the only benthos which dominated its biofacies since the Early Serravallian in both areas of EA, and within the same area its occurrence might be dominant or rare. Thus, in Ngjeqar section and Ballsh-1/s, the *S. carinata* prevails, while in Vllahina and Turbull it rarely occurs. In all these cases it could be met at the same stratigraphic level corresponding with the *First Occurrence Datum* (FOD) of *Orbulina universa*. On contrary, in Ndroqi section, *S. carinata* appeared rare since Langhian, but with the FOD of *O. universa* its occurrence became frequent, whereas its abundance in Ballshi-1/s and Ngjeqar section (Fig. 2) suggested that its different occurrences are probably much more controlled by lithological compositions of sections of different studied regions than by paleobathymetry itself. In contrast, other biofacies in the forthcoming paragraph mentioned became frequent or prevailed from the Late Serravallian to Pliocene. In addition, likely their occurrence was primarily paleobathymetrically controlled in both areas.

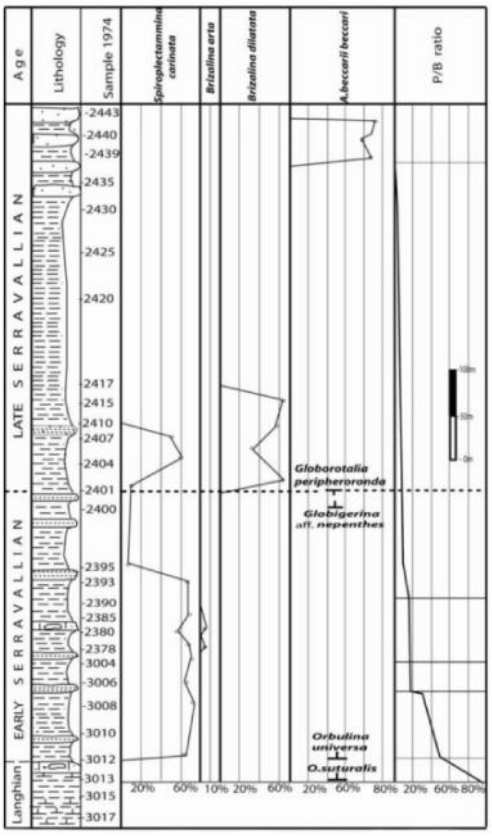

Fig. 2: The percentages of several benthos taxa among total fauna and plankton/benthos ratio in samples of Ngjeqar section.

In the area created due to Paratethys, the differences in content and occurrence of faunas between Late Serravallian and Pliocene occurred due to a final regressive cycle causing a significant shallowing by the end of the Serravallian, and the closing of the sedimentary basin from the Early to Middle Tortonian throughout the area (bioprovince) outside the PAF, e.g., in Ngjeqar and Turbull sections the disappearance of plankton in sample 2435 and 375 (Fig. 3), respectively corresponds with the beginning of the *Ammonia beccarii* Acme zone (Prillo and Hasanaj, 1990). Such a disappearance of plankton also occured in the Middle Miocene or up to Badenian/Sarmatian boundary (Rogl, 1985), which corresponds also with the uppermost part of the Serravallian. In the Serravallian Age, several plankton taxa such as *Globigerina subcretacea*, *Globigerina tarchanensis*, *Globorotalia bykovae*, *Globorotalia transsylvanica*, *Globigerinoides grilli* and genus *Velapertina* which are present in Badenian stage of the Central Paratethys, particularly in its upper part lacked. On the other hand, the absence in the Serravallian Age of the aforementioned planktonic taxa and the presence of frequent species such as *Globigerina falconensis, G. peripheroronda* (during Early Serravallian), *Globigerina decoraperta* (Takayanagi & Saito), *G. falconensis*, *G. miozea*, *G. menardii*-3 (during Late Serravallian) prove that no direct connection between the Central Paratethys and the Mediterranean (External Albanides) in the aforementioned Age has occured.

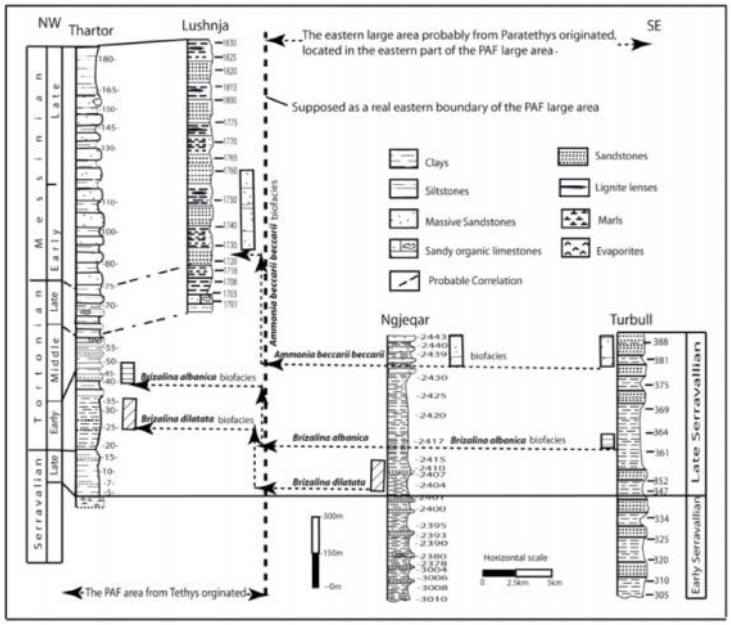

Fig. 3: Stratigraphy, migration of three different biofacies and correlation of the sections at Turbull, ngjeqar, Lushnja and Thartor.

On the other hand, the data related to these sections, especially those starting from disappearance of *Brizalina dilatata dilatata* and *Brizalina dilatata albanica* to the top of the both sections or towards *Ammonia beccarii* (Acme) zone show that there are almost no differences in content and distribution of foraminifera between them. In these sections located outside PAF and in the Thartor Section located within PAF, the differences in faunas became evident in the Late Serravallian. Likely, the source is the vertical and lateral migration only across the boundary between two large areas of the biofacies such as *B. albanica* and *B. dilatata* (Fig. 3). Other biofacies such as *Ammonia beccarii beccarii* could have migrated vertically not only between two large areas but also within the same area or from one geotectonic zone to another. Here, the difference between these two biofacies is a great vertical migration from Late Serravalian to Early Messinian of the eastern large area of the PAF.

The following biofacies could be distinguished in the deposits of EA based on migration, and frequency and dominance tendencies of several species of *Bolivina*, *Brizalina* and *Ammonia* genus dating between Late Serravallian to Pliocene:

***Brizalina arta* biofacies** could be met outside the PAF area (upper bathyal habitat). This frequent biofacies in B-1/s of Ballshi region, (Fig. 4) occurred after FOD of *Orbulina universa* d'Orbigny up to above LOD of *G. peripheroronda* (Blow & Banner) during the Early Serravallian's transgressive cycle. This borehole is represented by abundant occurrence of *S. carinata* and rare occurrence of other benthic foraminifera such as *Melonis pompiloides*, B. dilatata*, Bolivina reticulate* Hantken, *Bolivina scalprata miocenica, Bulimina costata, Bulimina inflata* Uvigerina gallowayi, Uvigerina barbatula*, Uvigerina rutila*, Uvigerina spp,. Gyroidinoides soldanii*, Ceratobulimina contraria, Siphonina reticulate*, Hoeglundina elegans*, Cibicides dutemple*i*, *Cibicides pachyderma** (frequent), while *Brizalina arta* Macfadyen comprise about 20% of the aforementioned mentioned benthos. Plankton makes up 40 to 30% of total fauna. Based on Jorissen, (1988); Barbieri, (1991) almost all the associated benthos of *B. arta* biofacies suggest for an upper bathyal palaeoenvironment.

ii) Located in the Thartor section from the sample 7 to 17, within PAF (upper bathyal habitat), ***Brizalina arta* biofacies** remains more or less lithologically unchanged as between samples 5 and 7 (Fig. 5). The sandstone beds' thickness varies from 0.3 to 0.5 meter and the P/B ratio (40 to 30%) remains stable. Figure 6 depicts the biofacies found in Kavaja section, between the samples 2020 and 2027. Its upper boundary in both sections corresponds approximately with FOD of G. menardii-4.

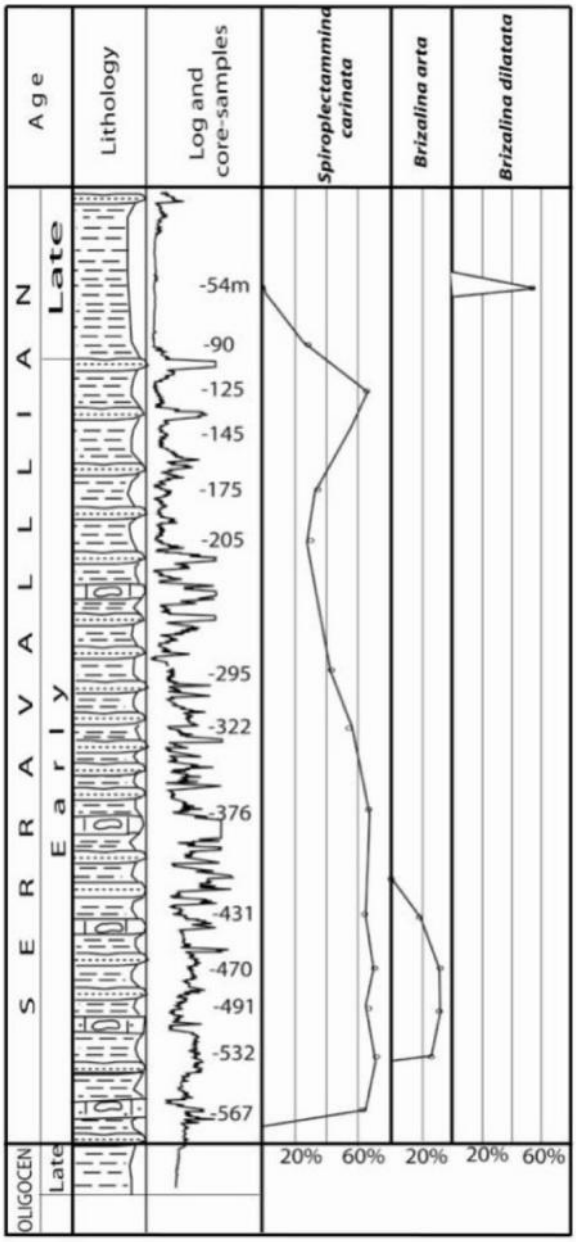

Fig. 4: The percentages of several benthos taxa among total fauna in Ballshi-1/s borehole.

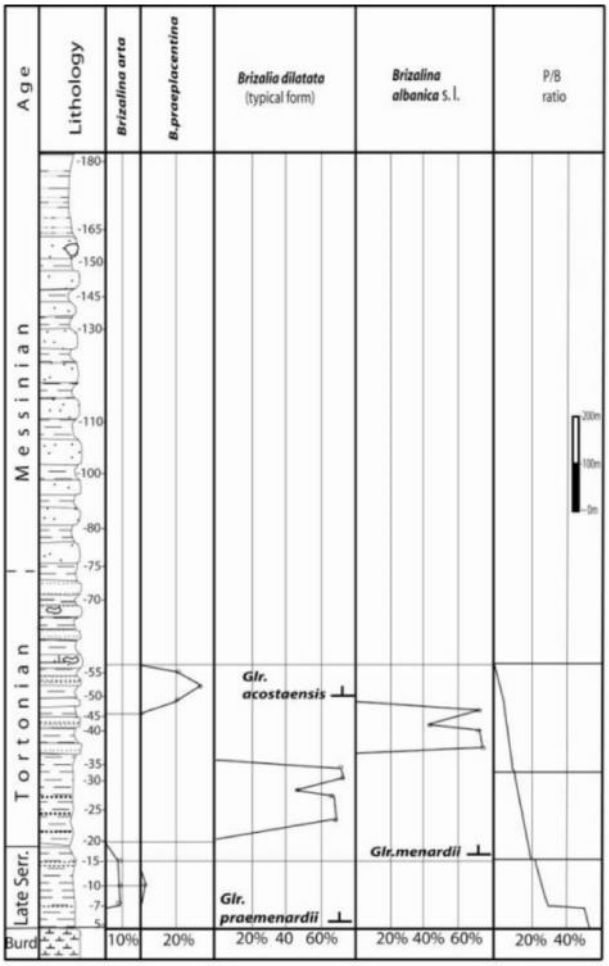

Fig. 5: The percentages of specimens of the Bolivinitidae's species among the total benthos and plankton/benthos ratio in samples of Thartor section.

Kavaja section is almost lithologically similar to the Thartor where the *B. arta* and *Uvigerina peregrina* are the most frequent species, comprising 10% and 14% of the total number of benthos, respectively. In the Kavaja section, they comprise 12% and 16% of total number of benthos, respectively. The *B. arta* dominates the bolivinitid faunas where *B. dilatata, Bolivina antique, B. praeplacentina* and *B. scalprata miocenica* could be rarely met. The benthos marked with* are common for both biofacies, outside and inside the PAF area. Moreover, all the aforementioned species and other benthos such as *U. peregrina* Cushman (frequent), *Uvigerina striatissima* Perconig,

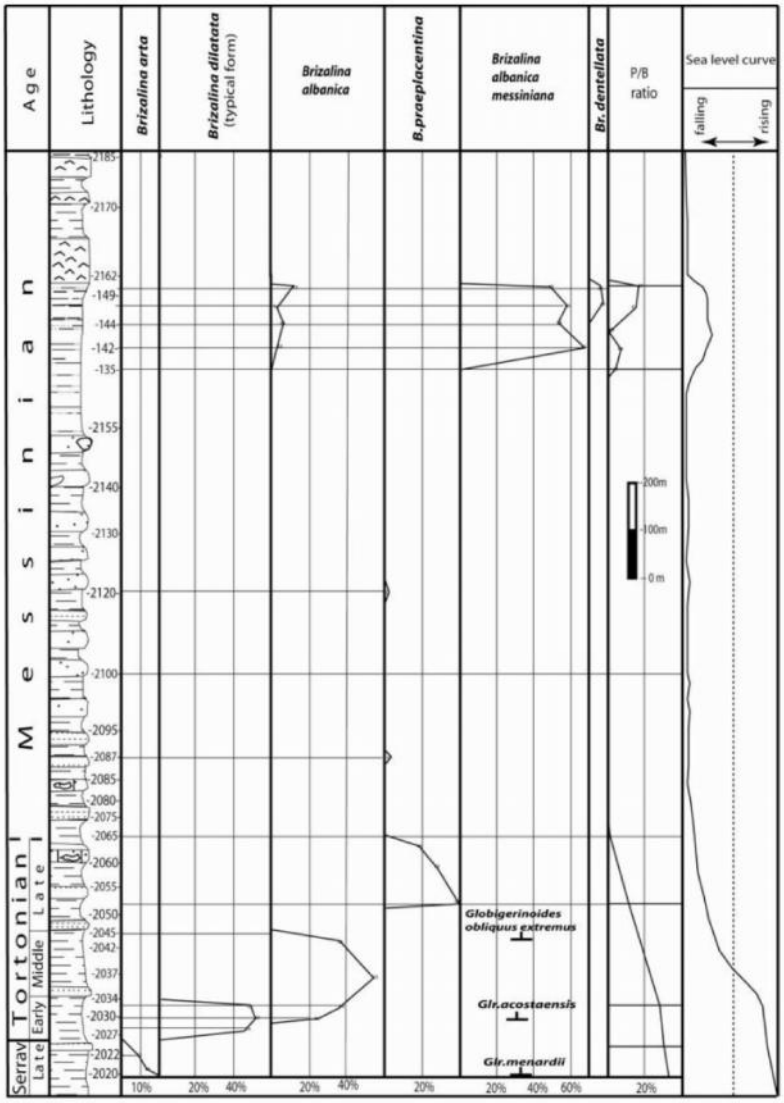

Fig. 6: The percentages of specimens of the Bolivinitidae's species among the total benthos and plankton/benthos ratio in samples of the Kavaja section.

Gyroidinoides altiformis R.E. and K.C. Stewart (frequent), *C. pachyderma* Rzehak (frequent), *Anomalinoides helicinus* Costa, *Planulina ariminensis* d'Orbigny and *Cassidulina laevigata* d'Orbigny occured in these biofacies. Plankton makes up 40% of total foraminifers. These characteristics of foraminiferal assemblages and the presence of the aforementioned benthos imply a rather open sea paleoenvironment. Its frequent occurrence during Early

Serravallian transgression in Ballshi region outside the PAF area, and during the unconformable (may be transgressive) Late Serravallian, in the zone inside the PAF report that the frequent occurrence of *B. arta* is likely due to the transgressive cycles, occurred in the *Late Tortonian* trasgression age, in the Durrës-Bisht Palla region. Regardless the same denomination, these biofacies are different not only in their benthic faunal content but also in their relative age. Likely, the source is the migration itself, affected by the presence of two different large areas inside of EA or more exactly of two neighbouring different bioprovinces. Rogel (1985) introduced the notion "bioprovince" based on a previously published paper. The same can be said for the following biofacies with the same denomination between them.

***Brizalina dilatata* biofacies** could be met outside the PAF (upper bathyal habitat); in Ros-2, Ballshi-1/s borehole and Ngjeqar section. In all cases it appeared at or above LOD of *G. peripheroronda* and prior to FOD of *B. albanica* or its biofacies of the Late Serravallian as in core sample at a depth of 455 m, in Ros-2 borehole. In Ros-2 borehole, *B. dilatata* makes up over 60% of total benthos. Here, there is a high diversity in species related to the rare occurrence of other benthos such as *B. scalprata miocenica* Macfadyen, *B. costata* d'Orbigny, *B. inflata* Seguenza, *U, barbatula* Macfadyen, *Uvigerina gallowayi* Cushman, *Oridorsalis umbonatus* Reuss, *and Hoeglundina elegans* d'Orbigny. Plancton to benthos (P/B) ratio is about 30%. *B. dilatata* typical form associated with such benthos indicates an upper bathyal habitat when the water depth becomes about 150m and deeper (Brun *et al*., 1984), whereas shallower than 150 m water depth it may be replaced by next *B. albanica* species or its biofacies.

***Brizalina albanica* biofacies,** which could be met outside the PAF (outer neritic), is the only biofacies or species appeared first in late Serravallian (after the LOD of *G. peripheroronda*) at core sample of the Ros-2, at a depth of 420m (Fig. 7) and in Turbull section (sample 361). In both cases they are lithologically represented by clays with rare and thin sandstone and siltstone beds. Above the sample 361 there is an increase in number of sandstone beds and their thickness. Both samples are not rich in foraminifera, particularly in plankton which make up only 2-3 % of total fauna. *B. dilatata* was completely replaced in Ros-2 by *B. albanica*. The latter was preceded in Turbull by faunal assemblages consisting of the same benthic taxa characterising the aforementioned *B. dilatata* biofacies such as: *Bulimina costata, U. barbatula, U. gallowayi, H. elegans, Cibicides pachyderma*, which based on Jorissen (1988) and Barbieri (1991) imply an upper bathyal habitat from Early to Late Serravallian. On the other hand, in these two locations, the aforementioned

biofacies, after a short stratigraphic sequence occurred almost without any fauna at a depth of 380 m and sample 375, respectively, are characterized by faunal assemblages where in both cases subspecies of *Ammonia beccarii* prevail. Consequently, Prillo and Hasanaj (1990) and Prillo *et al*., (1994) imply for an inner neritic environment. Thus, the paleobathimetric studies estimated the position of the *B.albanica* extending from Outer to Inner neritic zones. Likely, the source is a final regressive cycle which caused a significant shallowing by the end of the Serravallian throughout the area out of the PAF.

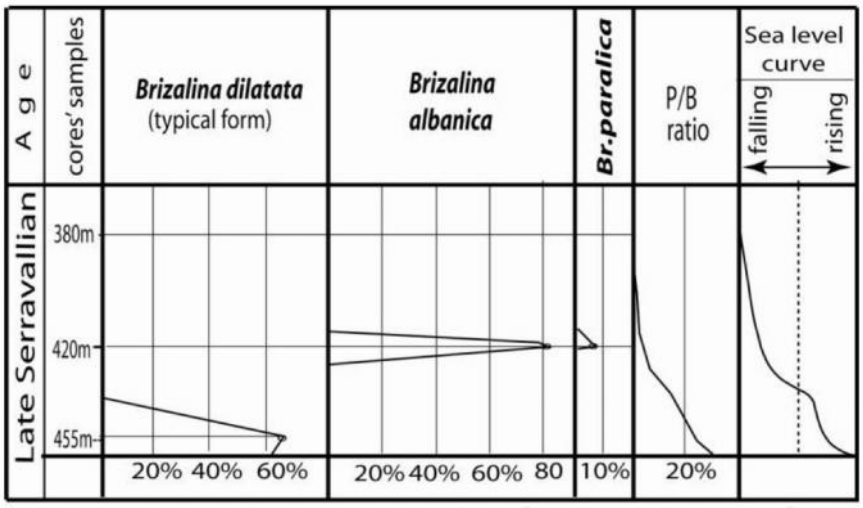

Fig. 7: The percentages of specimens of the Bolivinitidae's species among the total benthos and plankton/benthos ratio in the Roskovec -2 borehole.

Brizalina albanica s.l. **biofacies** could be met in the PAF area (outer neritic), at a depth of 1945-1947 and 1995-1997m in the Narta-2 well core's sample (Fig.8), which is located between the FOD of *G.menardii* 4 and LOD of *Globorotalia mayeri* Cushman & Ellisor corresponding more or less with the surface eroded by the Late Tortonian's transgression. The sample which is located at the depth 1995-1997m is characterized by the frequency of planktonic foraminifera. The P/B ratio is about 15%, and the *B. albanica* makes up over 80% of total benthos. The upper sample which is located at the depth 1945-1947m is characterized by the abundance of plankton. The P/B is about 70% and *B. albanica* dominates over other benthos, making up over 70% of total bentho. The two samples have the same foraminiferal content; with no significant bathymetric benthic taxon except for presence of the dominant species, and *Valvulineria bradyana* rarely found not only in the aforementioned samples, but also in some others, especially in its lower part dating since the Late

Serravallian. The species is recorded as outer and inner neritic one or more exactly as a species collected from 130 to 10 m water depth (Jorissen, 1988). Moreover, the *Brizalina paralica* (Perconig) could be sporadically met in its core sample, at the depth 1945-1947 m and 2512-2515 m. Such an occurrence of this species and its subspecies forma *nigeriana* are given within oligotypic assemblage in Upper Oligocene-Lower Miocene sediments of the Niger Delta, and its bathmetric range is given from upper bathyal to middle neritic (Brun *et al*., 1984). A frequent occurrence of the species within oligotypic assemblages is given for the preevaporitic Messinian sequence of the Po Basin, in northen Italy (Agip, 1982), but we did not explain the absence of this species in the corresponding part of the preevaporitic Messinian sequence of our studied sections. As aforementioned said, the species is found only within oligotypic assemblages suggesting, its preference for a restricted paleoenvironment such as hypersaline environment as stated by Brun *et al*., (1984). The paleobathymetric position of the biofacies in Na-2 drilling can also be used to define its bathymetric range as for *B. albanica*. Figure 8 depicts three different paleoenvironmental conditions based on faunal content and P/B ratio of all cutting and core-samples from the bottom of the Narta-2 well (depth 2697-2699 m up to 1850 m) corresponding with Early to Late Serravallian up to the eroded surface by the Late Tortonian transgression. Consequently, the development of both *B. albanica* in Roskovec.-2 and Turbull section and *B. albanica* s.l (with some morphotypes) in Narta-2 and Ndroqi regions is probably due to eustatic changes in sea level during regressive cycles and both have the same bathymetric range.

Nevertheless, these seem to be different in space and time. Thus, the regressive cycle or falling level in case of Roskovec-2 (Fig. 7) and Turbull regions probably regressed during late Serravallian. As a final cycle it reported a significant shallowing in these regions and in others showing similarities with the latter. In Narta-2 and Ndroqi regions regressive cycle probably regressed during the latest Serravallian and brought about a relative shallowing of the sea basin in these regions only, but still not shallower than outer neritic depth. These differences show that these regressions belong to two different areas or bioprovinces, as well. On the other hand, the presence of *B. albanica* suggests in both cases that it is stratigrafically and paleoecologically controlled and is water-depth related species, as well as *B. dilatata*. So, the latter could be replaced by *B. albanica* when sea basin becomes shallower.

This biofacies does not date since the latest Serravallian of the Thartor section where these sediments overlied tectonically the Late Burdigalian (AGS, 2002). In the other regions of the PAF such as Tirana depression, the presence of *B. albanica* s.l. biofacies during latest Serravallian is not reported. The eastern part of the depression comprising the Kruja tectonic zone, or more the eastern

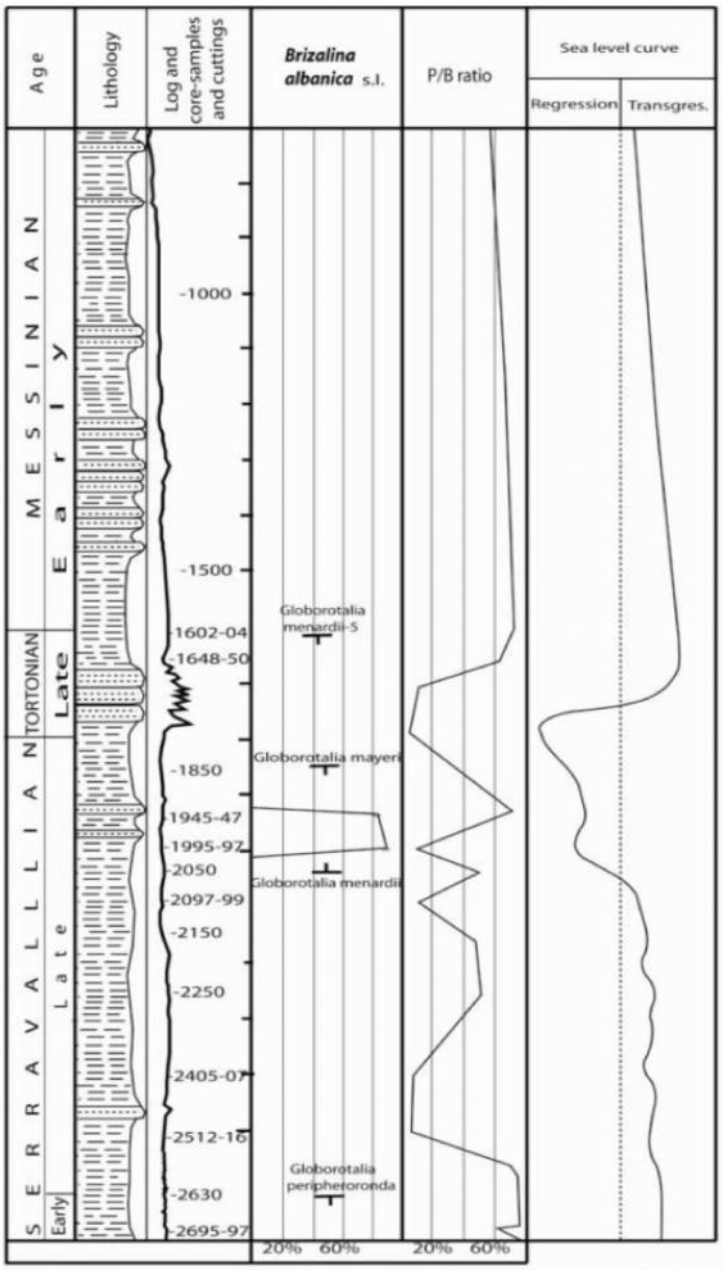

Fig. 8: The percentages of specimens of the Bolivinitidae's species among the total benthos and plankton/benthos ratio in the Narta-2 drilling.

part of EA, is represented by neritic, Upper Serravallian sediments that transgressed during Late Serravallian over the underlying Early Oligocene.

***Brizalina dilatata* biofacies** could be met within the PAF (upper bathyal habitat). It appeared in Thartor section from samples 19 to 30 after FOD of *G. menardii*-4, (Fig. 5), represented by unstratified clays with rare loosely-cemented sandstone beds in lower part which upwards become gradually stratified clays alternated with sandstone beds. In Kavaja section this biofacies appeared after FOD of *G. menardii*-4, from samples 2028 to 2032, represented by unstratified clays alternated with thin siltstone and occasionally with hard sandstone beds. Early Tortonian was developed likely due to the migration of *B. dilatata* biofacies of the older age (Late Serravallian) of another area. The latter is preceded in both sections by *B. arta* frequent and followed by *B. albanica* s.l. In Thartor section, *B. dilatata* was entirely replaced by *B. albanica* s.l. In Kavaja section this change occurs due to an interval in which *B. dilatata* and U. peregrina are almost abundant, and B. albanica is frequent. Likely, the transition between these biofacies in both cases might be related with gradual changes in paleoenvironmental conditions, primarily to water depth. However, the transitional interval in Kavaja section seems to consist also of other rare benthic taxa rich in bathyal taxa such as *B. costata, B. dilatata, C. pachyderma*, and probable displaced neritic species such as *Valvulineria bradyana, Elphidium crispum.* Turbidity, current and frequent eustatic changes in sea level probably by the end of the biofacies of Kavaja transporting shelf sediments dawnslope are a means to address these neritic species into upper bathyal habitat where *B. Dilatata prevails.* It follows that *B. dilatata* (Reuss) is the most water-depth related species and paleoecologically controlled.

Dating since the Tortonian (outer neritic), ***Brizalina albanica* s.l. biofacies** has the same name with previous one dating since Late Serravallian, or, as aforementioned said two *B .arta* or two *B. dilatata* biofacies developing in different space and period of time. The *B. albanica* s.l. biofacies developed at the same area and in younger age. The source is likely the lineage. These biofacies are preceded by *B. dilatata* and represent their replacement in both sections, from Early to Middle Tortonian. On the other hand, the Thartor section is characterized by very pyritized specimens *B. albanica* s.l. almost on entire its biofacies, by the absence of any bathyal taxa and rare occurrence of *B. praeplacentina, B. paralica* (Perconig) in its uppermost part. The plankton percentage (up to 10%) of total fauna in this biofacies reduces to 5% towards its top. In Kavaja section the plankton percentage (approximately 15%) of total fauna reduces to 7% by the end of the present biofacies. These data show that this biofacies especially in Thartor is characterazed by oligotypic foraminiferal assemblages where very pyritized of *B. albanica* s.l.'s specimens dominate, probably with a shortage of oxygen content proving a rather restricted

outer to middle neritic paleoenvironmental conditions, nearly with the same conditions as previous *B. albanica* and *B. albanica* s.l. biofacies.

***Bolivina praeplacentina* biofacies** (outer to middle neritic) appeared in Thartor after FOD of *Globorotalia acostaensis* Blow, between the samples 47 and 55. It appeared in Kavaja after FOD of *Globigerinoidesextremus* Bolli & Bermudez between the samples 2052 and 2063 (Fig. 6). This pattern becomes almost lithologically the same over the entire biofacies of both sections, represented by unstratified clays and fine to coarse grained thick sandstone beds which gradually become thicker upward of its top, ending with a remarkable sandy limestone bed for both sections. This bed or horizon is vertically variable with regard to its lithology and faunal content, and laterally variable regarding its thickness. As it is part and parcel of the same biofacies, this horizon migrates from Early Tortonian (Thartor) to Late Tortonian (Kavaja).

Occurring very sporadically, the plankton disappears by the end of this biofacies. In Thartor and Kavaja section (in particular samples) *B. praeplacentina* makes up to 37 per cent of total benthos. *Lenticulina rotulata* (Lamarck), *Ammonia inflata*, *Florilus boueanum* (d'Orbigny), *Elphidium crispum* (Linne), *Elphidium complanatum* (d'Orbigny), *U. Peregrine* Cushman and *Cibicides dutemplei* (d'Orbigny) have the same frequency. Figure 9 depicts the same biofacies found in Patos section, in the south of PAF. Its faunal assemblage is more abundant and very well preserved. Its frequency in B. praeplacentina seems to be affected by a shallow sea transgressive cycle of the Late Tortonan, which is replaced gradually by a Messinian regressive one. It is represented in Patos section by unstratified clays on the basal horizon which is more than 7 m thick and with a sequence of about 75 m of the present biofacies occurring from sample 2 to 6. The latter gradually alternate with siltstone beds 15 meter thick in the uppermost part of the sequence where the *B. praeplacentina* disappeared. The latter likely belongs to next *A. inflata* dominant biofacies. In fact, as can be seen in fig.9, in this section can be distinguished *A. inflata* frequent and next *A. inflata* dominant, the frequent one appears before *B. praeplacentina* biofacies and both end at sample 7. Nearby this section could be observed that the bituminous Messinian sandstones transgressed over the underlying Serravallian (without *G. menardii* lineage), therefore this transgression seems to represent the reliable eastern boundary of the PAF. The *B. praeplacentina* biofacies in Kercukje is not the same with that of its next Kavaja section because between them a tectonic boundary makes room supporting also by the seismic data (Guri *et al*., 2003).

The aforementioned data and those of the other benthic foraminifera accompanying *B. praeplacentina* (the most occurring here are the living benthos) suggest for their sedimentation in a neritic, rather middle neritic habitat (Jorissen, 1988).

***Ammonia inflata* biofacies** (middle to inner neritic) represent intermediate biofacies between *B. praeplacentina* frequent and *A. beccarii beccarii* dominant. In Kavaja section, an alternate occurrence between the present biofacies and the overlying biofacies has been reported. Here, *A. inflata* dominant was found between samples 2065 and 2103; 2113 and 2129; 2140 and 2153. In Thartor section it was found between the samples 57 and 71. In Lushnja section it was found since the beginning of the age, from sample 1703 to 1714. In Patos it was found higher up the section. Figure 9 depicts the dominant biofacies met above the lithology of *B. praeplacentina* biofacies, 35m deep, from sample 7 to 11. It is lithologically represented by siltstone alternated with thin sandstone beds.

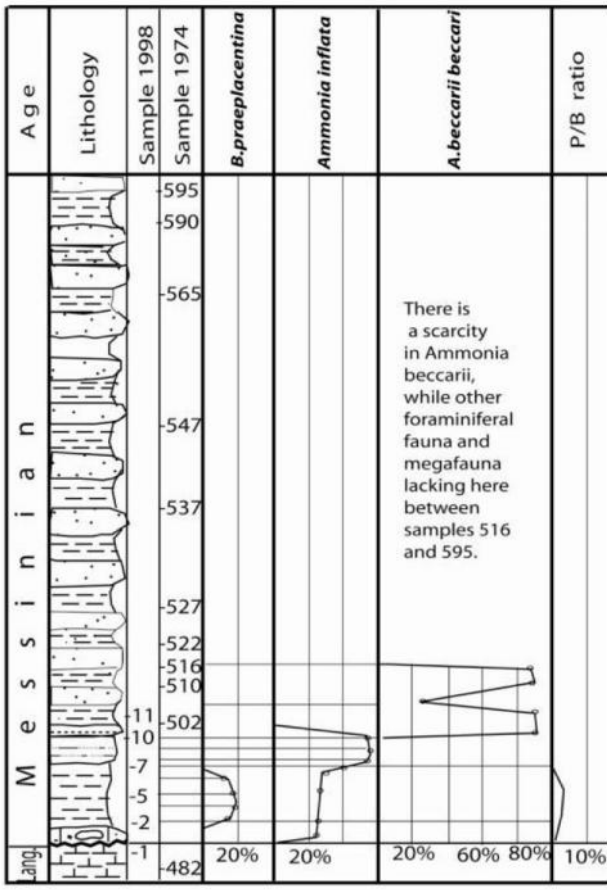

Fig. 9: The percentages of the Bolivinitidae's species and species of Ammonia genus among the total fauna and plankton/benthos ratio in samples of Patos section.

In Kërçukja section (Fig. 10) *A. inflata* is represented only by sample nr.50 which seems to be not valid. It consists of mixed fauna where *A, inflata* makes up over 40% of total benthos, likely sedimented as turbidites in the upper bathyal habitat which in sample nr.50 is represented by *S. carinata, U. peregrine, Gyroidinoides altiformis* and *C. pachyderma*. Plankton in this sample makes up 5% of total fauna.

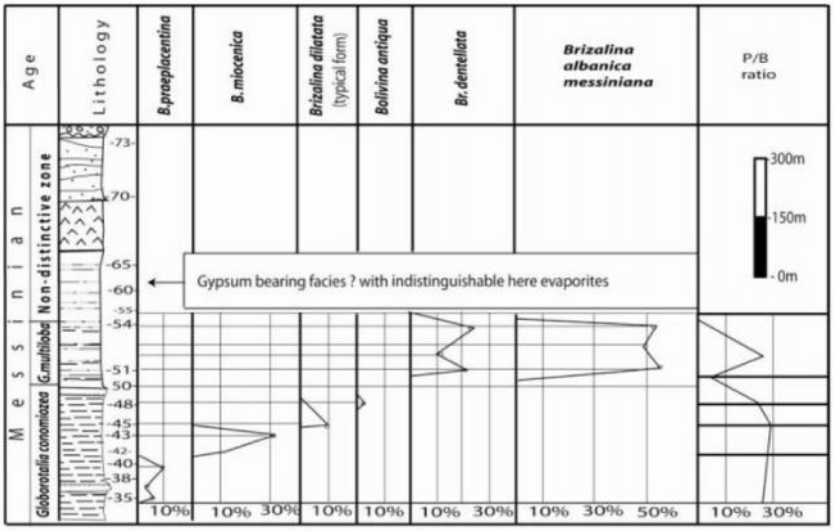

Fig. 10: The percentages of specimens of the Bolivinitidae's species among the total benthos and plankton/benthos ratio in samples of Kërçukje section.

Lithological and faunal similarities among the three sections report that biofacies in the Lushnja section has been affected by a regressive cycle as in Thartor and Kavaja section (Fig. 11 and Fig. 3).

Here, and in the Patos section, the aforementioned biofacies represent a transgressive phase and their faunal similarities relate to the species such as transitional subspecies between forma *inflate* and forma *beccarii*, rare *Elphidium crispum, Florilus boueanum,* and in the overall cases dominated by forma *inflate*. Such a occurrence has been reported in (Jorissen, 1988). He said that the populations dominated by forma inflate are also present on the clayey substrata (less than 2% sand fraction) along the Italian coast, between 20 and 60 m water depth. Consequently, the aforementioned biofacies developed in these sections in the late Tortonian and Messinian, has preferred the same sea water depth between 20 and 60 m or from inner to middle neritic (Fig. 12).

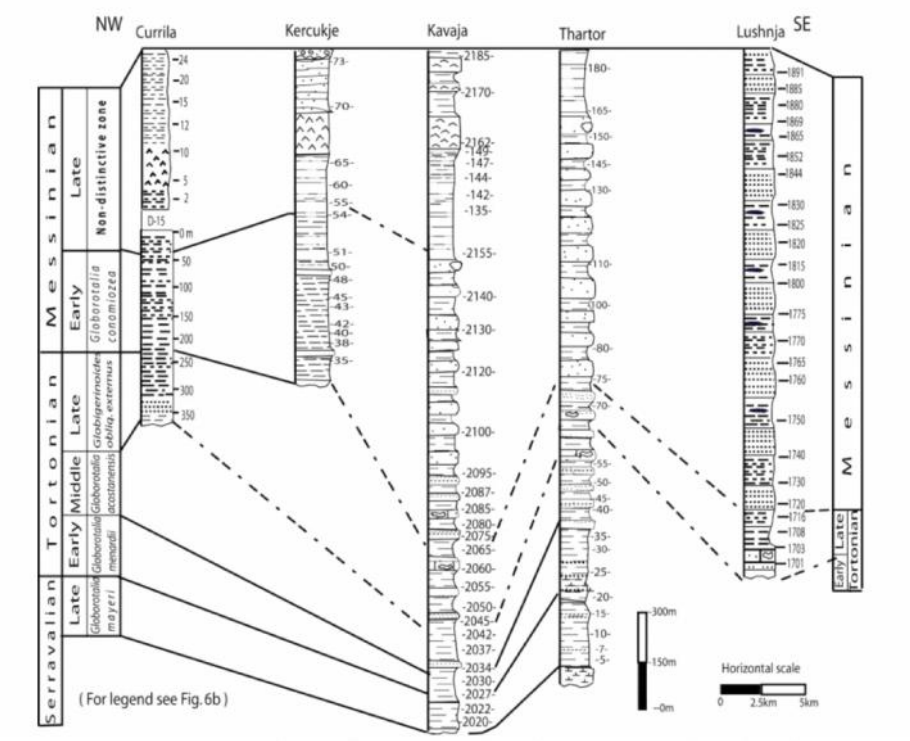

Fig. 11: Stratigraphy and correlation of the sections at Lushnja, Thartor, Kavaja, Kërçukje and Currila (Durrës).

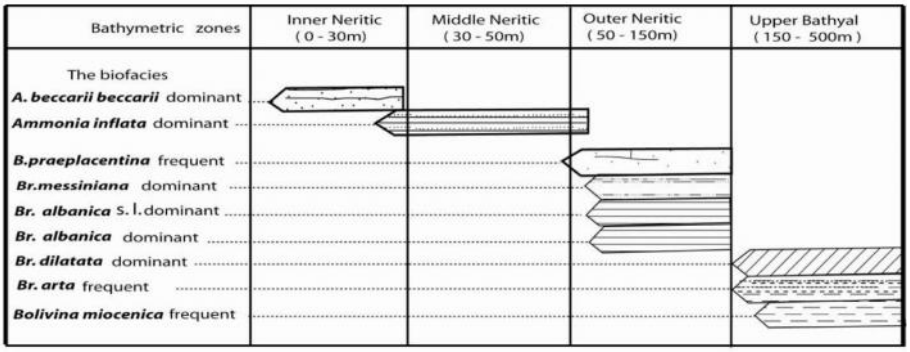

Fig. 12: The paleobathymetric distribution of the dominant and frequent distinguished biofacies in the present study. The bathymetric zones are according to Brun *et al*. (1984)

***Bolivina miocenica* biofacies** (upper bathyal), its lower boundary in D-15 borehole at the depth 340 m coincides with the FOD of *Gs.extremus* which is also accompanied by a prominent lithological change of the cuttings samples, from almost the sandstone cuttings pass into only clayey cuttings. From 340 m borehole depth up to 200 m, or from Late Tortonian up to lower part of *G. conomiozea* Zone, this biofacies is lithologically represented only by clays rich in plankton. The P/B ratio is about 60%. The *B. miocenica* frequent could be met in Bisht-Palla section (unpublished paper), which is 7 km in north-west of Durrës-15 or Currila (Durrës) section (Fig. 13).

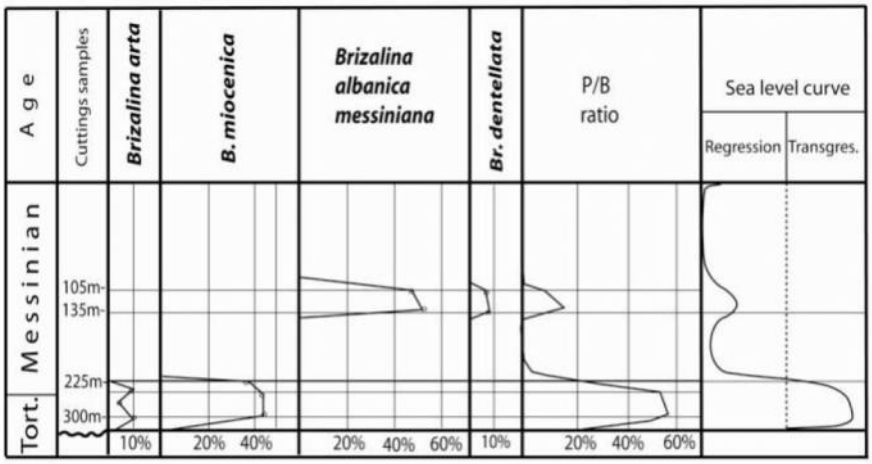

Fig. 13: The percentages of specimens of the Bolivinitidae's species among the total benthos and plankton/benthos ratio in the Durrës-15 borehole.

This biofacies in Bisht-Palla is characterized by analogy with D-15 one with regard to their lithology, stratigraphical range and foraminiferal content. The lower lithological boundary might be at the same time the stratigraphical boundary of the present biofacies in both Bisht-Palla and D-15. The latter is located between an underlying sequence with almost only sandy lithology that seems to be Early Tortonian and the overlying sequence with mainly clayey sediments of the Late Tortonian, which probably ascribed to a transgressive cycle (Fig.14).

In an unpublished paper, the biofacies was named *B. miocenica- B. arta* as in the Bisht-Palla section *B. arta* and *B. miocenica* (Gianotti) occur nearly in equal number, while in the section of D-15 borehole *B. arta* is not frequent. The *B. miocenica* in particular cuttings represents about 50 per cent of total benthos. Such biofacies is also recorded in two samples of Kërçukja section (sample 43, 44 in Fig. 10), where *B. miocenica* is associated with a many other benthos which also frequently occur such as *S. carinata, B. dilatata, U. peregrina, U. rutila, G. altiformis, Planulina ariminensis*, while plankton

makes up over 40% of total fauna. The following biofacies is more landward and with a prominent vertical migration but ought to be described here based on age order.

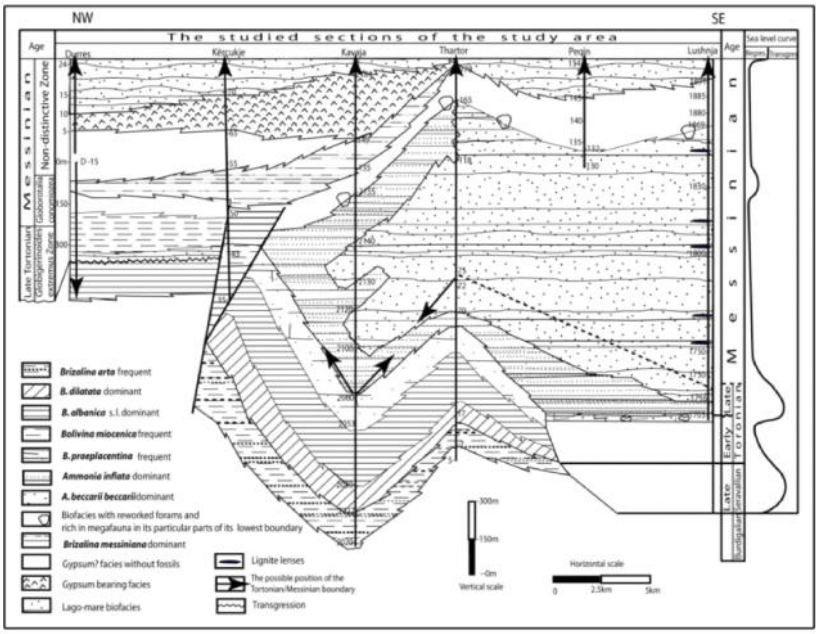

Fig. 14: The lateral and vertical distribution of dominant and frequent benthic foraminifera biofacies, based on surface and borehole sections of study area.

***Ammonia beccarii beccarii* biofacies** (inner neritic) is different from the aforementioned Paratethys originated biofacies. The differences relate to restricted geographic range of the previous biofacies (70 m thick in Ngjeqar section, nearby Roskovec town (Dalipi *et al.*, 1974)). *Ammonia beccarii beccarii* biofacies has a vast extension and the previous one belong to the latest Serravallian-Tortonian or so called "old Tortonian", whereas the present biofacies belong to Tortonian-Messinian or so-called "young Tortonian" that originated from Tethys. It is clearly reported in the Lushnja section, between samples 1716 and 1869 reaching a thickness of over 1000 m. In Thartor, it is recorded from samples 70 to 118 and not certain to the sample 165 reaching a thickness of over 800 m. In Kavaja section it is alternated with the aforementioned *A. inflata* biofacies and occurs between samples 2100 and 2112, 2130 and 2140. The lignite lenses within this biofacies in Lushnja section did not show any sea episode during their sedimentation. In all the samples here investigated, a high level of *Ammonia beccarii* dominance occurs especially in the Lushnja section. Here, in all its samples *A. beccarii beccarii* comprises

over 90 per cent of total benthos and in most of its samples a great number of *Cyprideis* specimens occur. The representative of this genus is not frequent in Kavaja section. However, in all cases representative of this genus dominating among other ostracods fossils indicate for their sedimentation in brackish water paleoenvironment (Sissingh, 1972). Its vertical migration occurred from latest Tortonian to early Messinian. The migration becomes greatest in earlier ages-older biofacies (Roskovec region) to the present one. Therefore, the vertical migration of biofacies increased as its bathymetry decreased. However, it is impossible to have such a migration within the same bioprovince. Therefore, it seems to be also some other data in the presence of two bioprovinces or two different areas within external Albanides, and the eastern real boundary of the PAF ought to be drawn between them.

Brizalina albanica messiniana **biofacies** (restricted outer neritic) could be met only within preevaporitic sequence of Kavaja section from samples 136 to 149, where between samples 146 and 149 either occurrence of the *Bulimina* genus and that of *Bolivina-Brizalina* genera in equal numbers or a slight prevalence of *Bolivina-Brizalina's* specimens was reported. Such an event documented too in the living faunas of the western Mediterranean by Bizon & Bizon (1985) by a change from a *Bolivina*-dominated microfauna below a water depth of about 80 m to one dominated by Bulimina above. This biofacies occurs too in Kërçukja section, from samples 51 to 55, and in D-15 borehole in interval between 105 and 135 m depth. In all sections, it is lithologically represented by unstratified clays, occasionally with intercalated clays, thin siltstone and sandstone beds. Both the FOD and the LOD of *Globigerina multiloba* Romeo and of *Globorotalia acostaensis* Blow dextral coiling dominant occur within this biofacies. In almost all the aforementioned samples there is slight dominance of *B. messiniana*. In the biofacies of Kavaja section *Br. messiniana* makes up over 85 per cent of total benthos. In Kërçukja section, between samples nr.51 and 52 a great anomaly in occurrence of plankton could be met. In sample 51 they make up 10 per cent of total fauna. In sample 52 make up about 35 per cent of total fauna. Between other samples of this section and that of other sections differences in occurrence of plankton were merely met. The other benthos such as *Bulimina aculeate,* d'Orbigny, *Brizalina dentellata* Tavani, *Quinqueloculina* and *Valvulinerina bradyana* are more frequent and probably typical of this biofacies. Jorissen (1988) said that the latter was not found at a depth of 130 m sea water. In Kërçukja section, most of the samples consist of pyritized fauna. The presence in this biofacies of the low species diversity with single species dominance and the occurrence in their foraminiferal assemblages of an anomaly in P/B ratio justifies their preferences for restricted paleoenvironment from outer to inner neritic.

The next "lago-mare" biofacies occurred by the end of Miocene sequence

(Cita *et al*., 1980). Figure 14 depicts the biofacies overlying the gypsum bearing Formation in the gypsum bearing regions. In the other sections this biofacies is located between underlying *A. beccarii beccarii* dominant and overlying early Pliocene sediments (Prillo and Hasanaj, 2002).

The stratigraphical distribution of Bolivinitidae

The stratigraphic distribution of more frequent occurred species and subspecies of Bolivinitidae during the Middle and Late Miocene was established by comparison with the associated planktic foraminifera using the Mediterranean planktic foraminiferal zonation (Iacccarino, 1985; Prillo et al., 1994).

Consequently, the first and last occurrence of bolivinitids species and subspecies, their frequency and dominance in foraminiferal assemblages were determined. Apparently, migration characterizes Sazan, Ionian and Kruja Tectonic Zones (External Albanides) as within the latter probably takes place the boundary between two different neighbouring areas. Figure 15 clearly depicts a very low diversity in bolivinitids' species represented by rare specimens before the Late Serravallian. From the late Serravallin to late Messinian, they were characterized by a relatively high diversity and some of them developed frequent and dominant biofacies. In addition, some of them are stratigrafically important due to their restricted vertical range, since their first and last occurrences occurred within time interval here reported. The species *Bizalina dilatata* typical (Reuss), which is more similar to holotype (Reuss, 1850), occurs sporadically from the Late Oligocene to Late Serravallian and is frequent or abundant from Late Serravallian to Early Tortonian, while from Late Tortonian to Early Messinian occurs again sporadically (Fig. 15). The notion "typical" is here used to separate this species from *Brizalina dilatata* sensu Cimerman & Langer (1991) or *Brizalina catanensis-B.dilatata* group (Prillo, 1988). The latter have never been found in the Miocene sediments of Albania, and their stratigraphical distribution during Pliocene of the EA are distinctly related to the water depth of the sedimentary's sea basin. Once Pliocene sediments were deposited shallower than upper bathyal depth, the typical *B.dilatata* was replaced by *Brizalina catanensis - B. dilatata* group, as for the replacement of typical *B. dilatata* during Middle and Late Miocene by *B. albanica.*

Bolivina praeplacentina Prillo is another species that occurred frequently from Tortonian to Early Messinian. In our opinion, until 1995 this new species was wrongly determined as *B.scalprata miocenica* Macfadyen. The latter is characterized by a lanceolate, while *B.praeplacentina* is characterised by an elongate test exhibiting in this way affinity with an Early Pliocene species such as *Bolivina placentina* Zanmatti, descended from *B.praeplacentina*. Moreover, the lineage relationships between them are also based on the presence of sutures with nearly hook-shaped lobes in the median part of the test, especially

in adult and developed morphotypes of both *B.placentina* Zanmatti and *B.praeplacentina* species.

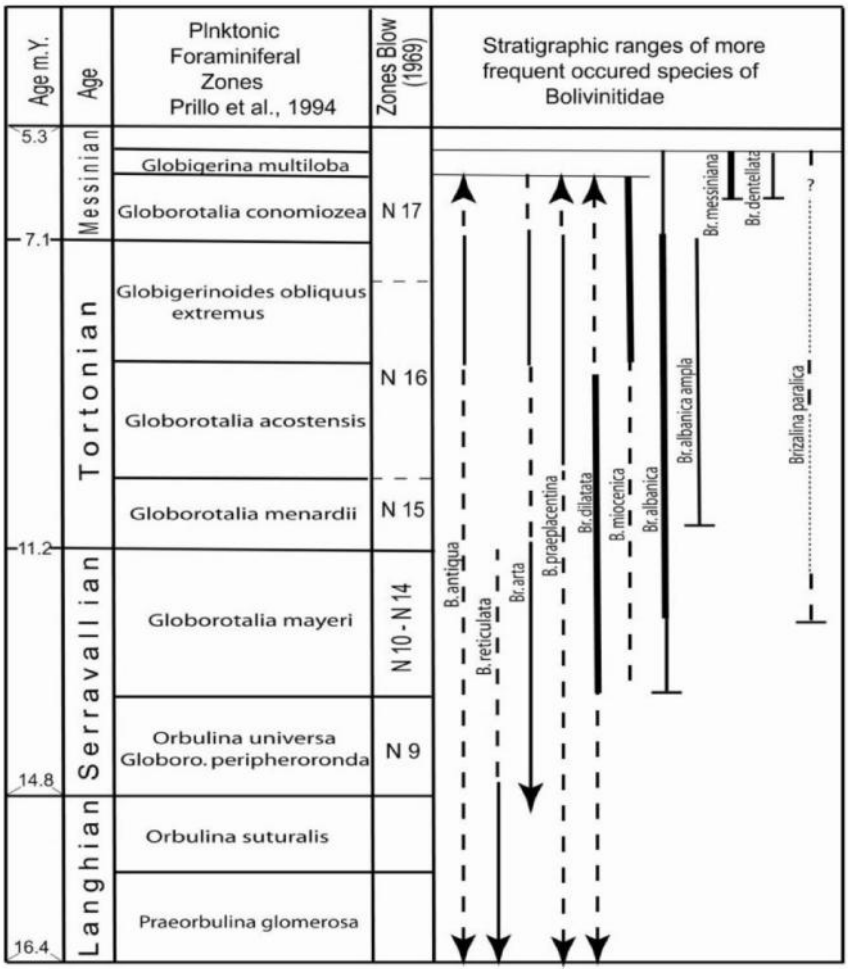

Fig. 15: Stratigraphic distribution of more frequent accured species of Bolivinitidae inside and outside of the Peri Adriatic Foredeep (PAF), during Middle and Late Miocene. The absolute age after Gradstein (1996)

Brizalina albanica Prillo and its varieties such as *B. albanica ampla* within Tortonian and *B. albanica messiniana* within Late Messinian (Fig. 15) are of the greatest stratigraphic significance due to its restricted vertical range (from Late Serravallian to Late Messinian). The morphologic characteristics of the *B.albanica* are likely comparable with that of the *B. dilatata* and/or *B. spathulata's* morphotypes. Consequently, defining whether forma *albanica* has evolved from *B. dilatata* or *B. spathulata.* (Williamson) would be difficult.

Their stratigraphical distribution in the aforementioned sections would be necessary, as the *Brizalina spathulata* species has never been mentioned in the previous Miocene studies, but only *B. albanica* s.l. or *B. dilatata***.** There are two aspects of the *B. dilatata* and *B. albanica's* occurrence in relation to each other during time interval from Late Serravalian up to Early Tortonian, whereas their development in late and the latest Serravalian and Early Tortonian were probably affected by lineage and migration.

CONCLUSIONS

The dominance and the frequency patterns of several species of the Bolivinitidae and certain other benthos here investigated were determined based on paleoecology, evolution and migration. Lineage, migration and different regressive cycles within the EA have been of great impact for the development of *B. albanica.* Paleoecology has been of great impact for .the development of *B. arta* and *B. dilatata* biofacies, but *B. arta*'s development is likely related to different transgressive cycles. In contrast, the other biofacies probably shallower ones such as *Bolivina praeplacentina*, *Ammonia inflate* and *A. beccarii beccarii* migrated to the same area, whereas between two different areas their vertical migration become greater or the greatest. These data show the presence of two different neighbouring bioprovinces within the EA. The western bioprovinces or the PAF area originates from Tethys. The Eastern bioprovinces probably originated from Paratethys. Moreover, the development of *B.albanica* is affected by a final regressive cycle during Late Serravallian that resulted in a significant shallow by the middle of the Tortonian throughout the area. On the other hand, in other places such as Vlora region of Na-2 drilling, the development of *B.albanica* s.l. was affected also by a regressive cycle during latest Serravallian that resulted in a relative shallow, from bathyal to outer neritic depth of the sedimentary basin, which in this case is located to west of the previous area. All these data are a means to address the separation of EA into two bioprovinces on basis of presence or no of representatives of keeled globorotalids taxa, and the migration of all different biofacies only across the boundary between them from an older age to a younger one within External Albanides. Consequently, every bioprovince is here characterized by the presence of different tectono-sedimentary regimes in space and time. Therefore, the boundary between them is the eastern boundary of the PAF area. Nevertheless, only in Tirana depression this boundary is determined based on the data here reported, whereas the boundary drawn through and in north of Kuçova's does not represent the eastern boundary of the PAF, but it could represent only the most eastern boundary of the young Tethyan area in Albania.

REFERENCES:

Albanian Geological Service (AGS). **1983**. Harta Gjeologjike e RPS të Shqipërisë, shkalla 1: 200 000. Tirana.

Albanian Geological Service (AGS). 2002. Geological map of Albania, scale 1: 200 000. Tirana, 2002.

Agip S.p.A. 1982. Foraminiferi Padani (Terciario e Quaternario). Atlante iconografico e distribucione stratigrafica. Seconda Edizione.Agip, S.p.A. San Donato Milanese.

Barbieri R. 1991. Phenotypic variation in *Gyroidinoides altiformis* (Stewart & Stewart) and *Gyroidinoides subangulatus* (Plummer) (Foraminifera). *Journal of micropaleontology*. **9 (2)**: 239-244. March.

Bizon G, Bizon JJ. 1985. Méthode d'étude et mode de prélèvement des sédiments d'ECOMED: In J. J. Bizon & P. F.Burollet (Eds): Écologie des microorganismes en Méditerranée occidentale. "ECOMED" Ass. Fr. Techn. Petr., Paris.

Brun L, Chierici MA, Meijer M. 1984. Evolution and morphological variations of the principal species of Bolivinitidae in the Tertiary of Gulf of Guinea. *Geologie Méditerranéenne*, **11(1)**, 13-57.

Cimerman F, Langer M. 1991. Mediterranean Foraminifera. Razred za naravoslovne vede, classis lV: historia natyralis, opera 30, 1-118, pls.1-93. Slovenska Akademia, Ljubljana.

Cita MB, Schilling VA, Bossio A. **1980.** Stratigraphy and paleoenvironment of the Cuevas del Almanzora section. (Vera Basin). *Riv. Ital. Paleont*. v. 86, nr. 1, pp 215-240 Milano.

Dalipi H, Nasto Th, Dalipi V, Prillo S. 1974. Stratigrafia e paleogjeografia e depozitimeve të Miocenit të Mesëm, Miocenit të Sipërm dhe Pliocenit te U.P.A. Fondi i I.GJ.N.G. Fier.

Gradstein FM. 1996. Geologische Zeitscala der Mark Bradenburg in: Atlas zur Geologie von Bradenburg, Landesamt für Geowissenschaften und Rohstoffe, Kleinmachnow.

Guri S, Rakipi N, Bonjaku S. 2003. Studimi kompleks tektonikës sedimentologjisë dhe zonave hidrokarburmbajtëse duke përfshirë dhe atë detare. Fondi IGJNG, Fier.

Iaccarino S. 1985. Mediterranean Miocene and Pliocene planktic Foraminifera. In: Bolli, H. M., Saunders, I. B. and Perch Nielsen, K., Eds., Plankton Stratigraphy. Cambridge University Press: 283-314.

Jorissen PJ. 1988. Benthic foraminifera from the Adriatic Sea, principles of phenotypic variation. *Utrecht Micropaleontology Bulletin.* 37, 5-174.

Prillo S. 1985. Konkluzione biostratigrafike në bazë të mikrofaunës

(foraminifera) të kampioneve e shllameve te pusit Narta-2. Fondi IGJNG Fier.

Prillo S. 1988. Foraminiferet, biostratigrafia dhe paleoekologjia e depozitimeve nga Akuitaniani deri në Helvecian (përfshirë). Disertacion per graden shkencore "Kandidat i shkencave". Fondi Institutit Gjeologjik Naftës e Gazit Fier.

Prillo S, Hasanaj L. 1990. Perkatesia moshore e depozitimeve qe permbajne *Ammonia beccarii* dhe *Cyprideis (Ostracoda*). Bul. Shkencave Gjeologjike No-3, Tirana 1990.

Prillo S, Hasanaj L. 1999. Biostratigrafia dhe interpretime paleoekologjike për depozitimet e Pliocenit në Shqipëri. Fondi IGJNG Fier.

Prillo S, Hasanaj L. 2002. Biostratigraphy and paleoenvironments of the late Messinian sediments of the Durres-Lushnja area, Albania. *Bulletin T.CXXV de l'Académie serbe des sciences et des arts, Classe des sciences mathématiques et naturelles*, **41**, 89- 96, Belgrade.

Prillo S, Hasanaj L, Çobo L, Mahmuti L. 1994. Studimi kompleks biostratigrafik i depozitimeve të Miocenit të mesëm e të sipërm për konkretizimin e kateve Langhian, Serravallian, Tortonian e Messinian sipas stratotipeve te Mesdheut. Fondi IGJNG Fier.

Reuss AE. 1850. Neue foraminiferen aus den Schichten des österreichischen Tertiärbechens Denkschr K. Österreichische Akademie der Wissenschaften, Wien, mathem, naturwiss Cl. 1, pls 1-6, Wien.

Rogl F. 1985. Late Oligocene and Miocene planktic foraminifera of the Central Paratethys. In: Bolli, H. M., Saunders, J. B., and Perch-Nielsen, K., Eds., Plankton Stratigraphy. Cambridge University, Press: 315-328.

Sissingh W. 1972. Late Cenozoic Ostracoda of the south Aegean Island Arc. Utrecht Micropaleontological Bulletins. **6**, 1-187.

Tjalsma RC. 1971. Stratigraphy and Foraminifera of the Neogene of the Eastern Guadalquivir Basin, S. Spain. *Utrecht Micropaleontology Bulletin*. 4, 1-161.

A COMPARATIVE EVALUATION OF THE QUALITY OF ALBANIAN WHEAT CULTIVARS

Artiona LAZE and **Valentina ARAPI**
Agriculture University of Tirana, Faculty of Biotechnology and Food, Kamëz, Tiranë, Albania
Vladimir MALO
The Transfer Center of the Agriculture Technology, Lushnje, Albania

ABSTRACT

Chemical-technological properties such as humidity, ash, protein content, wet gluten, gluten Index and Zeleny sedimentation of four Albanian soft wheat cultivars sown in the experimental plot of Lushnja region from 2012 to 2013 are evaluated. Results reported a statistically strong positive correlation between the value of wet gluten and the protein content (r = 0.971) and between wet gluten and Zeleny sedimentation (r = 0.985). The present paper aims to: i) evaluate the qualitative properties of Albanian soft wheat cultivars and, ii) determine the ratio between wet gluten content and grain protein content in those cultivars.
Keywords: cultivars, soft wheat, wet gluten, gluten Index

1. INTRODUCTION

The Balkans is mentioned for soft wheat (*Triticum aestivul L*) of high quality due to good agroclimatic conditions. In Lushnja region, Albanian 18 thousand ha of wheat are annually cultivated making the region responsible for the 22-24 % of the total production in the whole country (Ministry of Agricultural and Food and Consumer Protection 2011).

There are many factors that determine wheat quality such as: physical grain properties, protein percentage and composition, and starch content and composition. Among all, the most important factor that influences the bread making quality was found to be the protein content (Dowell *et al*., 2008), therefore the high content of proteins, and the amount and quality of gluten have a very positive effect on the volume and shape of bread (Pomeranz, 1988).

Also, the quantity and quality of gluten was considered to be an important

quality parameter of wheat flour. Wet gluten content is determined by washing the dough obtained from wheat flour, with water or other solutions (e.g. NaCl solution), in certain conditions, in order to remove the starch and other soluble compounds of the sample (Mis, 2000). The rubbery mass that remains after washing is the wet gluten. The gluten content is directly correlated to the grain's protein. Wheat protein quality was found to be highly influenced by environmental factors (Garrido – Lestache *et al*., 2004) and by the cultivar (Curic *et al*., 2001).

The gluten index (GI) value expresses a mass fraction of gluten remaining on a sieve after automatic washing in a salt solution and centrifugation (Curic *et al*., 2001; Dowell *et al*., 2008). Curic *et al.,* (2001) said that 60 □ GI □ 90 provides the optimum bread making quality for Central European cultivars. Ratios between wet gluten content and grain protein content showed that wet gluten/Protein (WG/P) ratio is considered as an indicator of wet gluten production per protein unit. Simic *et al*., (2006) reported that Croatian wheat with WG/P ratios ranging between 2.7 and 3.0 have gluten with optimal baking characteristics, while cultivars with strong gluten characteristics showed the WG/P ratio closer to 2.3.

The present paper aims to: i) evaluate the qualitative attributes of some autochthonous cultivars and, ii) determine the ratio between wet gluten content and grain protein content in those cultivars.

2. MATERIALS AND METHODS

2.1 Materials

The present investigation involves four Albanian soft wheat cultivars that were sown in the experimental plot of Lushnja region, Albania from 2012 to 2013 (latitude 40˚ 50' 38, 07"N; longitude 190 44' 44,37"; elevation 12 m), characterized by an average annual precipitation of 1289 mm and annual average temperature of 15 °C.

Table 1. Wheat genotypes

No	Wheat genotypes	Symbol
1	Dajti	G01
2	L.V.S	G02
3	Progresi	G03
4	Linja 4	G04

Each wheat genotype was planted in three replications based on the Randomized Block Scheme (RCBD). The wheat samples were grounded in the experimental automatic mill (Pulverisette 14). Table 1 reports wheat genotypes here involved.

2.2 Chemical analyses

Wet Gluten and Gluten Index values for all flours samples were determined using the Glutamatic system (Petern Instrument AB, Stockholm, Sweden) and applying the AACC (2000) method 38-12.02. The Kjeldahl method was applied to determine the protein content. Sedimentation value (K-SDS) was determined based on (Zeleny, 1947). Moisture content and ash were analyzed applying the AOAC (1995) methods 44-10 and 08-01, respectively. The specific nitrogen to protein conversion factor 5.7 was used for the calculation of crude protein content in flour.

2.3 Statistical analyses

All measurements were carried out with three repetitions; the descriptive statistical analyses for obtained results were reported as the mean ± standard deviation (SD). The statistical results were performed using the statistical software SPSS 17 program.

3.RESULT AND DISCUSSIONS

The physical and chemical properties of the four cultivars of soft wheat are in table 2 reported. They have an optimum amount of humidity (11.04% Dajti -14.79% L.V.S). Ash content of in the flour ranged from 1.44 % (Linja 4) to 1.58 (L.V.S). The total protein content, an indicator of the quality of the wheat, ranged from 11.68% (Progresi) to 14.28% (L.V.S). The proteins content was similar with the previous study done for the soft wheat genotypes (Arapi *et al*., 2013). The source is bran fraction (seed coat and embryo) within the wholegrain wheat flour.

Table 2. Physical and chemical attributes in four cultivars of soft wheat

Cultivar	*Moisture (%)*	*Ash (%)*	*Wet gluten (%)*	*Protein (%)*	*Gluten Index (%)*	*K-SDS (ml)*	*Wet gluten /protein*
Dajti	11.04± 0.09	1.52±0.08	24.7±1.34	12.03±0.21	72±1.32	31.25±0.58	2.28
Progresi	12.54±0.21	1.56±0.02	25.4±1.15	11.68±0.27	74±1.16	34.70±0.85	2.17
L.V.S	14.79±0.14	1.58±0.06	30.9±1.10	14.28±0.31	73±1.23	44.90±1.14	2.17
Linja 4	12.09±0.31	1.44±0.09	25.0±0.98	12.10±0.19	75±0.99	31.25±0.65	2.07

The content of wet gluten ranged from 24.7% (Dajti) to 30.9% (L.V.S). Sedimentation values (K-SDS) ranged from 31.25 ml (Dajti, Linja 4) to 44.90 ml, (L.V.S). The gluten index values varied from 72 (Dajti) to 75 (Linja 4).

Curic *et al*., (2001) said that all the cultivars provided optimum bread making quality (Gluten Index > 60%). The results of wet gluten in these cultivars agree with those of Përmeti (1997), who reported a high value of wet gluten in domestic wheat accessions, with an average of 28.40%. In regards to the ratio between the wet gluten content and grain protein content, these values ranged between 2.07 (Linja 4) to 2.28 (Dajti). Simic *et al*., (2006) stated that only the cultivar Dajti has strong gluten characteristics.

The value obtained for L.V.S cultivar indicates that this cultivar has better baking properties compared to other cultivars, with sufficient protein quantity (14.28%), considerable wet gluten quantity (30.9%), a high value of gluten index (73%) and good Zeleny sedimentation (44.90 ml).

Chemical-technological parameters (e.g. moisture, ash, Zenely sedimentation, protein, wet gluten and gluten index) were a means to address the correlation coefficients for a better understanding of the cultivar properties. Results of the Table 3 report that wet gluten shows significant positive correlation with the content of protein (r = 0.971) and K-SDS (r = 0.985).

Table.3. Pearson Correlation coefficient between Chemical – Technological Indices

	Moisture	Ash	Protein	K-SDS	WG
Moisture	1	1	1	1	1
Ash	0.581	0.479	0.918	0.985*	-0.201
Protein	0.871	0.727	0.971*	-0.204	GI
K-SDS	0.963*	0.621	-0.260		1
WG	0.952*	-0.542			
GI	0.060				

*Correlation is significant at the 0.05 level.

Gooding *et al*., (2013) found that bread-making quality, determined by the Zeleny sedimentation test (K-SDS), was more severely affected by drought stress before the end of the grain – filling than by temperature stress or by latter drought. Consequently, a positive linear correlation between moisture and K-SDS (r = 0.963) exists. The high coefficient of linear correlation 0.9424 and 0.9709 respectively, between protein content – wet gluten and wet gluten – K-SDS is in Figure 1 depicted.

This positive correlation means the higher the amount of gluten is, the higher protein content and level of sedimentation in the flour are.

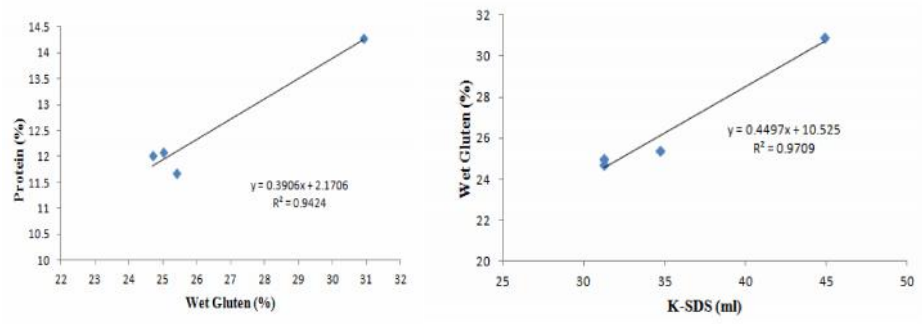

Fig. 1. Linear regression between Protein-Wet Gluten and Wet Gluten – K-SDS.

4. CONCLUSIONS

In the present investigation the following conclusions are drawn: i) all the Albanian cultivars showed an optimum level of protein content (11.68% - 14.28%) and high level of gluten Index (72% - 75%), ii) positive linear correlation between wet gluten and protein, and between wet gluten and K-SDS, i.e., the higher the amount of wet gluten, the higher the protein content and sedimentation value (K-SDS) are and, iii) the flour obtained from the L.V.S cultivar exhibits better physical and chemical properties compared to all other flours obtained from other cultivars, i.e., better baking properties compared to other cultivars.

REFERENCES

AACC International. 2000. *Approved Methods of the American Association of Cereal Chemists. 10th Ed. Method 38-12.02*. The Association: St. Paul, MN.

AOAC. 1995. *Official Methods of Analysis of AOAC International*; Method No. 08-01 and No. 44-10.

Arapi V, Laze A, Elezi F, Bano V. 2013. Evaluation of some soft wheat Accession of AUT collection created in the country, based on the qualitative indicators. *International Journal of Environmental Application and Science*, **8 (4),** 658-662.

Ćurić D, Karlović D, Tušak D, Petrović B, Đugum J. 2001. Gluten as a standard of wheat flour quality. *Food Technology and Biotechnology*. **39**, 353–361.

Dowell FE, Maghirang EB, Pierce RO, Lookhart GL, Bean SR, Xie F, Caley MS, Wilson JD, Seabourn BW, Ram MS, Park SH, Chung OK. 2008. Relationship of bread quality to kernel, flour, and dough properties. *Cereal Chemistry*. 85, 82–91.

Garrido-Lestache E, Lopez-Bellido RJ, Lopez-Bellido L. 2004. Effect

of N rate, timing and splitting and N type on bread-making quality in hard red spring wheat under rain fed Mediterranean conditions. *Field Crops Research*. **85**, 213–236.

Gooding MJ, Ellis RH, Shewry PR, Schofield JD. 2003. Effects of restricted water availability and increased temperature on the grain filling, drying and quality of winter wheat. *Journal of Cereal Science*. **37**, 295–309.

Ministry of Agricultural and Food and Consumer Protection (MAFCP). 2011. *Statistical year book*. Tirana, Albania.

Mis A. 2000. Some methodological aspects of determining wet gluten quality by the Glutomatic Method (a laboratory note*).International Agrophysics*, **14**, 263-267.

Përmeti M. **1997**. Contibute on genetic improvement of wheat in Albania. *Albanian Journal of Natural and Technical Sciences.* 3, 3-7.

Pomeranz Y. 1988. *Composition and functionality of wheat Flour components. In Wheat: Chemistry and Technology (Vol. 2), ed. Pomeranz Y*. American Association of Cereals Chemists, St Paul, MN, USA, pp 219-370.

Šimić G, Horvat D, Jurković Z, Drezner G, Novoselović D, Dvojković K. **2006**. The genotype effect on the ratio of wet gluten content to total wheat grain protein, *Journal Central European Agriculture*, **7(1)**, 13-18.

Zeleny LA. 1947. Simple sedimentation test for estimating the bread – baking and gluten qualities of wheat flour. *Cereal Chemistry*. **24**, 465–475.

DIMENSIONAL STABILITY OF MONOFILAMENTS AND THE PERFORMANCE OF ARTIFICIAL TURF

Blerina KOLGJINI
Department of Textile and Fashion Faculty of Mechanical Engineering, Polytechnic University of Tirana, Albania
Department of Textile, University of Ghent, Belgium
Ilda KOLA and **Ermira SHEHI**
Department of Textile and Fashion Faculty of Mechanical Engineering, Polytechnic University of Tirana, Albania
Paul KIEKENS
Department of Textile, University of Ghent, Belgium

ABSTRACT

Dimensional stability of monofilaments is very important for the performance of artificial turf. It could be obtained during the heat treatment of monofilaments along with the properties of the final product. Although the process itself is rather easy, the impact of weather conditions remains unknown. However, recent investigations have revealed that elevated temperatures are of primary importance. Dimensional stability and long standing properties of artificial turf are closely related to heat treatment.
***Keywords*:** monofilaments, shrinkage, dimensional stability

1. INTRODUCTION

Artificial turf is a complex system consisting of several layers (Patents application US 6723412 B2, 2004), some of which stand together even before installing it on real fields and define the position of monofilaments. The latter are components of the pile layer. The higher the performance of the top layer (pile layer), the higher the performance of the entire system is (FIFA, 2006).

In addition, monofilaments generally are produced from linear low density polyethylene (LLDPE) by extrusion and, stretched on melting and solid stage at different stretching ratios. One of the most important properties is the bending behaviour (on static and dynamic mode or resilience) of monofilaments (Schoukens, 2009).

Many noted papers provide information about the impact of processing parameters of monofilaments on classical mechanical properties and bending behaviour (Sandkuehler, *et. al.*, 2010). Consequently, related to the long standing of artificial turf, monofilaments recover completely after bent under the action of the players and the ball (Rambour and Schoukens, 2009).

In addition to processing parameters (Kolgjini, 2012) of monofilaments and the type of polymeric materials (Sandkuehler *et. al.*, 2010), geometrical aspects like profile cross section, length and thickness of monofilaments (Young, 1989) have a great impact on the performance of monofilaments/ pile layer.

Most of the formulas concerning the strength of materials express the relations among the form and the dimensions of a product, the loads applied thereto, and the resulting stress or deformation. Any of such formulas are only valid within certain limitations and applicable for certain problems.

Theoretically, a beam of known cross section geometry will bend under the application of a specified load and load distribution (Young, 1989) (figure 1).

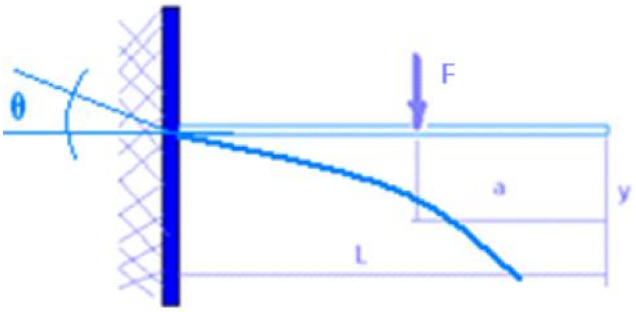

Fig.1. The position of bending of a straight beam is represented schematically, equivalent with a one side fixed monofilament on artificial turf.

Deflection at the unsupported end: $\mathbf{y = \frac{FL^3}{3EI}}$

and the slope measured by θ: $\theta = \frac{\mathbf{F(L - [a)]^2}}{\mathbf{2EI}}$

where:

E	Modulus of Elasticity	(N/m^2)
I	Moment of Inertia	(m^4)
F	Load	(N)
s	Stress at the cross-section being evaluated	(N/m^2)
y	Deflection	(m)
L	Distance as indicated	(m)
a	Distance as indicated	(m)

The moment of inertia is the function of the cross section and the distance from the neutral axis to the edge of the beam geometry.

The diamond shape cross section, as the most used profile cross section on monofilaments (Patents application US 6432505B1, 2002) and the deflection (bended) of unsupported end are here considered as the most possible deflection happening on real conditions of artificial turf (Kolgjini, *et. al*., 2012).

For diamond shape, the moment of inertia is: $I = \frac{bd^3}{48}$ or $\frac{db^3}{48}$;

where b and d are the distance from centroid to extremities.

Theoretically, any dimension change of monofilaments is unavoidably related with the bending properties such as resilience and static bending.

Practically, based on a study carried out by the Department of Textiles, University of Ghent, Belgium, the bending force shows an exponential correlation with the free pile length $F \approx 1 / L^3$ (Kolgjini, 2012).

Monofilaments mostly are products of the polyolefin. The LLDPE is the mostly used polymer and as such, it is likely to show poor retention, poor creasy resistance and poor shape retention. Appropriate dimension stability of monofilaments is important for the producers, therefore, once tufted, the pile layer becomes irreplaceable and influences the performance of the system while using it.

Once tufted, the carpet of artificial turf goes through the coating line which is very important for securing the position of the monofilaments. The process is performed at elevated temperatures.

Even though the coating process is applied on the back of the carpets, practically, the temperatures on the upper part (part of the pile layer) vary from 75 to 80°C—sufficiently high for dimensional change in length and thickness of monofilaments.

The exposure of the artificial turf on real conditions is very important. The temperatures on real condition are around 40°C—sufficiently high for structural and dimensional changes. It is well known that the structural changes happen at the crystallization temperature and below the melting temperature (Peacock, *et. al*., 2000).

Heat setting or annealing is performed on the monofilaments before tufting the carpet to prevent monofilaments from the dimensional, physical and mechanical instability.

Here, in the present paper, only the dimensional stability of monofilaments is reported. Information about the influence of heat settings on other properties will in a subsequent paper be reported.

The present paper aims to find the conditions of heat settings performance with regard to temperature and the state of heat settings (fixed or not-fixed ends) on the production line. Heat settings were performed at different temperatures with fixed and free ends.

2. MATERIALS AND METHODS

Materials

The polymer material here involved was provided by the Dow Chemical Company (DOWLEX TM): DOWLEX™ 2035G linear low density polyethylene (LLDPE) with a density of 0.919 g/cm^3 and a melt index of 6 g/10min.

The line of monofilament production

For a realistic approximation of the monofilaments, the production of monofilaments was carried out on a pilot monofilament line from Oerlikon Barmag type 3E/24D installed at the Department of Textiles, University of Ghent, Belgium. Production criteria of monofilaments were based on (Kolgjini, *et. al*., 2012). Monofilaments with cold draw ratio (CDR) 7.2; 6.2; 5.5 and 3.3, with dTex of approximately 1980 [g/10km] have been selected. These samples' behaviour was significantly different (Kolgjini *et. al*., 2012). The extruder has a single screw diameter of 30mm and a length of 24D. The temperature in the die was 220°C. The die has 24 diamond–shaped openings with a cross section of 70mm^2 each. Once melted, the monofilaments (section I, figure 2) were dragged into water bath and passed through the oven, with air circulations at a temperature of 100°C (section I, figure 2). Cold drawing (CDR) of monofilaments, which relates with the first stage of the production line, occurred. Subsequently, shrinkage accurately occurred at a temperature of 100°C (section II, figure 2). The shrinkage was controlled by changing the speeds of the rolls before and after going through the oven, reaching a value of 10%. Once shrunk, the samples were annealed at a controlled temperature of 100°C for ten seconds (section III in figure 2).

A second series of samples were provided (see figure 3). Once stretched, the filaments underwent a heat setting at 120°C with fixed ends (the rolls on both sides have the same speed).

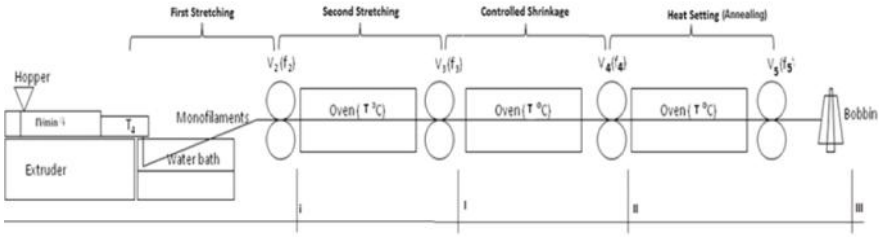

Fig. 2. Schematic representation of the production of monofilaments in laboratory conditions. n, V_2, V_3, V_4, V_5 are the speeds of rolls for each step of production. f_2 ,f_3, f_4, f_5, are the cross section of monofilaments for each step.

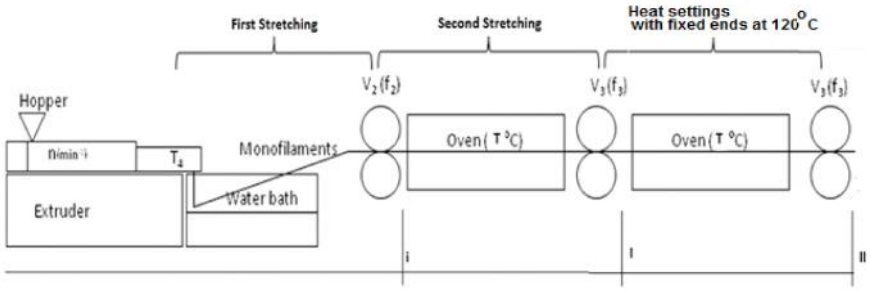

Fig.3. Schematic representation of the production of monofilaments with heat treatment with fixed ends at 120°C.

Test method

The internal standard modified for polyethylene material used at the University of Ghent (UGENT, Vakgroep Textilkunde) was followed for testing purposes. One meter yarn of monofilaments was exposed to elevated temperatures for 15 minutes at 75°C. A weight of 5g was placed on it to prevent monofilaments from being curled. Once heat treatment and conditioning of samples at normal temperatures were carried out, the length was measured again under the weight of 505g. The data were collected and shrinkage of products was calculated.

3. RESULTS AND DISCUSSIONS

After performing heat settings on different samples with different processing parameters and at different stages of production line of monofilaments, the shrinkage was calculated and the results are reported in Table 1.

Results reported that samples that did not pass the heat treatment (mentioned in table 1 as original products) showed higher values of shrinkage, like the samples that passed the heat settings but with fixed ends.

For the samples that underwent heat settings at 100°C on controlled shrinkage

(10%) and the annealing process, the percentage of shrinkage decreased after each of the steps of the production line.

Table 1. Shrinkage of the monofilaments at different temperatures for all the samples at different stages and with different CDR (Stretching ratio).

CDR (Stretching ratio)	*Original product* *Shrinkage in %*	*Fixed ends at 120° C* *Shrinkage in %*	*10% Shrinkage at 100°C* *Shrinkage in %*	*Annealed at 100 °C* *Shrinkage in %*
7.2	9.5±0.3	9.1±0.5	7.2±0.3	6.2±0.1
6.2	8.3±0.4	5.8±0.3	2.9±0.3	3.4±0.1
5.5	9.6±0.3	5.2±2.4	3.3±0.5	4.2±0.2

Heat settings or annealing is a process known to eliminate the internal stresses generated during fabrication, i.e. stretching (Peacock. 2000). The process itself is a means to address ductility, softness of the material, relief of internal stress and refinement of the structure by making it more homogeneous and improving the properties of samples stretched on solid stage.

Heat fixes the material in a relaxed state and thus avoids subsequent shrinkage as the internal stresses are relieved.

In addition to heat settings, the inverse proportional of the stretching ratio (CDR) with the percentage of shrinkage is very important for the monofilaments, as the higher induced stresses, the higher stretching ratio.

The most stable product are those that have stretching ratios varying between 5.5 and 6.2 and, have undergone at least once the heat treatment, on controlled shrinkage. Samples with a stretching ratio 3.3 do not show stability of values of shrinkage. The samples with stretching ratio 3.3 must unavoidably be submitted to the controlled shrinkage and annealing process. The samples with the stretching ratio varying between 5.5 and 6.2 showed stable values of shrinkage after the controlled shrinkage process.

Shrinkage results reported that the samples with fixed ends are unstable after controlled shrinkage and heat treatment, but only after passing these steps and carrying out the annealing process at elevated temperatures.

4. CONCLUSIONS

Dimensional stability is not aesthetically important for the monofilaments, but it unavoidably impacts the performance of the whole system. If dimensions of monofilaments change, the bending behaviour will change. The length of the pile layer has great impact on behaviour of the ball : ball rolling and ball rebounding.

Controlled shrinkage and heat settings at elevated temperatures are closely related to the stability of monofilaments. Samples with CDR 3.3 must be submitted to the controlled shrinkage and annealing process. Samples with CDR values varying between of 5.5 and 6.2 have stability of shrinkage. Once dimensions of monofilaments are stable, tufting might occur. Dimensions stability is a means to address the quality of artificial turf as monofilaments are fixed and could not be replaced.

REFERENCES

DOWLEX TM 2035 G (Cast Film), Polyethylene Resin. Tarragona Technical Centre, Tarragona Spain.

FIFA quality concept. 2006. Handbook of requirements for football turf. March 2006 edition [internet]. Available from: http://www.fifa.com/documents/fifa/FQCturf/FQC_Requirements_manual_March 2006.

Kolgjini B. 2012 .Structure and long properties of polyethylene monofilaments for artificial turf application" PhD theses ISBN 978-90-8578-544-6, October.

Kolgjini B, Schoukens G, Kiekens P. 2012. Influence of stretching on the resilience of LLDPE monofilaments for artificial turf application. *Journal of Applied Polymer Science*, **124**, 4081-4089.

Patents application US 6432505B1, Diamond cross section synthetic turf filament. (publication date: 13/08/2002).

Patents application US 6723412 B2. Synthetic Turf (publication date: 20/04/2004).

Peacock AJ. **2000**. Handbook of Polyethylene Structure Properties and Application. New York.

Rambour S, Schoukens G. **2009**. International Conference on Latest Advances in High -Tech Textiles and Textiles-based Materials. 23–25 September. Belgium.

Sandkuehler P, Torres E, Allgeuer T. **2010**. Performance artificial turf components — fibrillated tape. *Procedia Engineering*. **2 (2);** 3367–3372.

Schoukens G. 2009. Developments in textile sport surfaces. Advances in carpet Manufacture. Chapter 5, 102-137.Woodhead Publishing Com. Cambridge, UK.

UGENT, **Vakgroep Textielkunde** hot air retraction test for polyester PM/214 B.

Young WC. 1989. Roarks formulas for stress and strain, 6-th edition, ISBN 0-07-072541-1.

ENERGY ECONOMY IN THE APPAREL SECTOR

Elmira DUMISHLLARI
Department of Textile and Fashion, Polytechnic University of Tirana, Albania

ABSTRACT

Energy consumption is very important for the apparel sector as all the machines work with electricity. As alternative energy is costly, using traditional energy sources remains beneficiary. Information on energy-efficiency printing technologies and measures applicable to the textile industry is in the present paper reported.
***Keywords*:**energy, economize, apparel production companies, process

1. INTRODUCTION

Energy is one of the main cost factors in the textile industry. As energy consumption is costly and volatile, energy efficiency is of primary concern for textile industry (Bhurtun *et al*., 2014).

At the same time, it is very important for the apparel sector as all the machines work with electricity. As alternative energy is costly, using the traditional one remains beneficiary (Xhamaqi *et al*., 2014).

Energy efficiency improvements refer to a reduction in the energy used for a given service (heating, lighting, etc.) or level of activity. The reduction in the energy consumption is usually associated with technological changes, but not always, since it can also result from better organisation and management or improved economic efficiency (e.g. overall gains of productivity). Avoiding unnecessary consumption of energy or choosing the most appropriate equipment to reduce the cost of the energy decrease individual energy consumption without decreasing individual welfare and productivity (Bhurtun *et al*., 2006).

Energy efficiency is closely related to the quality and productivity improvements. Therefore, energy efficiency is essential for the sector to survive in the industry (Jananthan and Ameer, 2006).

The present investigation was carried out in an apparel production company in Tirana, Albania which produces sports clothing for different disciplines and operates “Full Package”. A full package garment supplier carries out all steps

involved in the production of a finished garment—including design, fabric purchasing, cutting, sewing, trimming, packaging, and distribution (Gereffi and Frederick, 2010).

2. MATERIALS AND METHODS

Working time for each working process was measured usinga stopwatch along with energy consumption per hour.

Once the results were obtained, efforts to reduce energy consumption were made involving all the stakeholders. In the present investigation ten of the so-called TSC model sport shirts were produced.

Garment production

Figure 1 depicts production procedures followed for the production of the 10 TSC model shirts (Glock and Kunz 2005; Ahmad, 2011; Dumishllari and Guxho 2014). The time required for each production procedure was measured using a stopwatch.

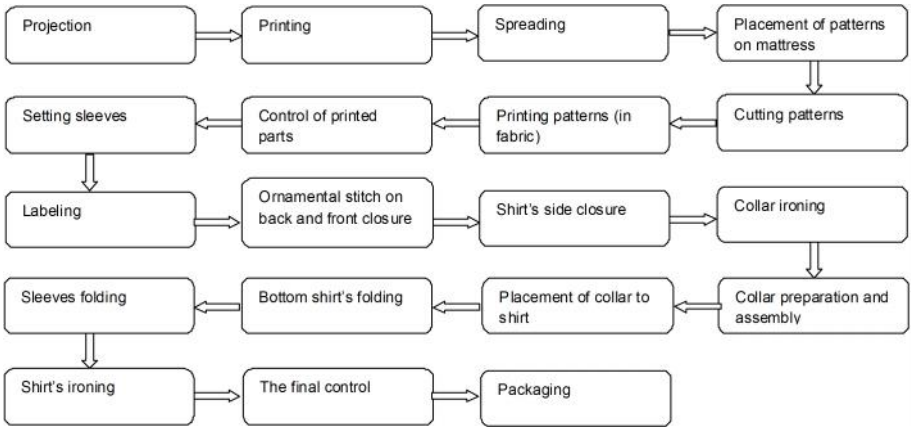

Fig.1. The step by step process of garment production.

In general, energy in the apparel production industry is mostly used in the form of electricity as a common power source for machinery, lighting and office equipment (UNIDY, 1992; Bhurtun *et al*., 2006; Shahidul and Khan 2008). Table 1 reports about the machines used to carry out the aforementioned production procedures along with the energy consumption.

Table 1. Equipment and machinery used in garment production, their energy consumption

Equipment/Machinery	**Energy Consumption [kW/hr]**
Computer	0.422
Printer	0.15
Printing machine	24
Saw	0.1
Lockstitch sewing machine	0.5
Labelling machine	2
Iron	1.2
Straight Stitch Sewing machine	0.5
Ornamental stitching machine	0.5
Machines for the realization of bottom/sleeves folding	0.5
Bulb Lights	0.04

Components of energy consumption

Working time was measured for all the production steps. Once the energy consumption for every machine/equipment is determined, energy consumption for resulting periods of time is determined as well. Energy consumption has been determined separately for the three components (machinery/equipment, lighting and repairs for each step of production).

Table 2 reports on production processes, time (adding the time required for repair of faults) and energy consumption from machines/equipment, lighting and repairs. Three defects were reported.

Table 2. Production process, time and energy consumption

Process	**Working time (For 10 shirts) added repair's time [s]**	**Energy consumption [kW]**		
		Machinery	**Lighting**	**Repairs**
Projection (in computer)	660	0.0774	0.01467	-
Printing	2571+770.4	0.107	0.074	0.0321
Spreading	182+47	0.005	0.0051	0.0013
Placement of patterns on mattress	32+26	0.0106	0.0013	0.0086
Cutting patterns	34.6+26	0.00095	0.00135	0.00072
Printing patterns (in fabric)	500+133	3.333	0.0141	0.886
Control of printed parts (organoleptic assessment)	105+27	-	0.00293	0.0006
Setting Sleeves	782	0.109	0.0174	-
Labeling	537	0.298	0.0119	-
Ornamental stitch on back and front closure of TSC	580+1020	0.0805	0.0356	0.142

Shirt's side closure	530	0.0736	0.01178	-
Collar ironing	77	0.0257	0.0017	-
Collar preparation and assembly	288	0.04	0.0064	-
Placement of collar to shirt	173	0.024	0.0038	-
Bottom shirt's folding	168	0.023	0.0037	-
Sleeve's folding	242	0.0336	0.0054	-
Shirt's ironing	418	0.139	0.0093	-
The final control(organol.)	740	-	0.0164	-
Packaging of TSC shirts	211	-	0.0047	-

3. RESULTS AND DISCUSSIONS

Results reported that printing has the highest energy consumption (74.31% or 4.23 kW of the total energy required for the production of 10 shirts TSC) and the defects that occurred during the process cover 15.56% of total power used and 82.7% of the power needed for repairs.

Figure 2 reports that 76.95% of the power is used by the machines, 4.24% for lighting and 18.82% of the power goes to the repair of defects.

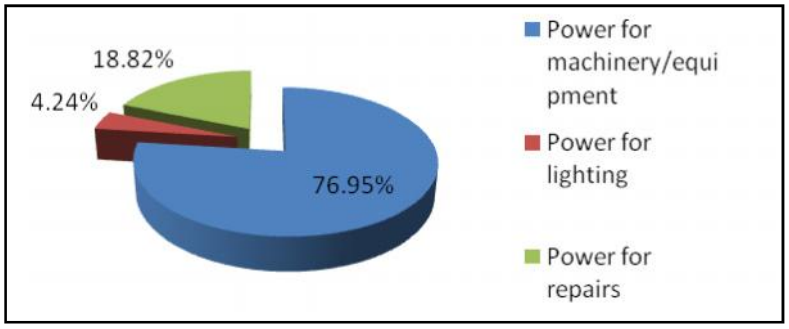

Fig. 2: Energy for machinery/equipment, lighting and repairs.

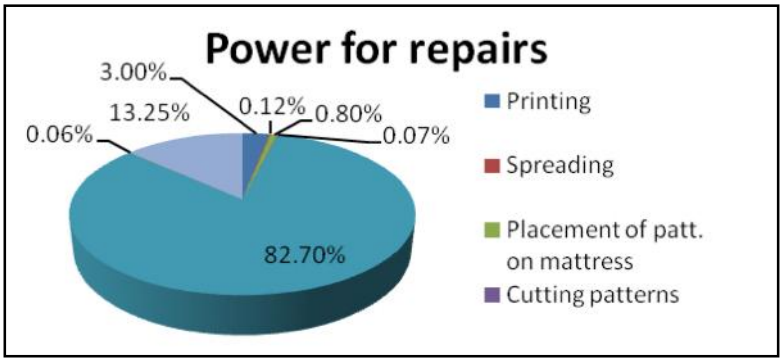

Fig. 3: Energy needed for repairs, according to the process (referring to the total power needed for repairs).

Figure 3 reports that the defects occurred during the printing require 82.7% ofthe total power necessary for the repairs. In “Ornamental stitch on back and front closure of TSC”, power for repairs occupied 13.25% of the total power necessary for repairs.

4. RECOMMENDATIONS

The following recommendations could be made: i) as machines consume considerably the energy(76.95% ofthe total energy), using energy economy machines would be necessary. The company here involved has currently put into function printing machines with low energy consumption (21.5 kW/ h from 24 kW/h). The new technology is easy to use and all the graphs could be printed at once and, ii) as repairing the defects is energy consuming, an organized control of all production processes would be necessary to prevent defects in time. Various defects occurred d throughout the production process and repairing them is both time (2049.4s) and energy consuming (1.071kW). The following cases could have been avoided:

Three shirts had defects when printed due to the printing ink. Repairing the defect is time consuming and reprinting is power consuming. Reprinting these shirts required 770.4s and 0.0321kW of energy.

Ironing is time consuming due to the return of the shirt back. If this process is conducted by an assistant, 40 s and 0.0133 kW of energy could be saved.

The ornamental stitching machine comprises a rotary mechanism where the newly stitching material passes. The machine was blocked twice due to untrained employee. In the first time, fixing the machine required 600s and in the second, 420s. In addition, 0.142kw of energy were lost.

Lightening is very important for the quality of work. Consequently, fluorescent bulbs of 25 W with of the same lightening quality as 40 W fluorescent bulbs would be a better option for energy efficiency.

Table3 reports on the power consumption for lighting in each working process.

Table 3. Power consumption for lighting: 40 W fluorescent bulb and 25 W fluorescent bulbs.

	Power Consumption [kW]	
Process	**40 W bulbs**	**25 W bulbs**
Projection (in computer)	0.01467	0.0092
Printing	0.074	0.0464
Spreading	0.0051	0.0032
Placement of patterns on mattress	0.0013	0.00081
Cutting patterns	0.00135	0.00084
Printing patterns (in fabric)	0.0141	0.0088
Control of printed parts (organoleptic assessment)	0.00293	0.00183
Setting Sleeves	0.0174	0.01086
Labelling	0.0119	0.0075
Ornamental stitch on back and front closure of TSC	0.0356	0.0222
Shirt's side closure	0.01178	0.0074
Collar ironing	0.0017	0.0011
Collar preparation and assembly	0.0064	0.004
Placement of collar to shirt	0.0038	0.0024
Bottom shirt's folding	0.0037	0.0023
Sleeve's folding	0.0054	0.0339
Shirt's ironing	0.0093	0.0058
The final control (organol.)	0.0164	0.0103
Packaging of TSC shirts	0.0047	0.0029

Power consumption for lighting by 40w fluorescent bulbs throughout the process was 0.24148kW. Power consumptionfor lighting by 25w fluorescent bulbs throughout the process was 0.18174kW.

5. CONCLUSIONS

The energy is very important for the apparel sector as all the machines work with electricity. As alternative energy is costly, using traditional one remains beneficiary.

The energy consumption of machinery/equipment is the highest.

Repairing, lightening and printing are energy consuming.

As efficacy and quality of work depend on working skills and technologies used, staff training is unavoidable.

New technologies including the alternative energy, staff training would be of great efficiency for the apparel sector.

REFERENCES

Ahmad GN. 2011. The step-by-step process of garment manufacturing.

Bhurtun C, KistamahN,Chummun J. 2006. Energy saving strategies in textile industry: the case of Mauritius.

Dumishllari E, Guxho G. 2014. Assessment of energy consumption in garment production.

Gereffi G, Frederick S. 2010. The global apparel value chain, trade and the crisis challenges and opportunities for Developing Countries.

Glock R, Kunz G. 2005. Apparel manufacturing sewn product analysis (Fourth Edition).

Jananthan R, Ameer S. 2006. Comparative study of energy assessment from apparel industries: the context of Sri Lanka.

Khan ShI. 2008. Energy efficient lighting.

UNIDY. 1992. Energy conservation in textile industry.

Xhamaqi M. 2013. Punim projekt diplome: Ndikimi i kohës së punës dhe kontrollit të procesit në konsumin e energjisë në ndërmarrjet e prodhimit të veshjeve. Universiteti Politekniki Tiranës, Departamenti i Tekstilit dhe Modës.

IDENTIFICATION AND EVALUATION OF PLANT GENETIC RESOURCES AND ALBANIAN TRADITION ILLUMINATED BY PROF. DR. KARL HAMMER

The symposium "Identification and evaluation of plant genetic resources and Albanian tradition illuminated by Prof. Dr. Karl Hammer" was organized by the Academy of Sciences of Albania in close partnership with the Agriculture University of Tirana.

This symposium was held on May 23rd in the framework of Science Education Program run by the Section of Natural and Technical Sciences, of the Academy of Sciences of Albania (ASA).

In his speech Acad. Prof. Dr. Salvatore Bushati, Head of the Section of Natural and Technical Sciences described the role that ASA plays in the realm of education and science as it aims to further intellectual pursuits by stating that the Academy, the Section of Natural and Technical Sciences is committed to further Science Education Program, because science improves our everyday life by ameliorating us both spiritually and mentally as scientists work beyond frontiers of any kind. He also pointed out the importance of ethnobotany and its correlation with Albanian traditions. In addition, he stated that Albanians must preserve traditions as part of their national identity and talking about Prof. Hammer was a difficult enterprise. He thanked Prof. Hammer for his efforts to conserve the Albanian plant species and to promote Albanian science.

A list of guests that included the representatives of the Ministry of Agriculture, Rural Development and Water Administration (MARDWA), Ministry of Environment, and many representatives of higher education and research institutes and centers such as Institute of Cultural Anthropology and University of Medicine demonstrated the rising awareness of the importance of ethnobotany to Albania's linguistics, traditions, biology and medicine.

Of great interest were the scientific presentations held by Dr. Helmut Knupffer and Mrs. Merita Spahillari-Hammer. Dr. Helmut Knupffer reported on collecting missions of German researchers in Albania and the actual situation of accessions with Albanian origin in the Gatersleben GenBank. He emphasised that Albania is characterized by a rich biodiversity. He concluded that the study of the original documents, the collecting lists and the corresponding gene bank accessions needs to be continued and information (geography, collection

numbers) needs to be further completed and corrected in GBIS-data quality improvement. Mrs. Hammer reported on Teodor Heinrich Hermann von Heldreich and crop plant research. She showed the efforts made by him to correlate Albanian linguistics with plants. She concluded as following:

Many of the species observed by Heldreich under cultivation are today very rare or even extinct in the Balkans.

With his flora of the cultivated plants Heldreich not only gives an exact picture of species, but it also allows the interpretation of history and evolution.

The "Nutzpflanzen Griechenlands" is an important source for our knowledge on crops and genetic resources in Greece, thus providing the country with one of the rare cases of agri- and horticultural floras .

Moreover, by including many observations with respect to Albanian cultivated plants (a first concise checklist by Hammer-Spahillari, Xhuveli and Hammer in our Arbëreshë book), it can be extremely helpful in the compilation of an Albanian agricultural flora. It also can serve as the basis of a future agri-and horticultural flora of the Balkans.

At the end of symposium greeting letters from colleagues of Prof. Hammer were read showing their appreciation towards this eminent personality.

FROM PLANT GENETIC RESOURCES TO AGROBIODIVERSITY

Karl HAMMER
Leibniz-institut für Pflanzengenetik und Kulturpflanzenforschung (Host),
D-06466 Gatersleben

INTRODUCTION

Food security has scientific dimensions. However, the tools, techniques and tactics of science need to adapt to a world of increasing political complexity. Here, appropriate policies would be of crucial importance for the biodiversity/ plant genetic resources. The latter are fundamental for the food and other needs of mankind. The present paper overviews briefly the interaction between science and policy in the realm of biodiversity/plant genetic resources
Keywords: Plant Genetic Resources

Nicolai Ivanovitch Vavilov (*November 25, 1887 – January 26, 1943)* was one of the most outstanding biologists, geneticists, geographers, agronomists and plant breeders of the XX century and the author of *Five Continents* (Vavilov, 1997). He was the founder and supporter of Plant Genetic Resources (PGR) and his geographical/taxonomic/genetic approach remains a precious guideline for PGR, regardless his tragic death in 1943. However, it took another 30 years until it turned into the "Plant Genetic Resources Movement" (Pistorius, 1997).

Plant Genetic Resources soon became the Movement of Plant Genetic Resources and the First Technical Conference on Plant Genetic Resources (Bennett, 1967) subsequently followed. The discussions were lead by Erna Bennett (Hanelt *et al*., 2012) and Sir Otto Frankel, with participation of Jack Harlan, Jack Hawkes and many others.

The Plant Genetic Resources Movement gradually led to intensive collection of cultivated plants and their wild relatives, especially in areas of diversity, the so called Vavilovian gene centres. The FAO (2010) estimated the largest numbers of accessions in the traditional and many newly founded genebanks of the world as 856.000 for wheat, 774.000 for rice and 467.000 for barley. The work on PGR was guided by "International Undertaking on Plant Genetic Resources for Food and Agriculture" (FAO, 1983).

Darwin (1859) stated that there were some very typical differences between cultivated and wild plants. In 1984 the domestication syndrome present in domesticated plants and animals was defined (Hammer, 1984), summarizing the progress since Darwin and using the advantages of the large collections. Within a relatively short time of about 10.000 years, humankind caused tremendous changes in the dependent plants and animals (see fig. 1after Hammer and Gladis, 1996). The organisms were not the only that changed. Neolithic revolution caused environmental changes leading to the Anthropocenic Age.

With the beginning of the 1990s, the traditional activities of genebanks and plant genetic resources researchers were unfortunately reduced and the "Movement" slowed down.

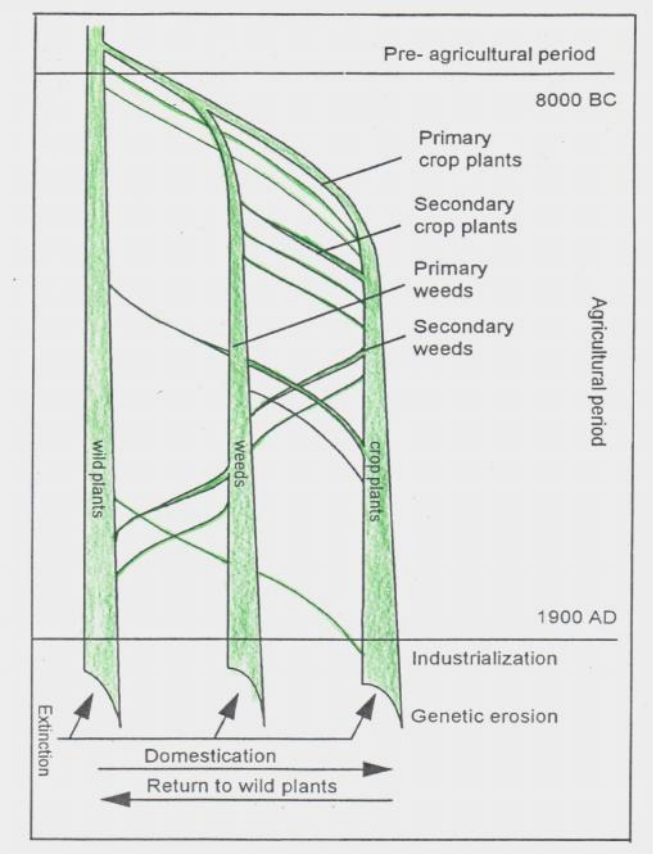

Fig.1. Crop evolution and terminology after Hammer and Gladis (1996). Agrobiodiversity.

The reasons of changes within the PGR sector have been manifold and influenced by political and scientific processes. New scientific input arose from the development of biodiversity. This term was first employed in the mid 1980s

during the conference "The National Forum on Biodiversity" in Washington (Wilson, 1988). Researchers in the PGR sector readily accepted the principles of biodiversity because of the larger scope of the concepts. Biological diversity considers ecological, genetic and organismic aspects (see fig. 2, after Heywood and Watson, 1995). A development of the predominantly genetically based PGR programmes seemed possible. Agrobiodiversity comprises all biological diversity in agriculture. One of the first treatments, originally called "domestic biodiversity" (Jeffries, 1997), was written by Hammer (1998; enlarged English edition 2003).

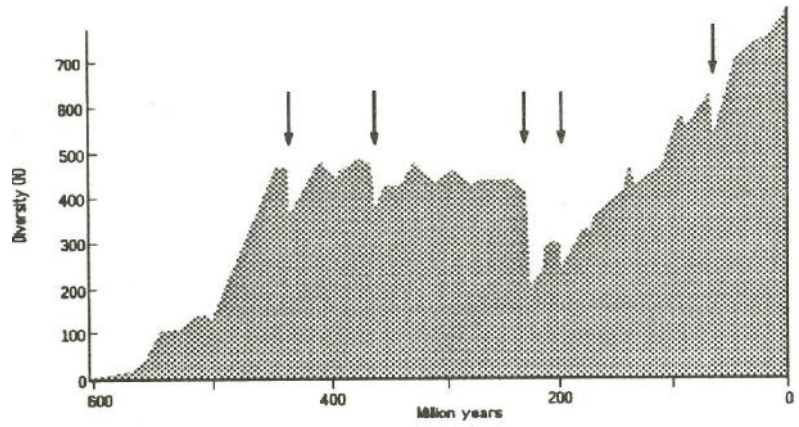

Fig. 2.Extinction events (arrows) and evolution of diversity in organisms.

Agrobiodiversity has addressed the inventory of different organisms participating in this ecosystem. The results of the first estimation of the domestic biodiversity are in Table 1 (after Hammer *et al*., 2012) reported proving the predominance of higher plants among the cultivated organisms for human needs. There was room for including cultural aspects and Szabó (1996) developed an ethno-biodiversity for studying the interaction between plants, animals, human societies and the inanimate world. PGR researches involve nowadays the cultural aspects as well, as human cultural and crop plants and domestic animals' evolution are correlated. The Arbëreshë in South Italy are a good example (Hammer *et al*., 2011). The study of evolution of PGR by botanical and genetical methods was supported by cultural, linguistic and other approaches as a means to address the evolution of the material (landraces), its collecting, maintaining and use for further production and breeding.

Table1. Groups from the domains Eucarya and Bacteria with cultivated species (after Hammer *et al*., 2012).

Groups	No. of species	No. of cultivated species (Mansfeld's approach)	Percentage (%) of cultivated species
Metazoa (Vertebrata only)	50.000	100	0.2
Fungi	1.600.000	62	0.004
Plantae	250.000	7.000	2.8
Rhodophytes	2.500	30	1.2
Bacteria (incl. Cyanobacteria)	1.500.000	2	0.0001

The gradual increase of biodiversity became evident (fig. 3). But also the loss of biodiversity can be demonstrated, formerly mainly caused by cosmic events. The loss of biodiversity in the present period promoted political actions. Within a relatively short time, the extinction rates reached an alarming level. Consequently, the Convention of Biological Diversity (CBD) was signed in Rio de Janeiro in 1992. This resulted in abandoning of the former Undertaking of PGR. The CBD, the more global concept of biodiversity, came into foreground of interest. The concepts of vulnerability and genetic erosion were still considered. Both agreements have only marginally taken each other into consideration (Hammer, 2003b).

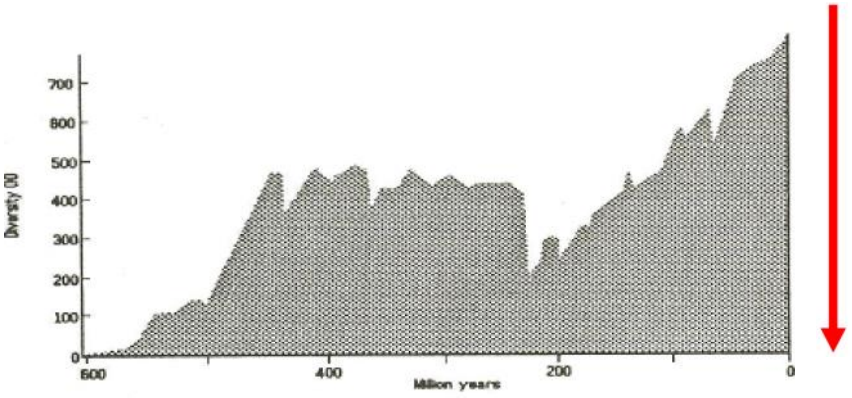

Fig. 3. Increase and loss (arrow) of biodiversity through the times.

Harmonizing the concepts

Amazing parallels exist between biodiversity and PGR. Both have provided a phenomenal increase in scientific knowledge. But soon after the introduction of CBD, a change was observed within the PGR sector, which has been

described as a paradigm shift (Hammer, 2003 a,b). Different constituents of biodiversity have been named differently and, accordingly, treated differently. The following shifts have been observed: i) *in situ* as opposed to *ex situ* maintenance of PGR, ii) inclusion of neglected and underutilized cultivated plants, iii) changes of methods of analysing diversity within and between taxa, iv) changes of methods for evaluation and, v) changes of storage and reproduction in genebanks.

Another challenge resulted from the rapid development of molecular biology and electronic data documentation, management and exchange.

The harmonization process was urgently necessary and resulted in the "International Treaty on Plant Genetic Resources" (FAO, 2001). This document is still in state of needing urgent improvements (Moore and Tymowski, 2005).

Comparison with other organisms

As has been recently confirmed, also other social organisms as leaf-cutter ants and termites are able to show agricultural behaviour (Mueller *et al*., 2005). These mutual adaptations reach back up to about 70 Million years and have to be seen as a symbiosis. The agricultural relations of man to other organisms are strong and relatively one-sided. Man is using and commanding the other organisms which accordingly show the domestication syndrome. Conclusions from biodiversity studies should lead to new alleys of mutual behaviour and consequently include ethnic aspects from the part of man (Hammer *et al*., 2010).

REFERENCES

Bennett E. (ed.), 1967. Record of the FAO/IBP technical conference on the exploration, utilization and conservation of plant genetic resources. Rome.

Darwin C. 1859. The origin of species by means of natural selection. London.

FAO. 1983. Revision of the international undertaking. CPGR, 1st Ext. Session, 7 - 11 November 1994, Doc. CPGR-Ex1/94/4 Alt. Rome.

FAO. 2001. International Treaty on Plant Genetic Resources for Food and Agriculture. FAO, Rome.

FAO. 2010. The Second Report on the State of the World's Plant Genetic Resources for Food and Agriculture. FAO, Rome.

Hammer K. 1984. Das Domestikationssyndrom. *Kulturpflanze* **32**, 11 - 34.

Hammer K. 1998. Agrarbiodiversität und pflanzengenetische Ressourcen. *Schriften zu Genetischen Ressourcen* **10**. ZADI, Bonn.

Hammer K.2003a. Resolving the challenge posed by agrobiodiversity and plant genetic resources - an attempt. *Journal of Agriculture and Rural Development in the Tropics and Subtroptropics.* Beiheft **76**. Kassel.

Hammer K.2003b. A paradigm shift in the discipline of plant genetic resources.*Genetic ResourcesandCrop Evolution.***50**, **(1)**; 3 - 10.

Hammer K,Gladis T. 1996.Funktionen der Genbank des IPK Gaterselbenbeider in-situ Erhaltung on farm.ZADI, Bonn.

Hammer K, Laghetti G, Pignone D. (eds), **2011:** Linguistic Islands and Plant Genetic Resources. The Case of the Arbëreshë. ARACNE, Rome.

Hammer K, Pignone D, Laghetti G. 2010.Plant domestication from syndrome to symbiosis - a comparison of different organisms. *Attidel IV Convegno Piante Mediterranee (Nova Siri)*, 43 - 48.

Hammer K, Piepho H.-P, Szabó A. 2012. Agrobiodiversity. In: E Shaarawi, Piegorsch A.K. (eds), Encyclopedia of Environmetrics, 2nd ed. John Wiley & Sons, Chichester.

Hanelt P, Knüpffer H, Hammer K. 2012. Erna Bennett (5 August 1925 - 3 January 2012). *Genetic ResourcesandCrop Evolution*. **59 (6);** 967 - 970.

Heywood VH, Watson RT.(eds). 1995. Global Biodiversity Assessment. UNEP, Cambridge University Press.

Jeffries MJ. 1997: Biodiversity and Conservation. Routledge, London & New York.

Moore G, Tymowsky W. 2005. Explanatory guide to the international treaty on plant genetic resources for food and agriculture. IUCN, Gland, Cambridge.

Mueller UG, Gerardo NM, Aanen DK, Six DL, Schultz TR. **2005**. The evolution of agriculture in insects. *The Annual Review of Ecology, Evolution, and Systematics*. **36**; 563 - 595.

Pistorius R. 1997. Scientists, Plants and Politics - A History of Plant Genetic Resources Movement. IPGRI, Rome.

Szabó AT.1996. Ethnobiodiversity: human diversity and plant genetic diversity in the evolution of crop plants, part 1. *Schriften Genetic*. *Resources.***4**, 130 - 161.

Vavilov NI. 1997. Five Continents. IPGRI, Rome.

Wilson EO.(ed.), 1998.Biodiversity.National Academic Press, Washington D.C.

THEODOR HEINRICH HERMANN VON HELDREICH AND CROP PLANT RESEARCH (1822 – 1902)

Merita HAMMER-SPAHILLARI
Dr. Junghanns GmbH Aue 182, D- 06449 Aschersleben
Karl HAMMER
Leibniz-Institut für Pflanzengenetik und Kulturpflanzenforschung (Host),
D-06466 Gatersleben

Theodor von Heldreich (fig. 1), well known botanist of his time, was born in Dresden (Saxony) on 03. March 1822, as the son of Conrad Friedrich Robert Heldreich and Amalia Charlotte Humbold in an aristocratic family. After his studies in philosophy in Freiburg, Germany, he began his botanical studies in Montpellier (1837), under Michel Félix Dunal (1789 - 1856) and Geneva during 1838 - 1842, under Augustin-Pyramus de Candolle (1778 - 1841) and Alphonse de Candolle (1806 - 1893). His first botanical studies led him to Sicily 1940 - 1941 where he worked as a successful plant collector there and described three new plant species. After coming back from Sicily, he became curator of the De Candolle Herbarium in Geneva. Pierre Edmond Boissier (1810 - 1885), the author of the famous "Diagnoses plantarum orientalium novarum" (1842 - 1859), described a new Cruciferae genus as *Heldreichia* Boiss, in honor of the successful young scientist. A tentative list of many species described in honor of Heldreich is presented by Baytop and Tan (2008).

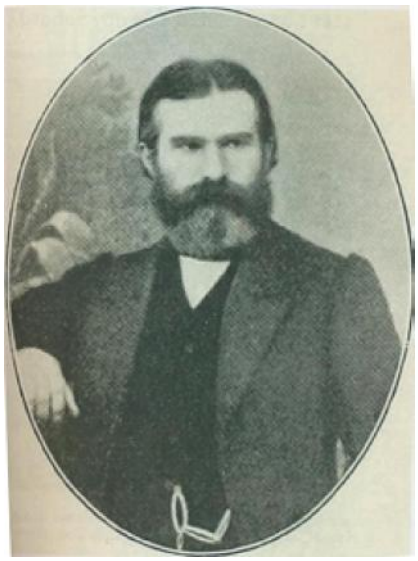

Fig. 1. Theodor von Heldreich.

Heldreich continued to collect plants in Italy, Greece, Asia Minor and Crete from 1843-1848.

From 1849 - 1850 he lived in England followed by a short term stay in Paris as a curator of P. Barker Webb's Herbarium.

From 1851 he settled permanently in

Greece. In 1855 he married Sofia, daughter of I. Katakuzenos and granddaughter of the Greek scholar and patriot Konstantinos Koumas. They had three daughters (Minna, Karolina and Ioanna). As supposed by Baytop and Tan (2008), who also presented pictures of the gravestones from an Athens cemetery, no direct descendants of Heldreich are still alive.

From 1856 - 1896 he published thirteen volumes of the "Herbarium graecum normale", served as director of the court garden for over 50 years until his death on the 2nd of September, 1902 in Athens. Heldreich was also director of the Natural History Museum in Athens (1858 - 1883). He detected and described seven new genera and more than 700 new species of higher plants.

His botanical work is well known (Stafleu and Cowan, 1970) and has been recently revised for Anatolia (Baytop and Tan, 2008). His work in Greece and the Balkans with yearly expeditions, including mountains and islands (fig. 2, distribution map of *Acer heldreichii*) is an example for scientific effectivity and intensity.

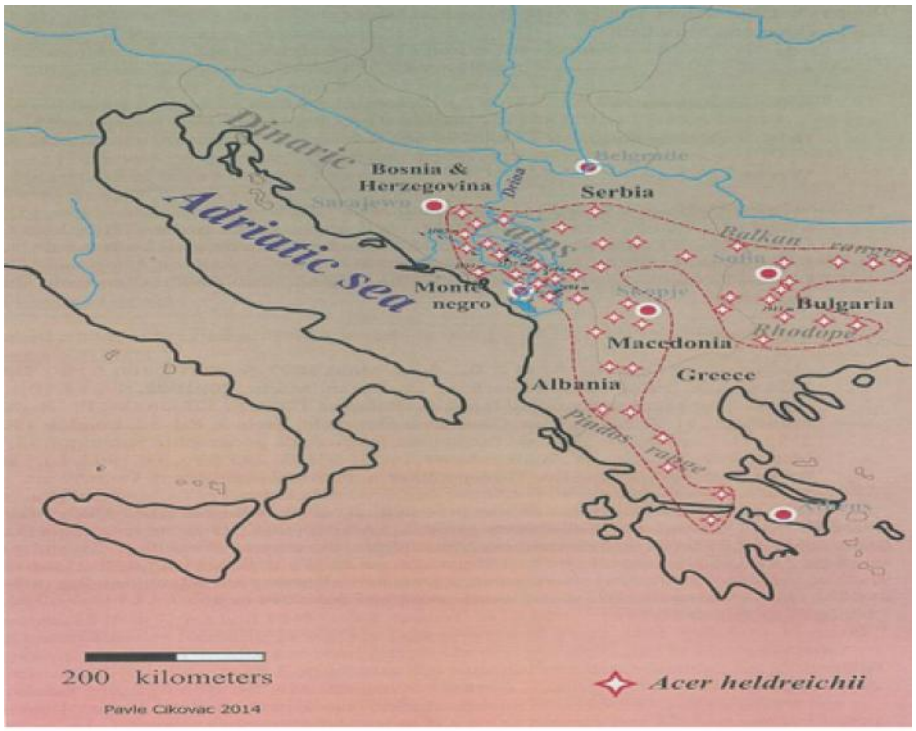

Fig. 2. Distribution map of *Acer heldreichi* after Baytop and Tan, 2008. Many collecting missions of Heldreich were carried out in this area

Widely known is his work concerning *Aesculus hippocastanum*, one of the most beautiful ornamental and alley trees in Europe. The origin of this tree was redetected for the Balkans (mountains of Greece, Macedonia and Albania) by Heldreich, contrary to former opinions proposing Asia Minor as the home country of this species.

Apart from botany, he was interested in mathematics (Botany in relation to mathematics, Athens 1901), zoology (La Faun de la Grèce, I. Animaux vertébrés, Athens 1878), wrote a romance entitled "Mussinitza" in 1878 and a sketch on the death of the Professor of botany and poet Theodoros G. Orfanides in 1889, among others. He published scholarly works in German, Greek, French, Latin and Italian.

Considering his manifold interests and especially his most important teacher, Alphonse De Candolle (author of Bot. Appl., 1856) with a part on cultivated plants and "Origin des plantes cultivées" (1882), the best treatment on cultivated plants of his time, Heldreich's engagement in cultivated plants is a logical consequence. In fact, Heldreich started intensive studies and finished his work "Die Nutzpflanzen Griechenlands" (fig. 3) already in 1862. This was one of the first agri- and horticultural floras from an old center of origin of agriculture (see also Heldreich's "Homeric Flora", Athens 1896). De Candolle (1882, cited after the English edition of 1967) appreciated the classical approach of Heldreich concerning Theophrastus: "These passages and others of ancient writers are quoted and interpreted by Heldreich better than by Hehn and other scholars" (p. 426) (De Candolle refers to the book by V. Hehn, Culturpflanzen und Hausthiere in ihrem Uebergang aus Asien nach Griechenland und Italien sowie in das uebrige Europa, Berlin, 1870). "Nutzpflanzen" is a synonym of cultivated plants as it was and is still used by German botanists.

Fig. 3. One of the first agri- and horticultural floras from an old center of origin of agriculture (1862). Book cover of the edition of NABU Press, 2010.

De Candolle (1882) made extensive use of Heldreich's agricultural flora and cited for the first time in a prominent place the Albanian plant names collected by Heldreich himself during his excursions. As can be seen from the title of Heldreich's book, he was investigating the "pelasgic" names. Dr. von Hahn (1854) tried to characterize the Albanian

language, present not only in the Greek Kingdom and its islands, but also in the whole of the Balkans (SE European Region located S of the Danube-Sava-Kupa river systems) as the language of the first pre-Slavic inhabitants of this area. The ideas of Hahn have been supported by Reinhold (1855), who claimed that the old Albanian language was the primary language of the Balkans from which Latin and Greek derived. Soon it became aware, mainly using linguistic considerations, that the Albanians are descendents of autochthonous Balkan populations, to which belong Illyrians, Thracians and Greeks (Lewis et al., 2014).

At any rate, the Albanian plant names have been collected by Heldreich, also using the practical advice and experience of Reinhold (1855), e.g. differentiating between determined and undetermined nouns, i.e. citing both forms in applicable cases and making notes on irregular plurals and others. The results have been approved by linguists (Kind, 1863). As already stated, the plant names have been introduced by De Candolle (1882) to international botanical circles. De Candolle added also other linguistic information from Heldreich (1877, 1879). Heldreich has already changed pelasgic to Albanian in his article of 1877. Special treatments of Heldreich on cultivated plants included *Humulus lupulus* (1885), *Tulipa* spp. (including ornamentals, 1862), recommended ornamentals of Greece (1861) and the genus *Leopoldia* (1878, with many ornamentals). He included information about cultivated plants into his continuing floristic publications (Flora of Cepahalonia, 1883, Flora of Thera, 1899).

His last excursion in 1901 resulted in finding a new wild species, *Myosurus heldreichii* described after his death in 1902 by A. Léveillé.

Some examples from Heldreich's "Nutzpflanzen Griechenlands" are given in the following, to present at least some impressions from this work. On page 3 he described some cereals as *Zea mays*, *Panicum miliaceum* and *Sorghum vulgare*. For the last one he uses a very wide concept similar to the present one when most *Sorghum* species are united into *Sorghum bicolor* (L.) Moench s.l. A closer analysis of the accompanying text shows that *S. dochna* (Forssk.) Stapf was cultivated for grains and fodder. Probably, *S. saccharatum* convar. *technicum* (Körn.) Tzvel was grown for the production of brooms. Kalambokj is the old Albanian name for *Sorghum*; later on it went also to mays.

Page 40 describes a species which is known today as *Ridolfia segetum* (L.) Moris. This aromatic plant is very rare in our days. Recently, it was only reported as a cultivated plant from Kuweit and Palestine.

Citrullus colocynthis is mentioned as a medicinal plant from gardens (p. 50).

Mesembryanthemum crystallinum is mentioned as a vegetable grown in gardens. This vegetable has been introduced by the Turks (p. 51).

Lavatera arborea is described from gardens where it is used as a vegetable. Leaves and flowers have been used. In 1996, Hammer found this species as a

garden plant in the small Island of Linosa (Italy), where it was grown as a fodder plant (Laghetti *et al*., 1998).

Gossypium herbaceum L. was cultivated on large areas as a fibre plant (p. 52). Today this old world species has nearly disappeared, whereas the new world *G. hirsutum* is occasionally cultivated.

Prunus insititia L. is a little plum, wild and cultivated, Heldreich mentioned several varieties, among others a very early ripening one with green fruits (p. 68).

Vicia ervilia is characterized as a commonly grown fodder plant (p. 71). Very few accessions of this species have been found in collecting missions carried out by Hammer in the 1990s.

Vigna unguiculata is mentioned as *Dolichos melanophthalmus* DC. (p. 72), an Old world bean, which was grown as a vegetable and for the dry seeds.

Many of the species observed by Heldreich under cultivation are today very rare or even extinct in the Balkans.

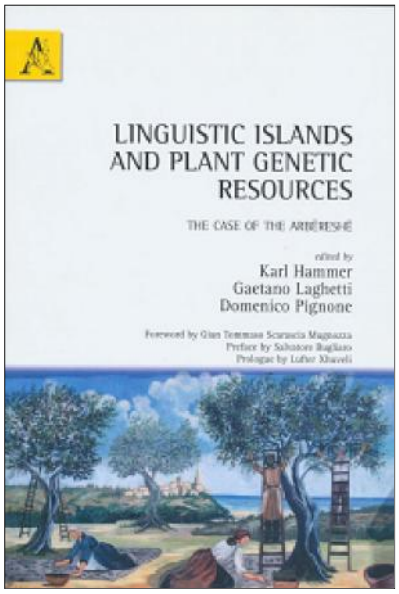

Fig. 4. Book on Arbëresh agriculture, Hammer *et al.*, 2011, Aracne editrice S.r.l., Rome.

With his flora of the cultivated plants, Heldreich not only gives an exact picture of the species, but it also allows the interpretation of history and evolution. The "Nutzpflanzen Griechenlands" are an important source for our knowledge on crops and genetic resources in Greece thus providing the country with one of the rare cases of agri- and horticultural floras. But, moreover, by including many observations with respect to the Albanian cultivated plants (a first concise checklist by Hammer-Spahillari, Xhuveli and Hammer in our Arbëreshë book, see fig. 4), it can be extremely helpful in the compilation of an Albanian agricultural flora. It can also serve as the basis of a future agri- and horticultural flora of the Balkans.

REFERENCES

Baytop A, Tan K. **2008**: Theodor von Heldreich (1822 - 1902) and his Turkish collections. *Turkish Journal of Botany.* **32**, 471 - 479.

De Candolle A. 1882 ('1883'). L'origine des plantes cultivées, éd. 1. Paris.

Hahn JG von. 1854. Albanesische Studien, Teil 1. Jena.

Hammer K, Laghetti G., Pignone D. (eds), **2011**. Linguistic Islands and Plant Genetic Resources. The Case of the Arbëreshë. ARACNE, Rome.

Hehn V. 1870. Culturpflanzen und Hausthiere. First ed.

Heldreich, von Th. 1862. Die Nutzpflanzen Griechenlands. Mit besonderer Berücksichtigung der neugriechischen und pelasgischen Vulgarnamen. Karl Wilberg, Athen.

Heldreich, von Th. 1877. Die Pflanzen der Attischen Ebene. Julius Bergas, Schleswig.

Heldreich, von Th. 1878. Über die Liliaceen-Gattung *Leopoldia* und ihre Arten. Typographie der Universität, Moskau.

Heldreich, von Th. **1879**. Verhandlungen des botanischen Vereins Brandenburg, 147.

Heldreich, von Th. 1882. Flora de l'ìle de Céphalonie. Georges Bridel, Lausanne.

Heldreich, von Th. 1895. Über den Hopfen (*Humulus lupulus*) und seinen Anbau in Griechenland. Athen.

Heldreich, von Th. 1899. Die Flora der Insel Thera. Georg Reimer, Berlin.

Kind Th. 1863. Pelasgisch - Albanisch - Griechisch. *Zeitung vergleich. Sprachforsch*. **12**, 207 - 211.

Laghetti G, Pignone D, Hammer K. 1998. Presence, history and uses of *Lavatera arborea* L. in Linosa island (Italy). *Economic Botany.* **51 (1)**, 129 - 130.

Léveillé A. Ranunculaceae *Myosurus heldreichii*. Bull. Acad. Int. Géogr. Bot. XI (1902) 296. http://www.ipni.org/ipni/idAuthorSearch.do;jsessionid=D561F44D136E7AEA71B33FCB36559812?id=12648-1&back_page=

Lewis MP, Simons GF, Fenning CD. 2014. Ethnologue: Languages of the World, 7th ed. SIL International, Dallas.

Reinhold Dr. 1855: Noctes Pelasgicae vel Symbolae ad cognescendas dialectos Graeciae Pelasgicas. 3 suul. (1856).

Stafleu FA, Cowan RS. **1970**. Taxonomic Literature, vol. II, H - Le. Utrecht and The Hague., Heldreich, Theodor von, 142 - 144.